AD-A082 688 GENERAL DYNAMICS CORP FORT WORTH TX FORT WORTH DIV F/G 20/4
V/STOL PROPULSION-INDUCED AERODYNAMICS HOVER CALCULATION METHOD--ETC(U)
FEB 80 W H FOLEY, J A SANSONE N62269-79-C-0212
UNCLASSIFIED NADC-78242-60 NL

1 OF 2
AD
A082688

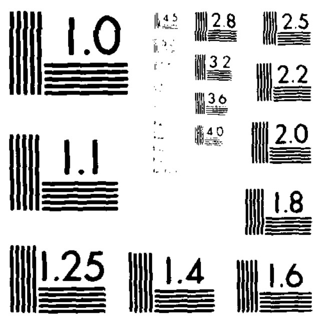
1.0
1.1
1.25
1.4
1.6
1.8
2.0
2.2
2.5
2.8
3.2
3.6
4.0
4.5

LEVEL II

NADC-78242-60

ADA082688

12

V/STOL PROPULSION-INDUCED AERODYNAMICS HOVER CALCULATION METHOD

by

W. H. Foley and J. A. Sansone

GENERAL DYNAMICS
Fort Worth Division

February, 1980

APPROVED FOR PUBLIC RELEASE; DISTRIBUTION UNLIMITED

Prepared For

NAVAL AIR DEVELOPMENT CENTER
WARMINSTER, PENNSYLVANIA 18974

80 4 3 031

NOTICES

REPORT NUMBERING SYSTEM - The numbering of technical project reports issued by the Naval Air Development Center is arranged for specific identification purposes. Each number consists of the Center acronym, the calendar year in which the number was assigned, the sequence number of the report within the specific calendar year, and the official 2-digit correspondence code of the Command Office or the Functional Directorate responsible for the report. For example: Report No. NADC-78015-20 indicates the fifteeth Center report for the year 1978, and prepared by the Systems Directorate. The numerical codes are as follows:

CODE	OFFICE OR DIRECTORATE
00	Commander, Naval Air Development Center
01	Technical Director, Naval Air Development Center
02	Comptroller
10	Directorate Command Projects
20	Systems Directorate
30	Sensors & Avionics Technology Directorate
40	Communication & Navigation Technology Directorate
50	Software Computer Directorate
60	Aircraft & Crew Systems Technology Directorate
70	Planning Assessment Resources
60	Engineering Support Group

PRODUCT ENDORSEMENT - The discussion or instructions concerning commercial products herein do not constitute an endorsement by the Government nor do they convey or imply the license or right to use such products.

APPROVED BY: E J Sturm DATE: 1/29/80

E. J. STURM, USN

UNCLASSIFIED

SECURITY CLASSIFICATION OF THIS PAGE (When Data Entered)

REPORT DOCUMENTATION PAGE

READ INSTRUCTIONS BEFORE COMPLETING FORM

1. REPORT NUMBER: NADC-78242-60	2. GOVT ACCESSION NO.
3. RECIPIENT'S CATALOG NUMBER	
4. TITLE (and Subtitle): V/STOL PROPULSION-INDUCED AERODYNAMICS HOVER CALCULATION METHOD.	5. TYPE OF REPORT & PERIOD COVERED: Final Technical Report For Period 1/19/79-1/19/80
	6. PERFORMING ORG. REPORT NUMBER
7. AUTHOR(s): W. H. Foley, J. A. Sansone	8. CONTRACT OR GRANT NUMBER(s): N62269-79-C-0212
9. PERFORMING ORGANIZATION NAME AND ADDRESS: General Dynamics Corp. Fort Worth Division Fort Worth, Texas 76101	10. PROGRAM ELEMENT, PROJECT, TASK AREA & WORK UNIT NUMBERS: Air Task No. A03V-320D/01B/7F41-400-000
11. CONTROLLING OFFICE NAME AND ADDRESS: Naval Air Development Center Warminster, PA 18974	12. REPORT DATE: Feb[redacted]1980
	13. NUMBER OF PAGES
14. MONITORING AGENCY NAME & ADDRESS (if different from Controlling Office)	15. SECURITY CLASS. (of this report): Unclassified
	15a. DECLASSIFICATION/DOWNGRADING SCHEDULE

16. DISTRIBUTION STATEMENT (of this Report)

Unlimited

T41400

17. DISTRIBUTION STATEMENT (of the abstract entered in Block 20, if different from Report)

Unlimited

18. SUPPLEMENTARY NOTES

19. KEY WORDS (Continue on reverse side if necessary and identify by block number)

V/STOL
Ground Effects
Suckdown
Fountain Forces

20. ABSTRACT (Continue on reverse side if necessary and identify by block number)

An empirical method has been developed to predict the propulsive-induced forces on a V/STOL aircraft hovering in proximity of the ground. This method is applicable to configurations employing two, three, or four circular exhausts. Planform contour, nozzle pressure ratio, and lift improvement devices are considered. Accuracies on the order of one percent of propulsive thrust are demonstrated.

DD FORM 1 JAN 73 1473 EDITION OF 1 NOV 65 IS OBSOLETE

UNCLASSIFIED

SECURITY CLASSIFICATION OF THIS PAGE (When Data Entered)

402104

FORWARD:

This study was conducted under contract to the Naval Air Development Center (Contract N62269-79-C-0212). The Technical Monitor was Mr. Campbell Henderson, Flight Dynamics Branch (6053), Aircraft and Crew Systems Technology Directorate.

TABLE OF CONTENTS

TABLE OF CONTENTS (Cont'd.)

TABLE OF CONTENTS (Cont'd.)

LIST OF FIGURES

LIST OF FIGURES (Cont'd.)

LIST OF FIGURES (Cont'd.)

LIST OF FIGURES (Cont'd.)

LIST OF FIGURES (Cont'd.)

LIST OF FIGURES (Cont'd.)

NOMENCLATURE

a	Average Planform Width (Figure 2.1-10)
C_S, C_F	Extrapolation Coefficients (Subsection 2.1.3)
d, D	Nozzle Diameter
d_{wa}	Thrust Weighted Nozzle Diameter (Eqn. 2.1-9)
$\bar{D}$	Equivalent Planform Diameter
d_E	Distance Between Nozzles
d_f	Distance Between a Nozzle and a Fountain
d_{je}	Equivalent Nozzle Diameter (Subsection 3.1.2)
F_j	Nozzle Thrust
h, H	Altitude
h_m	Altitude Where Jets Merge (Figure 2.1-15)
ΔL	Net Lift Loss (or Gain)
ΔL_j	Partial Lift Loss Due to Suckdown (Eqn. 2-1)
ΔL_F	Fountain Lift
ΔL_{FI}, ΔL_{FII}	Two-Nozzle Fountain Lift (Subsection 2.1.2.2)
ΔL_s	Lift Loss Due to Suckdown
$\Delta L_{s\infty}$	Lift Loss Out of Ground Effect
LID	Lift Improvement Device
N	Number of Nozzles
NPR	Nozzle Pressure Ratio
r	Planform Contour Radius
W	Planform Width (Figures 2.1-8 and 2.1-10)
$\theta_{1,2}$	Angular Section of Radial Ground Jet (Eqn. 2.1-10)

1. INTRODUCTION

The flow field in the immediate vicinity of a hovering V/STOL aircraft can be divided into six more or less distinct regions (Figure 1-1). Of particular interest here are regions 1, 2, 3, and 5, i.e., those regions wherein the engine exhaust flows combine with induced ambient air flows to produce forces and moments upon the airframe. In the case of aircraft with high engine exhaust velocities combined with appreciable planform areas, such as the AV-8A and the VAK-191B, these forces and moments are almost invariably both large and unfavorable. Consequently, a considerable amount of theoretical and experimental work (e.g., Ref. 1-15) has been devoted to the subject. During 1977, the Naval Air Development Center began work on a V/STOL Aerodynamic and Stability and Control Manual in order to reduce V/STOL test data and prediction methodologies to a form useful in a preliminary design environment - that is, to develop an engineering tool for doing rapid hand calculations of advanced aircraft performance during the conceptual stage of development. As a point of departure for this work General Dynamics has extended test and analysis work which was conducted both in house and under contract to ONR (Refs. 7 and 11) to develop empirical formulations for hover-induced lift effects for application in the manual.

The results of this program are presented in this report, and the methodology itself is contained in Section 3. This was assembled totally independent of the other sections of the report so that it may be removed and used separately from the body of the text. For this reason, the reader may note a certain amount of redundancy between Section 3 and the other sections.

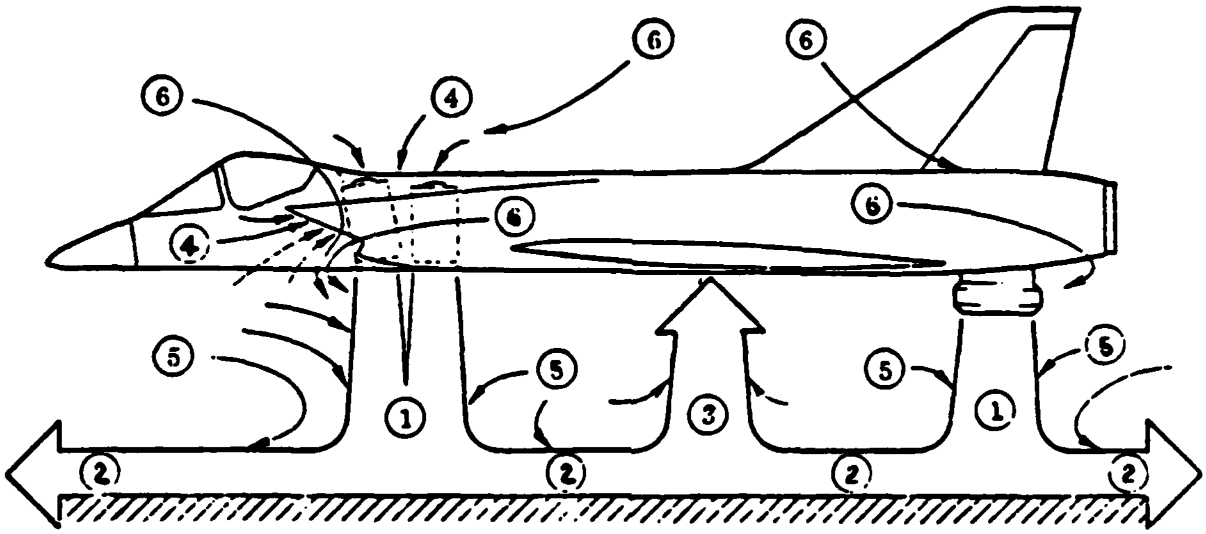

1 EXHAUST FLOW (FREE JET)

2 GROUND JET

3 FOUNTAIN JET

4 ENGINE INLET FLOW

5 & 6 ENTRAINED AMBIENT AIR

Figure 1.0-1 Flow Field Near a Hovering VTOL Aircraft

2. METHODOLOGY DEVELOPMENT GENERAL

The objective of this program is the development of an empirical method for the prediction of propulsive-induced effects upon the lift of a V/STOL aircraft hovering in ground proximity. To this end, two guidelines were established, namely, that the resulting empiricisms were to be covered in the simplest possible forms from the user standpoint regardless of the format which might be indicated from a purely scientific and analytic viewpoint (provided, of course, that the resulting empiricisms gave realistic results when applied to test data cases), and that no attempt would be made to structure the details of the flow field because, to do so, would have rapidly led the methodology afield into the area of an analytic formulation, rather than the desired tool for rapid use in aircraft preliminary design and evaluation. An example of the spirit with which these guidelines were observed can be seen by considering that the method of Karemaa et al. (Refs. 7 and 8), the point of departure for this work, was modified from

$$\frac{\Delta L}{F_j} = \frac{1}{F_j} \left\{ \Delta L_j + \Delta L_{fc} + \Delta L_{fi} \right\} \tag{2-1}$$

to

$$\frac{\Delta L}{F_j} = \frac{1}{F_j} \left\{ \Delta L_s + \Delta L_F \right\} \tag{2-2}$$

The terms ΔL_{fc} and ΔL_{fi}, in the Karemaa formulation, represent the incremental lift due to fountain buoyancy and the change to suckdown due to interference with the entrainment process by the fountain, respectively. In the Karemaa work, where the object was to develop an understanding of the physical processes involved in the flow field, it was most appropriate to distinguish between the two. Here, however, it was found that empirically the two could be combined so that only ΔL_F, the net fountain contribution, appears explicitly. Next, in the Karemaa formulation, ΔL_j represents the suckdown on those areas of the planform adjacent to each individual exhaust nozzle. Experimentally, ΔL_j was determined by measuring this force on the adjacent area with the non-adjacent planform areas physically present but non-metric. A predictive technique for ΔL_j would require the structuring of the induced flow fields because the locations of the non-adjacent areas change the flow field itself. Thus, suckdown, ΔL_s, which can be predicted empirically, is the summation of

the suckdown produced by each jet upon the entire planform area.

In all instances, justification for the empiricisms was made, ultimately, a posteriori, i.e., do they work to an acceptable degree of accuracy over a full range of likely configurations. As will be seen in Section 4, the complete methodology was tested against a number of configurations, which were not from the same data base from which the empiricisms were developed; the predictions obtained matched the test data within about 1% of the total lift, which is considered adequate for the applications envisaged for this methodology.

2.1 METHODOLOGY DEVELOPMENT

2.1.1 Suckdown

Wyatt (Ref. 4), one of the first investigators to conduct a parametric variation of the suckdown problem, obtained the empirical relationship

$$\frac{\Delta L_s - \Delta L_{s\infty}}{F_j} = -.012\left[h/(\bar{D}-d)\right]^{-2.30} \tag{2.1-1}$$

However, this expression did not correlate with the data of Spreeman and Sherman (Ref. 1) because experiments were conducted at different NPR's. Kuhn (Ref. 9) has derived a modified form of Wyatt's equation that empirically accounts for the NPR effect and gives better agreement, viz.,

$$\frac{\Delta L_s - \Delta L_{s\infty}}{F_j} = -.015\left[h/(\bar{D}-d)\right]^{-(2.2-.24(NPR-1))} \tag{2.1-2}$$

A close examination of the earlier results and the more recent work of Smith and Lummus (Ref. 11) (Figure 2.1-1) show that there is a fine structure to the suckdown that is a function of the area ratio $\bar{D}/d$. This structure consists of curves of the same family (Figure 2.1-2) which, in empirical, algebraic form, are described by the relation

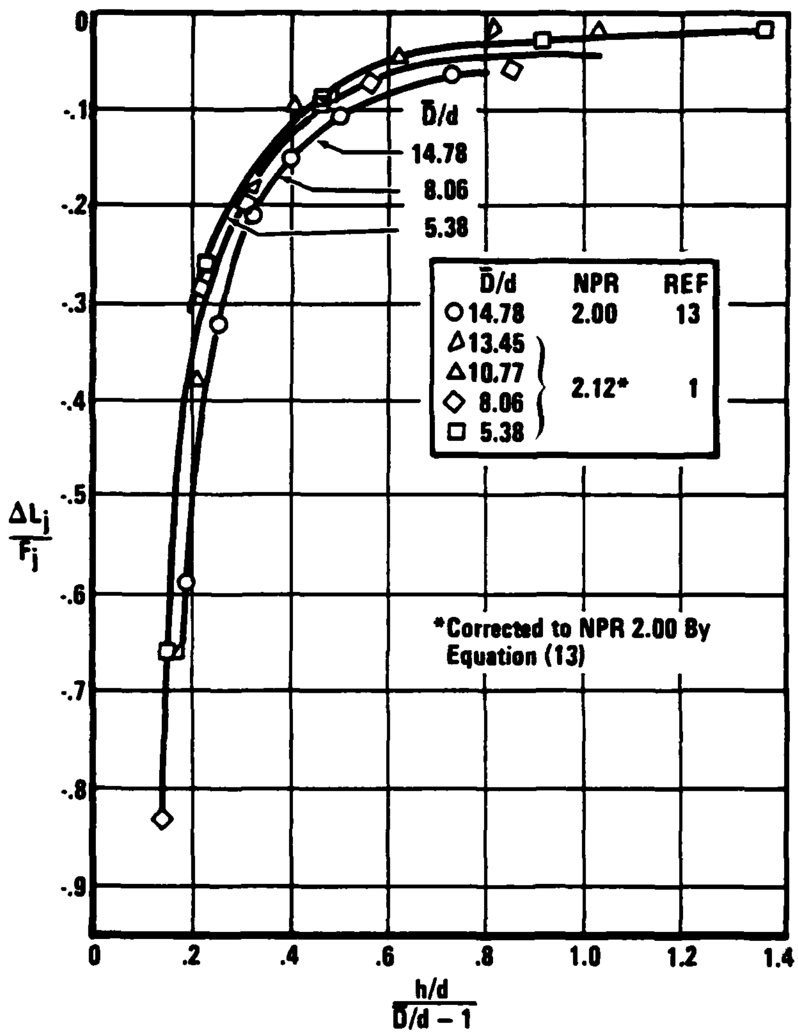

Figure 2.1-1 Suckdown Under Rectangular Planforms

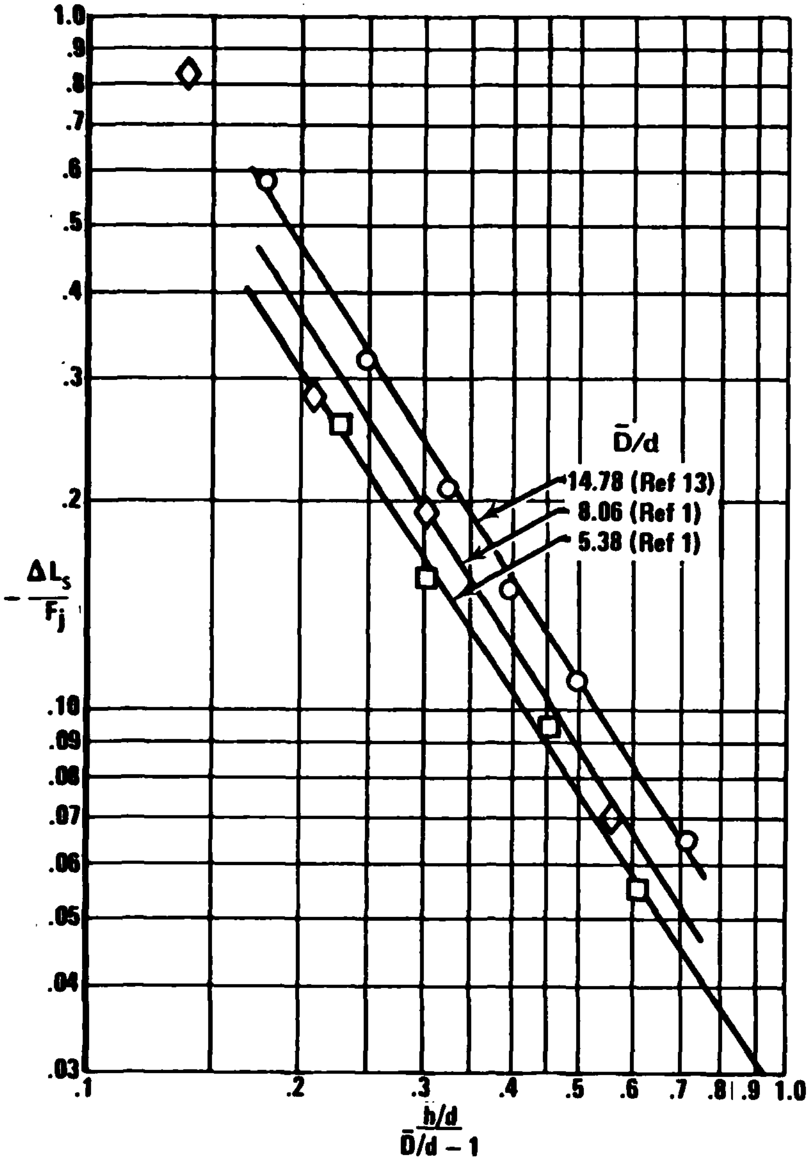

Figure 2.1-2 Suckdown Under Rectangular Planforms--Fine Structure

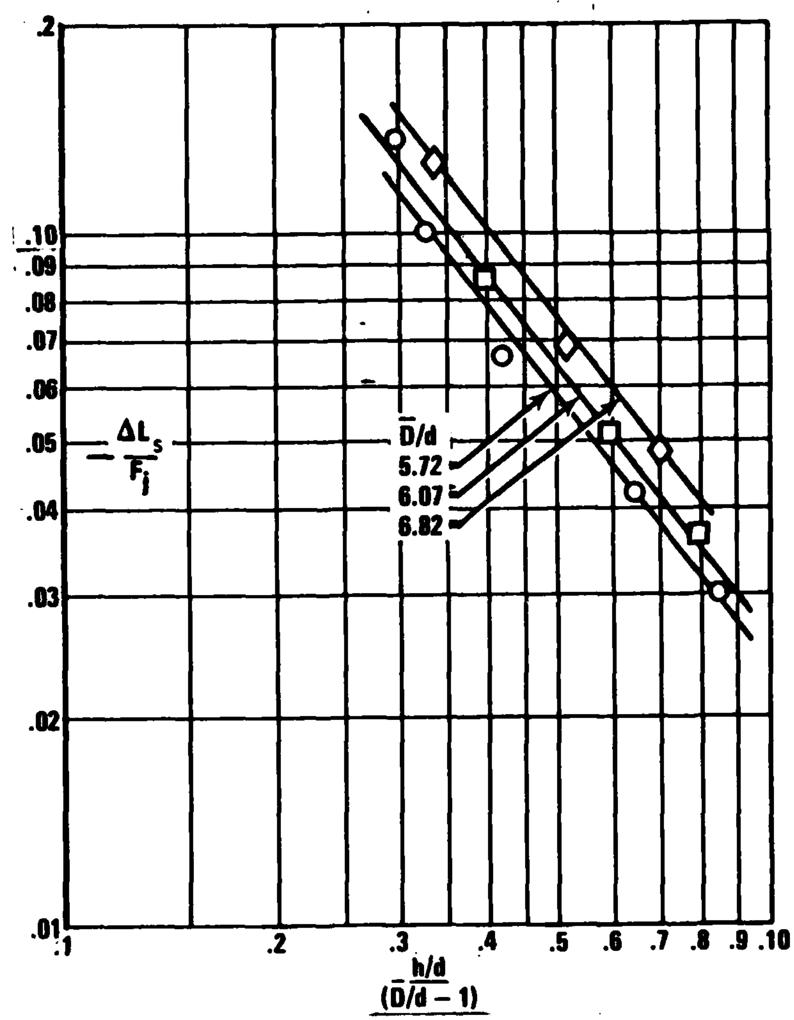

Figure 2.1-3 Suckdown Under Delta-Shaped Planforms--Fine Structure

$$\frac{\Delta L_s - \Delta L_{s\infty}}{F_j} = (.00125\ \bar{D}/d + .0185) \cdot \left[h/(\bar{D}-d)\right]^{-1.59} \qquad (2.1\text{-}3)$$

Wyatt's results for free-air suckdown may also have a fine-structure because of area ratio but, for the cases of interest, $\Delta L_{s\infty} \ll \Delta L_s$, so we use uncorrected from Wyatt's data,

$$\frac{\Delta L_{s\infty}}{F_j} = .0667\ (d/\bar{D} - .420) \qquad (2.1\text{-}4)$$

Delta planforms show a similar fine-structure (Ref. 15) (Figure 2.1-3); the suckdown is described by the relation

$$\frac{\Delta L_s - \Delta L_{s\infty}}{F_j} = -(.0072\ \bar{D}/d - .0166) \cdot \left[h/(\bar{D}-d)\right]^{-1.28} \qquad (2.1\text{-}5)$$

By definition, the suckdown for a configuration with more than one nozzle is obtained by calculating the individual suckdown for each nozzle and then summing and weight averaging by thrusts, that is

$$\frac{\Delta Ls}{F_j} = \sum_{i=1}^{N} \left(\frac{\Delta Ls}{F_j}\right)_i (F_j)_i \Big/ \sum_{i=1}^{N} (F_j)_i \qquad (2.1\text{-}6)$$

2.1.2 Net Fountain Buoyancy

The development of the empirical terms to predict fountain buoyancy required a much larger data base that was available from the previous work. To this end, a series of parametrical variations of the Ref. 7 configurations was made:

Test Series I. Two nozzles, variations in $\bar{D}$, Figure 2.1-4.

Test Series II. Two nozzles, variations in wing/fuselage area ratios, Figure 2.1-5.

Test Series III. Three nozzles, variations in $\bar{D}$, Figure 2.1-6.

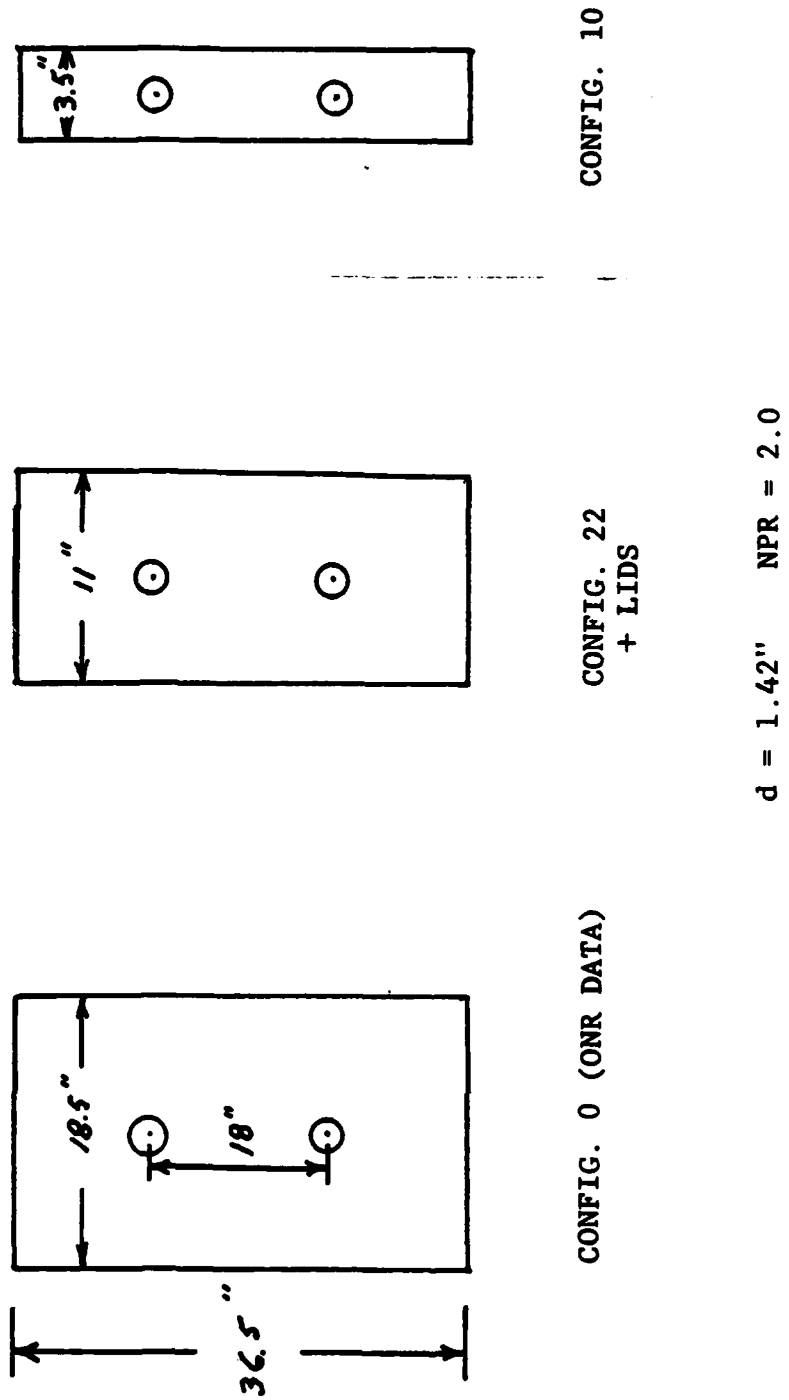

Figure 2.1-4 2 Nozzle Rectangular Planforms

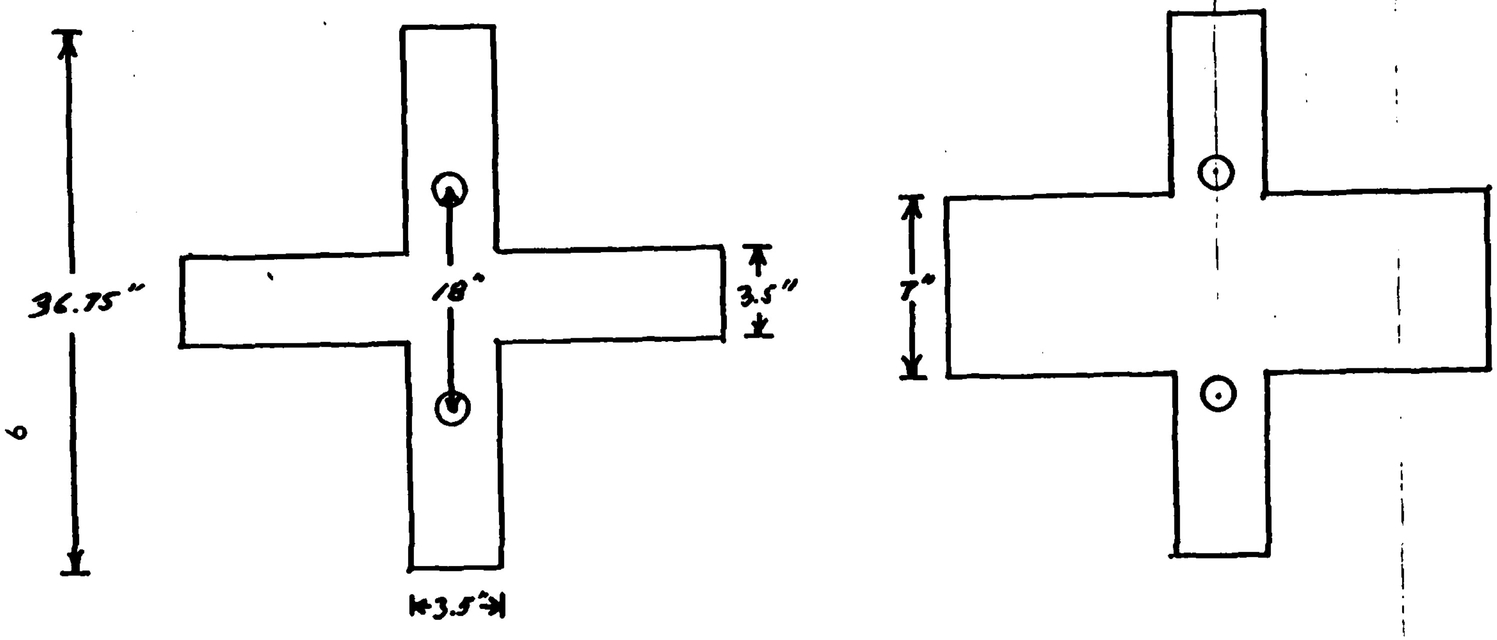

CONFIG. 1
+ LIDS
+ PLANFORM CONTOUR

CONFIG. 21
+ LIDS

d = 1.42"   NPR = 2.0

Figure 2.1-5 2 Nozzle Cruciform Planforms

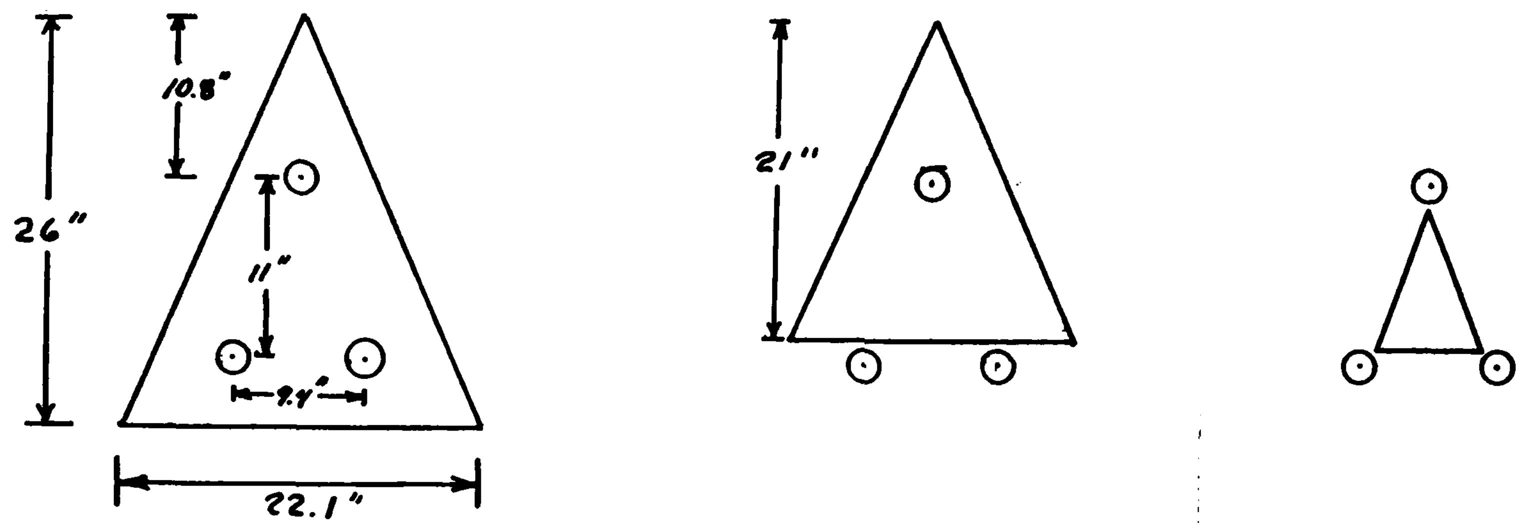

CONFIG. 6 (ONR DATA)
+ LIDS

CONFIG. 26
+ LIDS

CONFIG.`12
+ LIDS

d = 1.32"   NPR = 2.0

Figure 2.1-6 3 Nozzle Planforms

Test Series IV. Four nozzles, variations in $\bar{D}$ and d, Figure 2.1-7.

The experimental method of Ref. 11 was used to take force measurements of ΔL upon the planforms. As shown on Figures 2.1-4 through 2.1-7, most configurations were tested with and without lift improvement devices (LIDs). The planform undersurface contour was varied on Configurations 1 and 15. Finally, the fountain strengths on selected configurations were measured by total pressure surveys using the method of Ref. 7. The test results are shown in graphical form in Appendix A. They will be discussed below as appropriate during the methodology derivation.

For each configuration $\Delta L_f/F_j$ was obtained by subtracting the calculated suckdown from the $\Delta L/F_j$ obtained from the balance data, i.e.,

$$\frac{\Delta L_F}{F_j} = \frac{\Delta L}{F_j} - \frac{\Delta L_s}{F_j} \qquad (2.1\text{-}7)$$

2.1.2.1 Two-Jet Fountains

In the course of analyzing the experimental data, it became apparent that the fountain lift produced by the two-nozzle configurations was fundamentally different from those produced by either three or four nozzles in that the former were much more sensitive to planform area than the latter. The physical cause undoubtedly lies in the fact that a fountain produced by two jets has a fan shape that is much more diffuse than the compact, column-shaped fountains produced by three and four jets (Ref. 7).

Before beginning discussion of the methods by which $\Delta L_F/F_j$ are calculated, the terms $\bar{D}$ and d, which were used in the suckdown calculations, are redefined slightly for use in fountain calculations, namely,

$$\bar{D}_{wa} = \sum_{i=1}^{N} (F_j\bar{D})_i / \sum_{i=1}^{N} (F_j)_i \qquad (2.1\text{-}8)$$

and

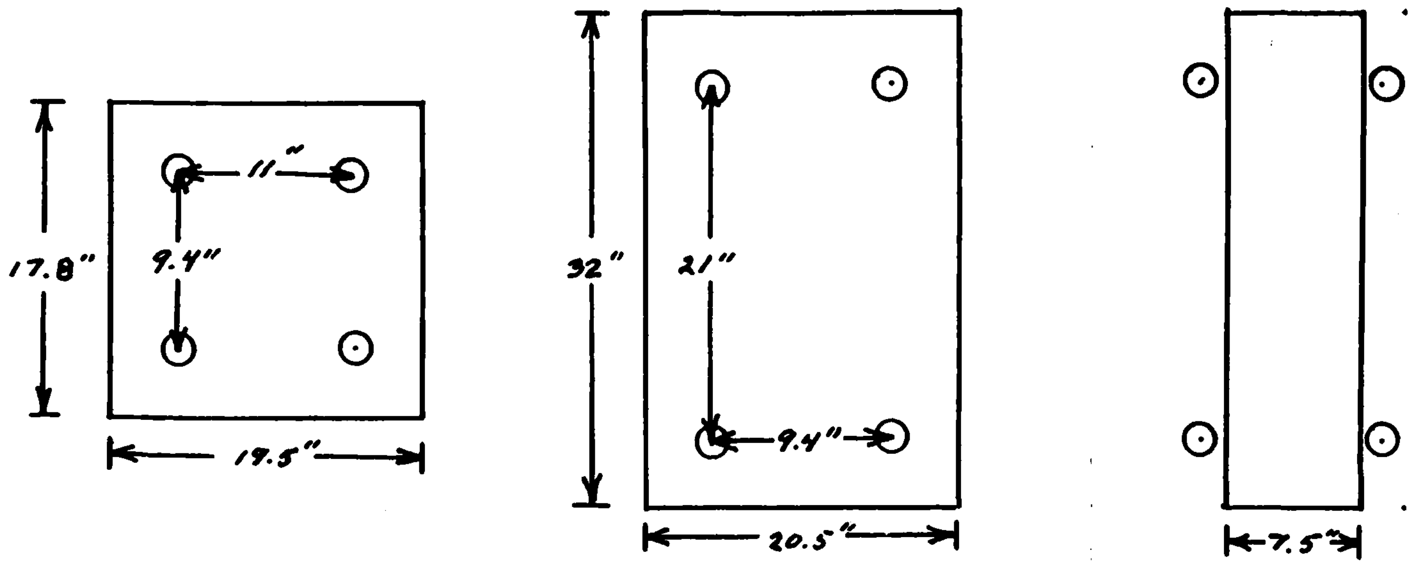

CONFIG. 13
+ LIDS
CONFIG. 2 (D=1.42"-ONR DATA)
NPR=2.0

CONFIG. 14
+ LIDS

CONFIG. 15
+ LIDS
+ CONTOUR

d = 1.61"

NPR = 1.5

Figure 2.1-7 4 Nozzle Planforms

$$d_{wa} = \sum_{i=1}^{N} (F_j\bar{D})_i / \sum_{i=1}^{N} (F_j)_i \qquad (2.1\text{-}9)$$

In other words, these geometric parameters now become thrust-weighted averages.

2.1.2.2 Two-Jet Fountain Lift

The test results from configurations 0, 10, and 22 (without LIDs) are used to begin the determination of the relationship between $\Delta L_f/F_j$ and $\bar{D}_{wa}/d_{wa}$. We begin by stating a priori that the fountain lift for a two-jet case is composed of two parts: $\Delta L_{FI}/F_j$ which is the lift obtained on a central, more or less rectangular, portion of the planform and $\Delta L_{FII}/F_j$ which is the lift obtained on the peripheral areas of a planform. As an example, in the case of a V/STOL with fuselage-mounted engines, the fuselage would comprise the central area and the exposed portion of the wing, the peripheral (see Section 3.1). However, inspection of these planforms shows that not only does $\bar{D}$ vary from configuration to configuration, but the planform area available to intersect the fountain also varies. In order to remove this second variable, the fountain buoyancies are normalized so that the data presented shows the fountain lift that would have been observed had the planforms in each case intersected the entire fountain. In this two-jet case, θ_1 is the angular section of each radial ground jet which after forming a fountain, intersects a given planform (See Figure 2.1-8)

$$\theta_1 = \tan^{-1}\left(\frac{W/2}{d_f + h}\right) \qquad (2.1\text{-}10)$$

Except for the point on a line connecting the two jets, the fountain does not impact normal to the planform. Therefore, to account for this, and again for purely geometric considerations, the fountain lift that a planform would experience if it intersected the entire planform is given by

$$\frac{\Delta L^1_{FI}}{F_j} = \left(\frac{\Delta L_F}{F_j}\right)_{TEST} \Big/ \int_0^1 \cos\theta\, d\theta = \left(\frac{\Delta L_F}{F_j}\right)_{TEST} \Big/ (\sin\theta_1)$$

(2.1-11)

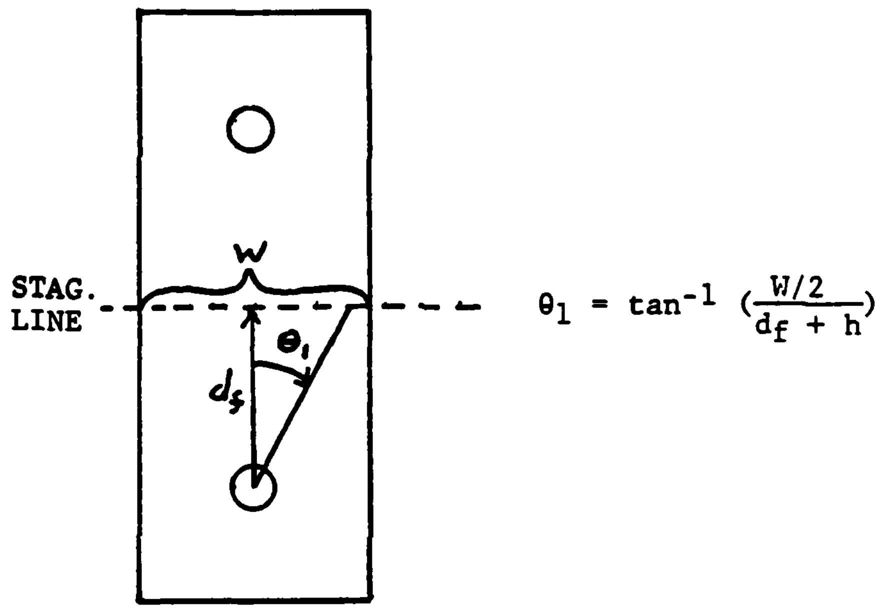

Figure 2.1-8 Portion of Fountain Which Intersects Central Planform

$\Delta L^1_{FI}/F_j$ is plotted vs $\bar{D}_{wa}/d_{wa}$ and h/d_{wa} on Figure 2.1-9, and the fountain lift on a given rectangular planform is obtained by

$$\frac{\Delta L_{FI}}{F_j} = \frac{\Delta L^1_{FI}}{F_j} \sin \theta_1 \qquad (2.1\text{-}12)$$

(A non-symmetrical planform is integrated by parts and then averaged (see Section 3.1).)

The calculation of the lift on the peripheral area, $\Delta L_{FII}/F_j$, proceeds in a similar manner (Figure 2.1-10) and

$$\frac{\Delta L_{FII}}{F_j} = \frac{\Delta L^1_{FII}}{F_j} (\sin \theta_2 - \sin \theta_1) \qquad (2.1\text{-}13)$$

where the sector $(\theta_2 - \theta_1)$ represents the portion of the fountain that intersects the peripheral planform. By comparison of the results of Configurations 1 and 21 with Configuration 10, $\Delta L^1_{FII}/F_j$ was obtained empirically. It is shown on Figure 2.1-11 as a function of h/d_{wa} and a/d_{wa}, where a is the average peripherial planform width normal to the fountain ground-plane stagnation line. Finally, the two-jet fountain lift is obtained by

$$\frac{\Delta L_F}{F_j} = \frac{\Delta L_{FI}}{F_j} + \frac{\Delta L_{FII}}{F_j} \qquad (2.1\text{-}14)$$

The calculation of fountain lift for three- and four-jet configurations is a much simpler matter since the concentrated fountain structure results in much less sensitivity to the planform area available for impact. As an example, Configuration 12, which has an extremely small planform area, was tested with different nozzle pressure ratios forward and aft in order to move the impact point of the fountain relative to the planform. As can be seen from Figure 2.1-12, it made relatively little difference to the net induced force; with a larger, more realistic planform, the differences would likely be even less. Therefore, a three- and four-jet fountain lift are simply functions of h/d_{wa} and $\bar{D}_{wa}/d_{wa}$ (Figures 2.1-13 and 2.1-14).

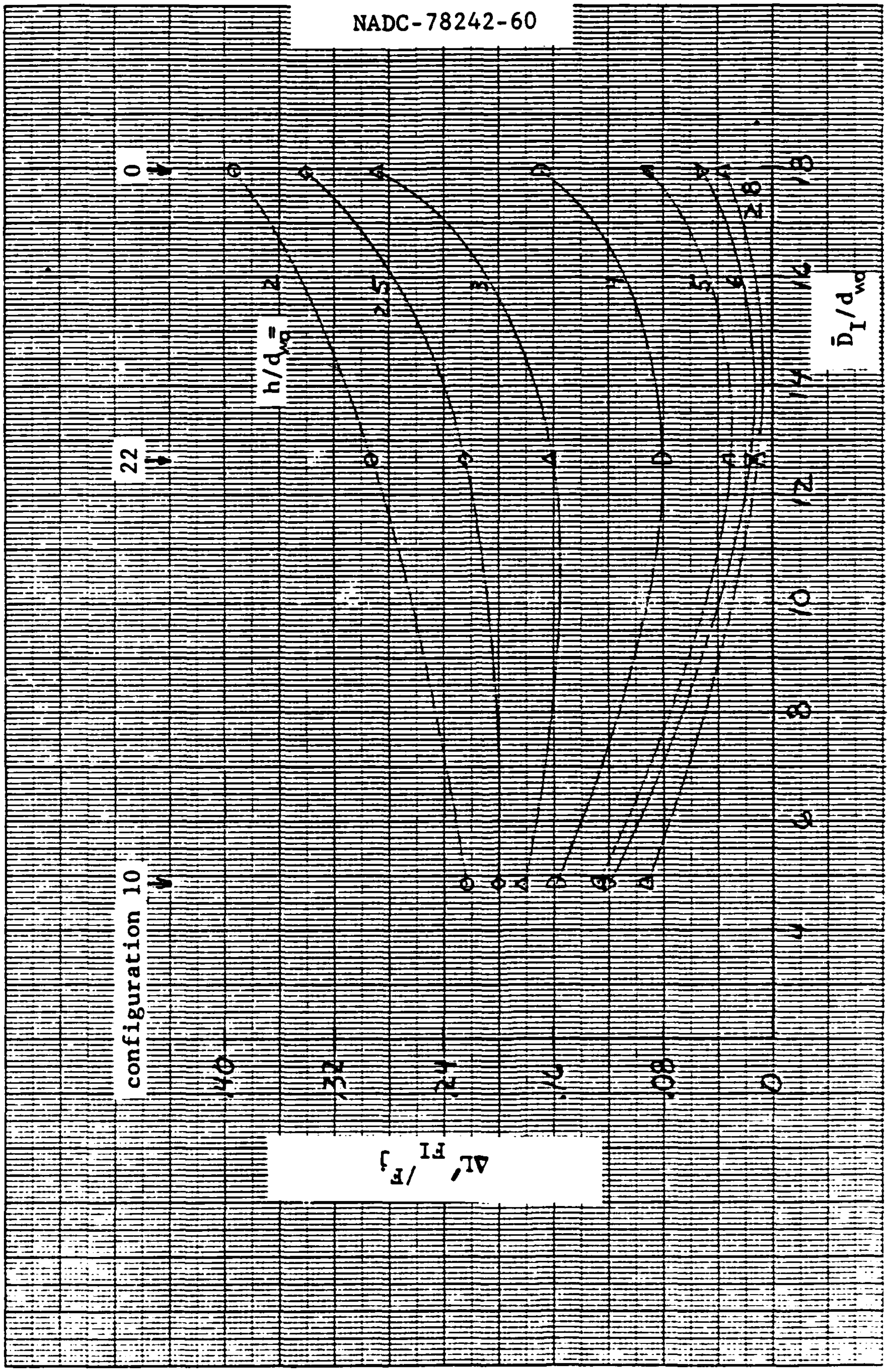

Figure 2.1-9 Fountain Lift, 2-Jet, Central Area

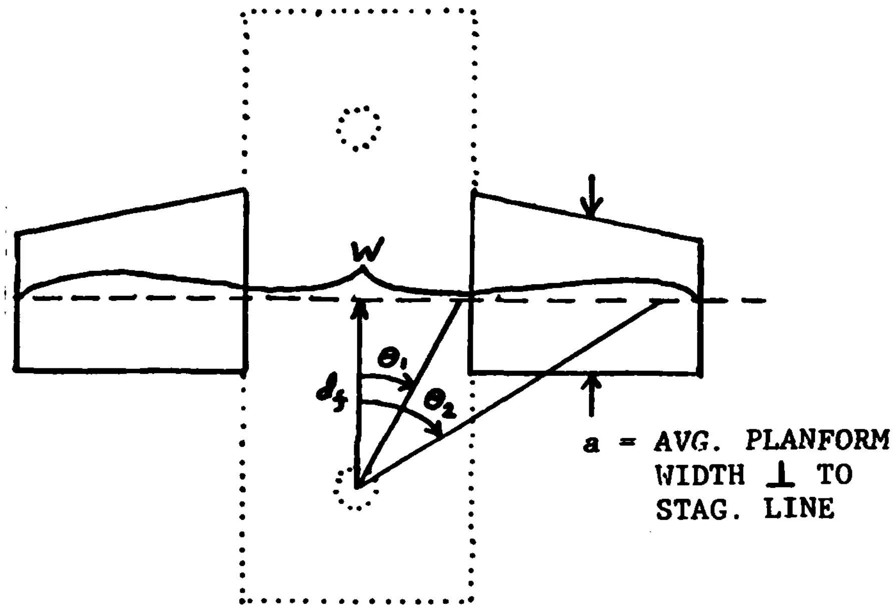

θ_1 FROM FIGURE 2.1-8

$$\theta_2 = \tan^{-1} \left(\frac{W/2}{d_f + h}\right)$$

Figure 2.1-10 Portion of Fountain Which Intersects Peripheral Planform

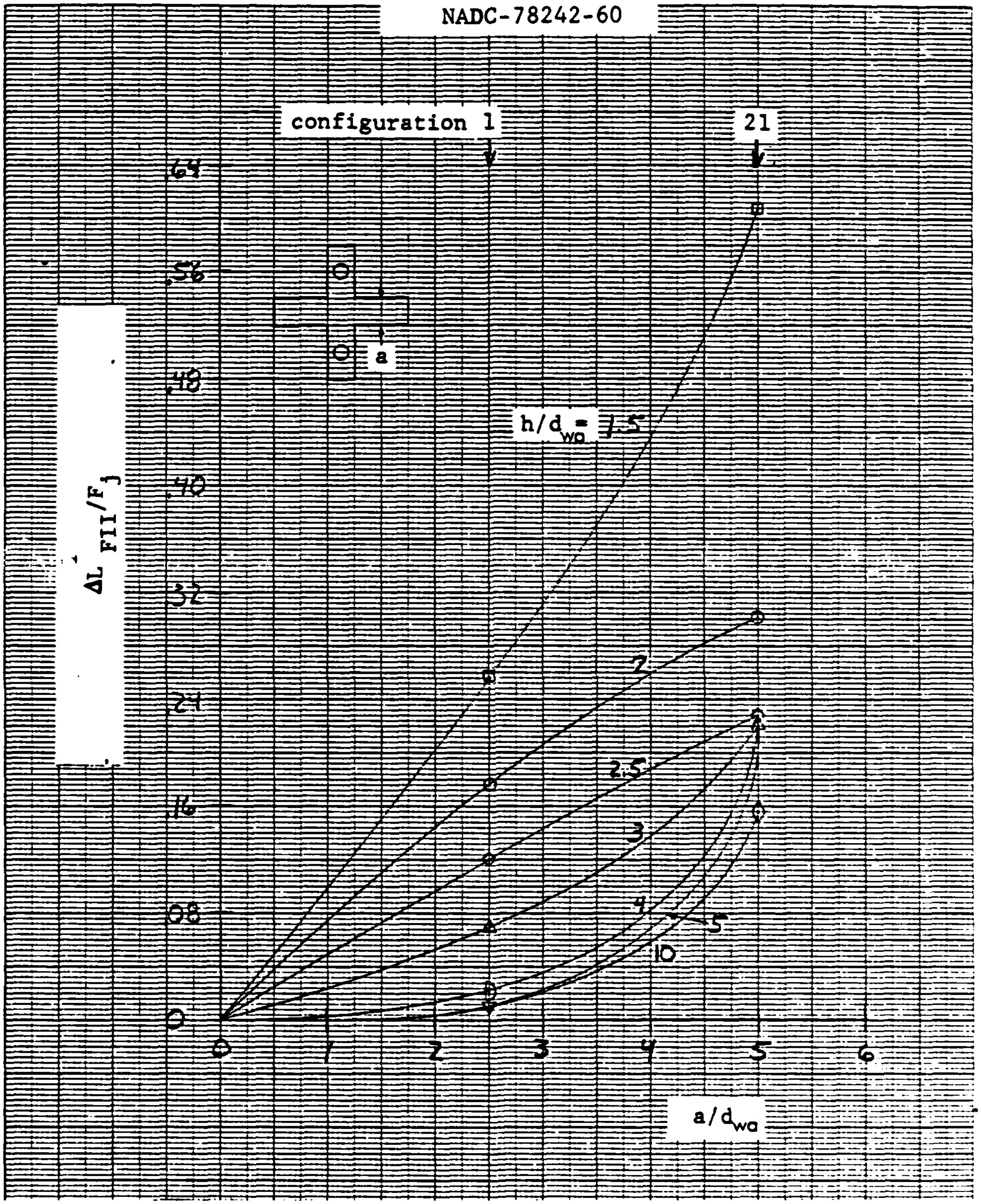

Figure 2.1-11 Fountain Lift, 2-Jet, Peripheral Area

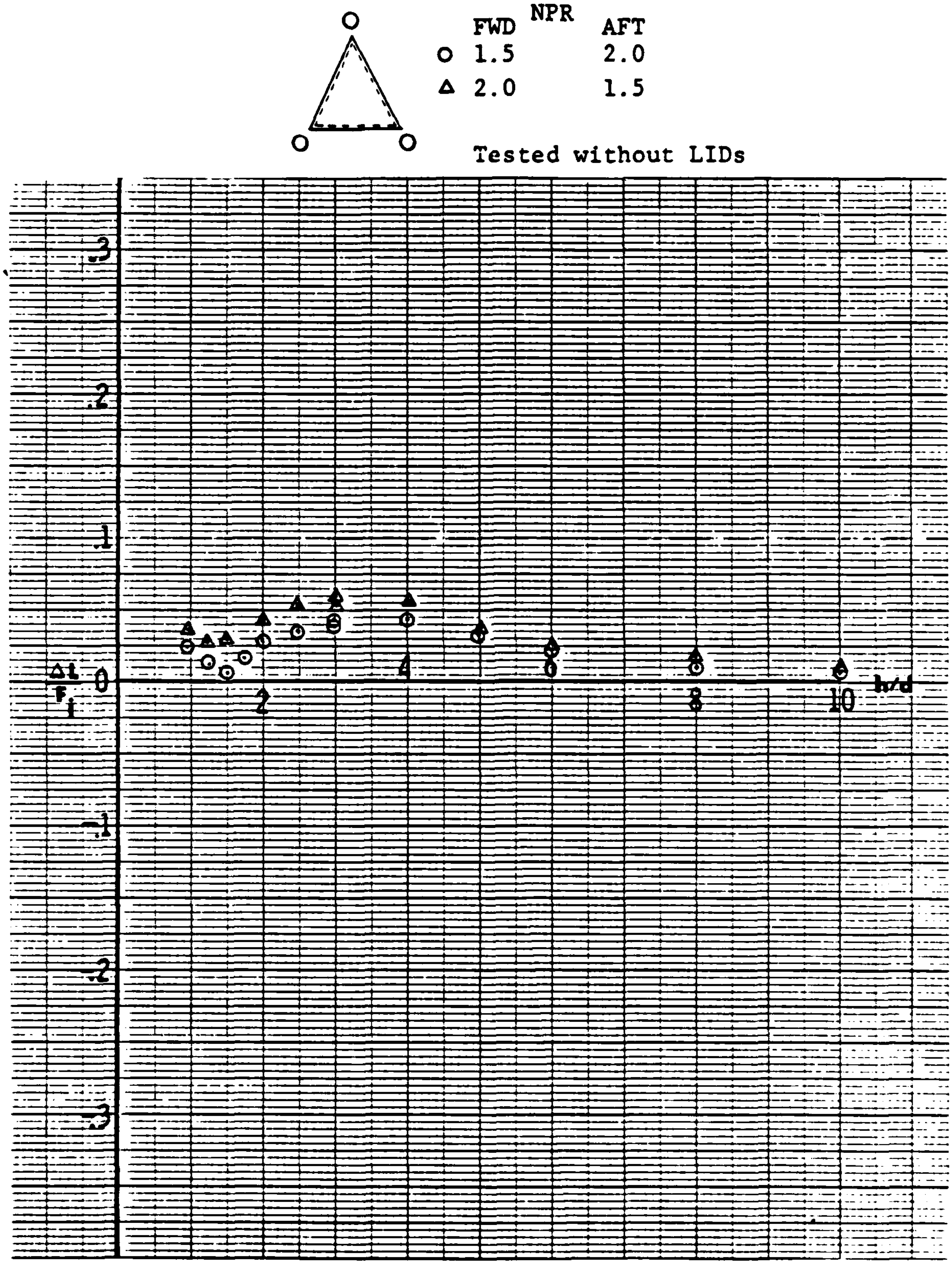

Figure 2.1-12 Configuration 12

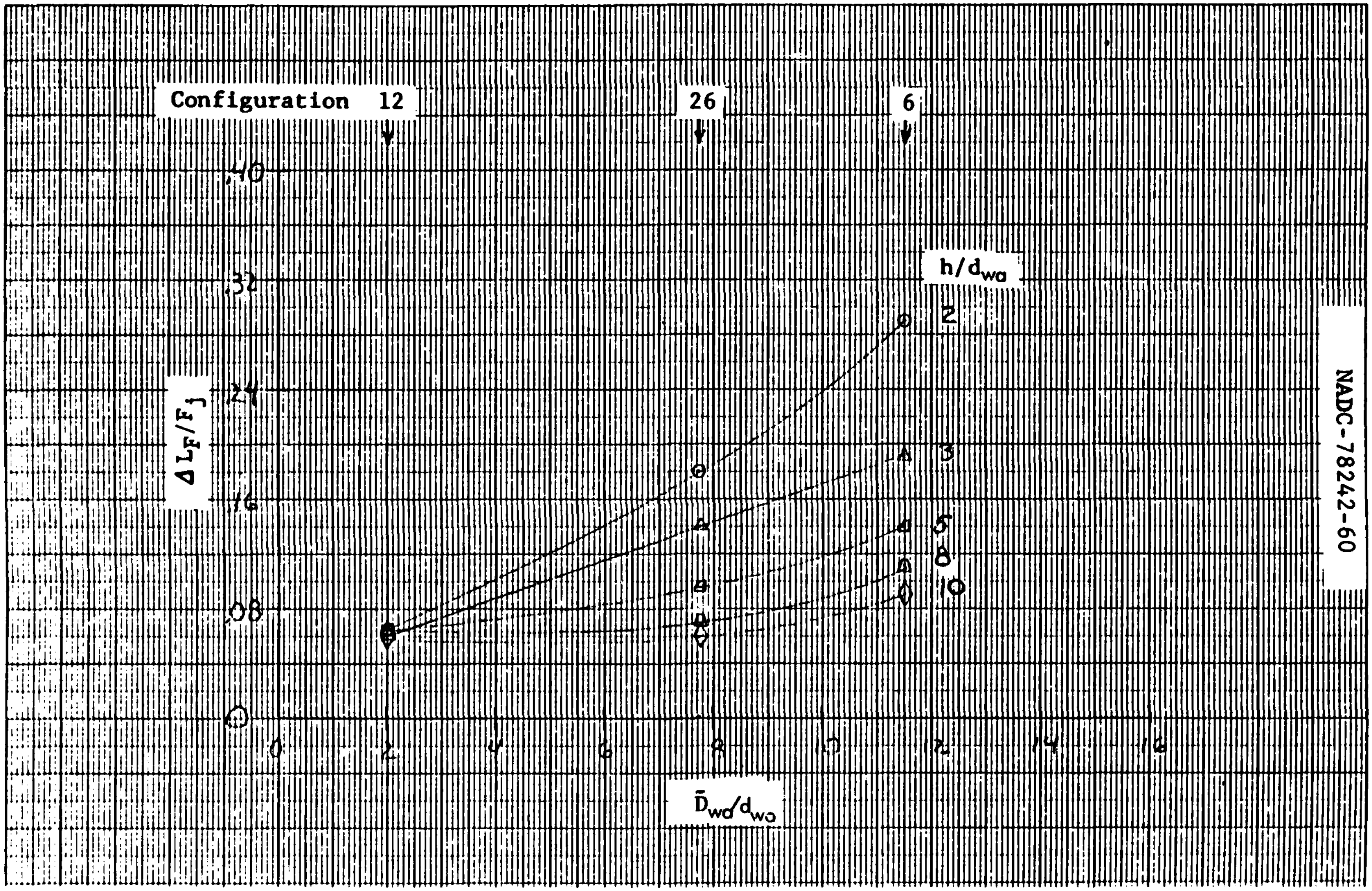

Figure 2.1-13 Fountain Lift - 3-Jet Configuration

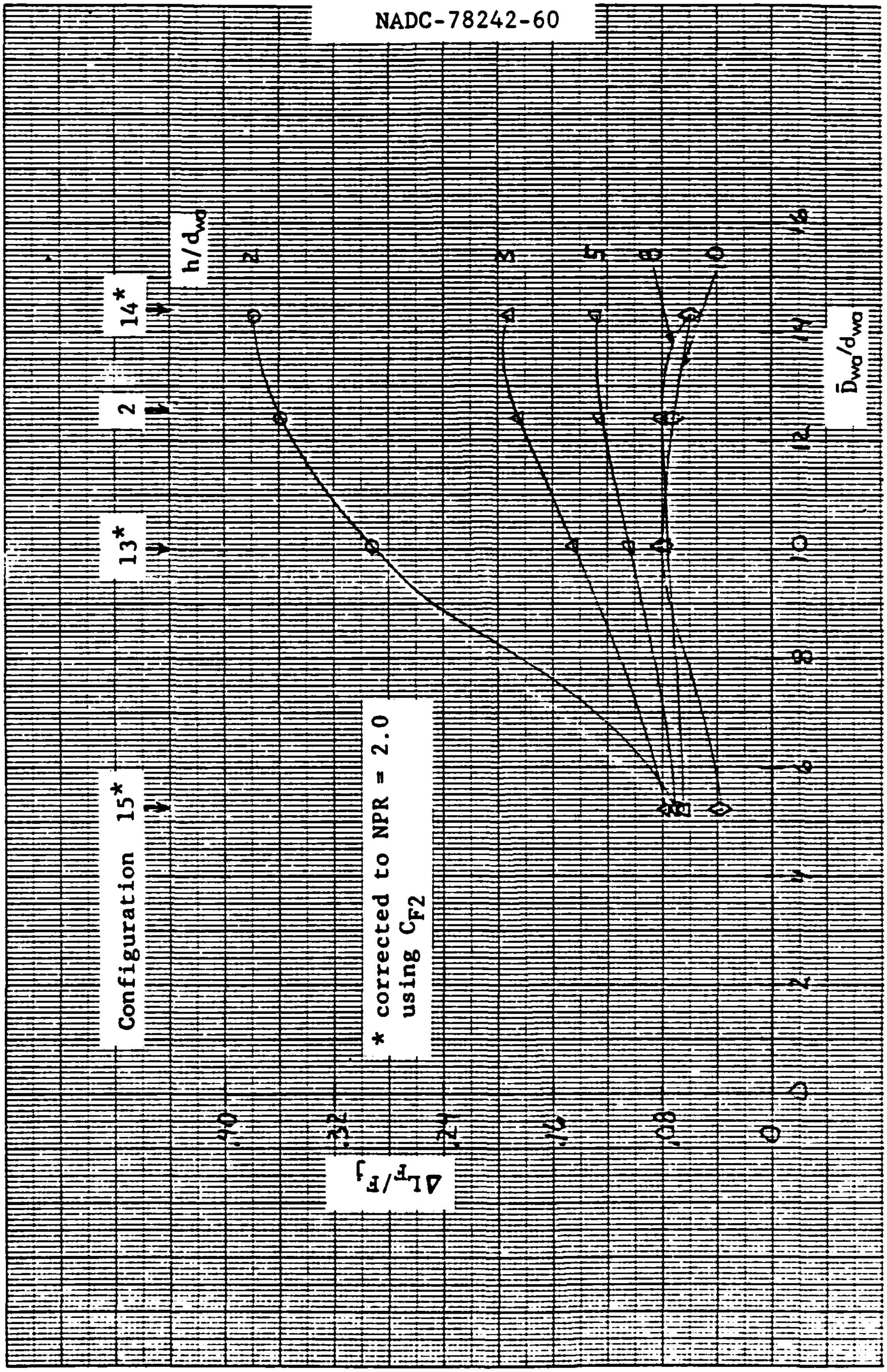

Figure 2.1-14 Fountain Lift - 4-Jet Configuration

2.1.3 Extrapolation Coefficients

Equation 2-2, as it stands, is useful only for calculating ground-induced forces on flat-plate models at low altitudes with nozzle exhaust NPR = 2.0. In order to extend the application of the methodology, a number of extrapolation coefficients are used to account for planform contour, NPR, etc., so that Equation 2-2 becomes

$$\frac{\Delta L}{F_j} = \frac{1}{F_j}\left[C_s\,\Delta L_s + C_F\,\Delta L_F\right] \tag{2.1-15}$$

2.1.3.1 Suckdown Extrapolation Coefficient C_s

Recent work on the effect of turbulence on suckdown (Ref. 11) has shown (1) the possibility of a large-scale effect and (2) a pronounced effect of NPR on suckdown. Therefore, let

$$C_s = C_{s1} \cdot C_{s2} \tag{2.1-16}$$

where C_{s1} is the extrapolation coefficient to account for the difference between model and full scale and C_{s2} for variations in NPR from 2.0.

As yet, there is not sufficient data available to quantify C_{s1} satisfactorily. It is being retained, however, against the time when it becomes available; in the meanwhile let

$$C_{s1} = 1.0 \tag{2.1-17}$$

The form C_{s2} has, however, been developed (Ref. 12) and is given by

$$C_{s2} \begin{array}{l} = 1.173-.2495 \ln (\text{NPR}) \text{ if NPR} \leq 2 \\ = 1.061-.0889 \ln (\text{NPR}) \text{ if NPR} \geq 2 \end{array} \tag{2.1-18}$$

2.1.3.2 Fountain Extrapolation Coefficient C_F

The fountain coefficient is a little more complex than the suckdown coefficient in that, not only are there terms to reflect scale and NPR, but also terms to account for the effects of jet merging before impact with the ground plane, planform contour, and LIDs. Therefore,

$$C_F = C_{F1} \cdot C_{F2} \cdots C_{F5} \tag{2.1-19}$$

where

C_{F1} is the effect of scale (interim value = 1.0)
C_{F2} is the effect of NPR
C_{F3} is the effect of jet merging
C_{F4} is the effect of planform contour
C_{F5} is the effect of LIDs.

For precisely the same reason that $C_{s1} = 1.0$, also $C_{F1} = 1.0$; it is reserved for use when the effect of scale becomes better known.

The effect of NPR on fountain lift has been extrapolated from Ref. 11 and is given by

$$C_{F2} = \begin{cases} .736 \ln \text{NPR} + .481 & \text{if NPR} \leq 2 \\ .035 \ln \text{NPR} + .930 & \text{if NPR} \geq 2 \end{cases} \tag{2.1-20}$$

In the case where NPR varies from nozzle to nozzle, the C_{F2}'s are thrust averaged and

$$C_{F2} = \sum_{i=1}^{N} (C_{F2}\, F_j)_i \Big/ \sum_{i=1}^{N} (F_j)_i \tag{2.1-21}$$

For any aircraft configuration with more than one nozzle, as altitude increases jets begin to merge so that the character of the fountains change. As an example, a three-jet configuration, as it gains altitude, will reach a point where two jets begin to merge (provided, of course, the nozzles are not equidistant apart). When this occurs, the character of the fountain will begin to change from that of a three-jet to that of a two-jet. At still higher altitude, when the two have completely merged, the fountain will become entirely a two-jet fountain. For many aircraft, such mergings can begin quite close to the ground.

The induced-lift data of the two-jet, subsonic V/STOL aircraft presented in Reference 13 was used to generate the dependence of C_{F3} upon altitude and nozzle spacing. When the suckdown and fountain lift were generated for this model ignoring jet merging, it was found that at low altitudes the correlation was good but that, as altitude increased above 1.374 d_E, the predicted fountain lift became optimistic. If the cause was due to jet merging the 1.374

d_E implies a spreading rate of 20 degrees, which is somewhat larger than the 10 to 15 degree range expected from free-jet tests. However, the presence of the stagnation zone next to the ground plane alters the spreading rate so that it was assumed merging was the cause. Thus, for the purpose of evaluating the effect of merging upon fountain strength,

$$h_m = 1.374\ d_E \tag{2.1-22}$$

was used. C_{F3} was then obtained by correcting the predicted fountain lift for the two-jet Reference 13 hence to agree with the data. The use of C_{F3}, shown on Figure 2.1-15, was further confirmed by successfully applying it to several multi-jet configurations as shown in Section 4.

The cross-sectional shape or contour of a planform has a very strong influence on the amount of available fountain lift that is actually recovered by the planform. In the case where the edges of the planform are rounded, the fountain, after impingement, will then tend to flow, Coanda-style, around the planform (Figure 2.1-16). The negative pressures, which are induced upon the planform and attend this turning, lower the lift. Herein, C_{F4} is used to reflect the lift loss due to contour and is dependent upon the type of fountain. For two-jet fountains, C_{F4} is shown on Figure 2.1-17 and was determined from the results obtained from contouring the planform of Configuration 1 and the results extrapolated from Ref. 14. Interestingly, C_{F4}, for two-jet fountains, is not a function of altitude but is very strongly dependent on contour. C_{F4} for three- and four-jet fountains was obtained from testing contours on Configuration 15 and is shown in Figure 2.1-18. Here, C_{F4} is a function of altitude but is not as sensitive to the contour as is the two-jet case. Undoubtedly, the difference is due to the different fountain structure.

Most of the configurations were tested with and without LIDs. By reversing the direction of the fountain flow (Figure 2.1-19), an LID is able to amplify the fountain lift. It can be seen from Figure 2.1-20 that, in many cases, the effect of a complete longitudinal and transverse LID system (i.e., the LIDs form a closed box) is to double the fountain lift; whereas, if the LIDs are left open on two ends, the lift increases by only 50%. The test series also indicated some other characteristics:

1. Except at very low altitudes, the depth of the LIDs is not particularly important (Figures 2.1-21 and 2.1-22).

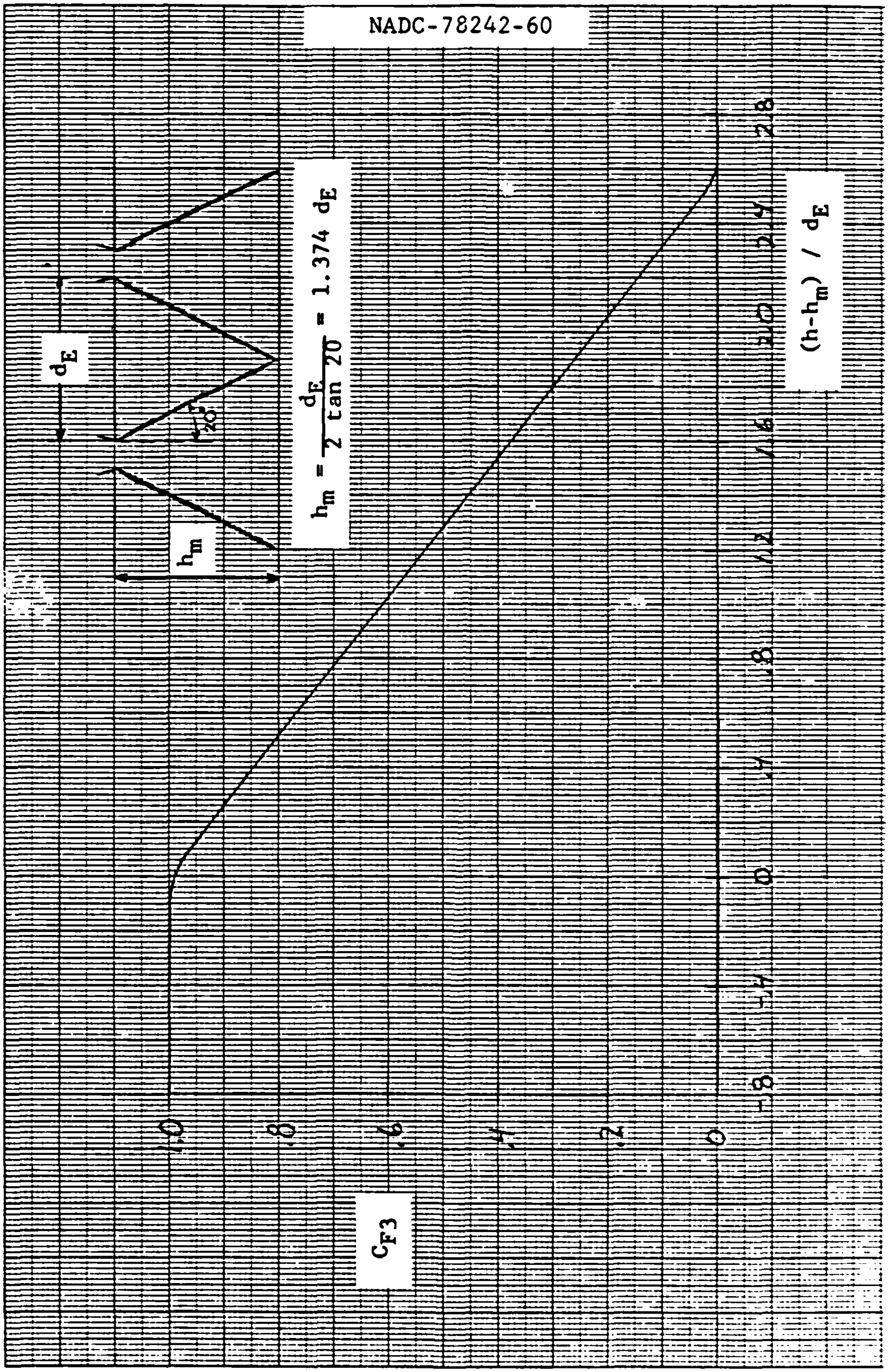

Figure 2.1-15 Effect of Jet Merging On Fountain Lift

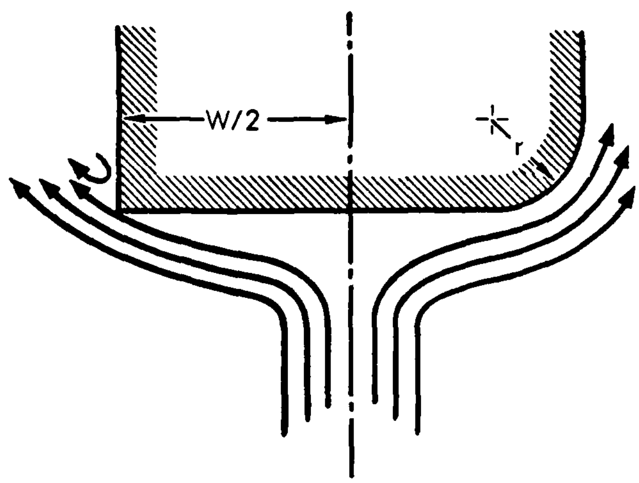

Figure 2.1-16 Fountain/Semi-Rounded Fuselages

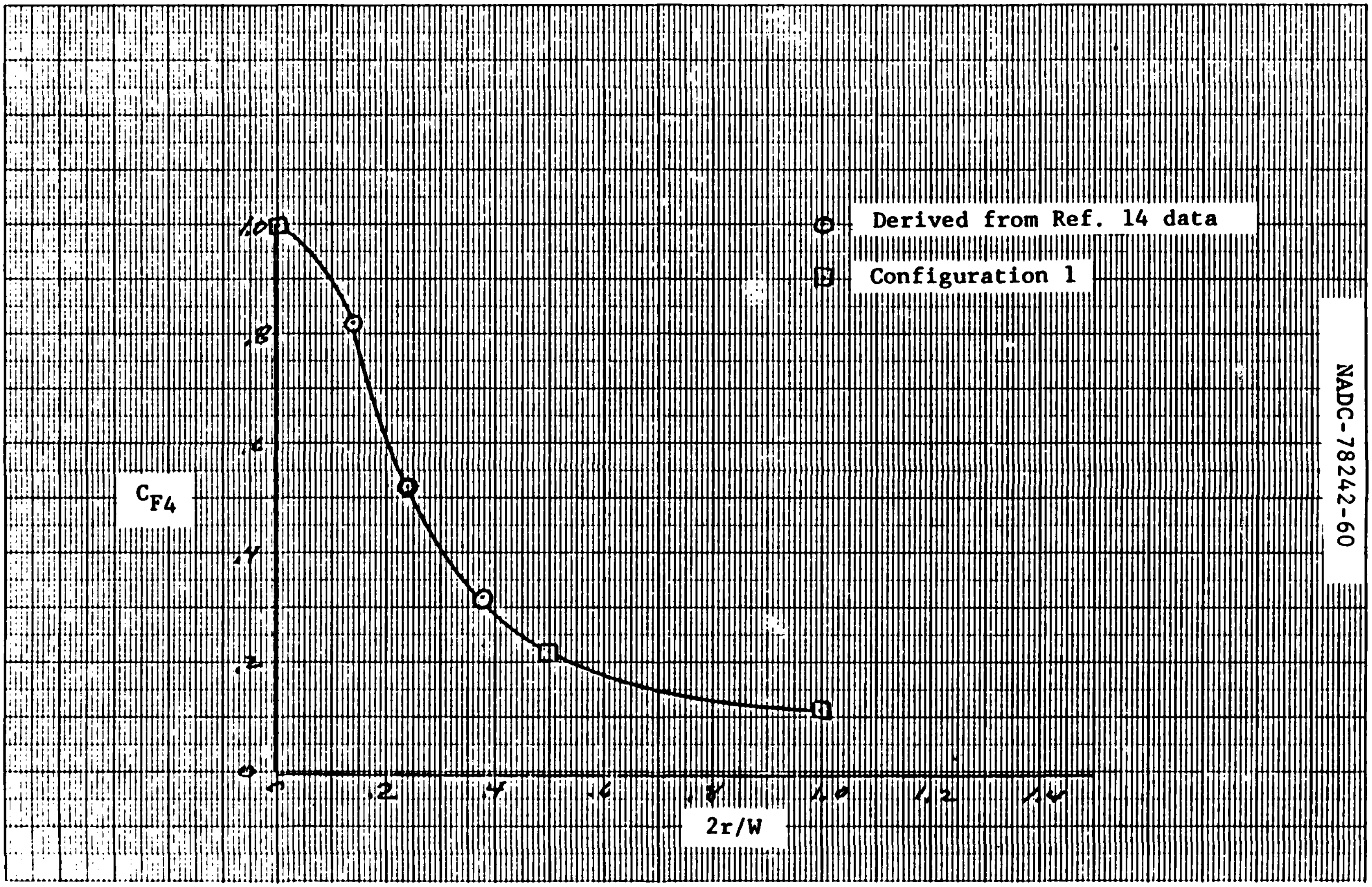

Figure 2.1-17 Effect of Planform Contour - 2 Nozzle Case

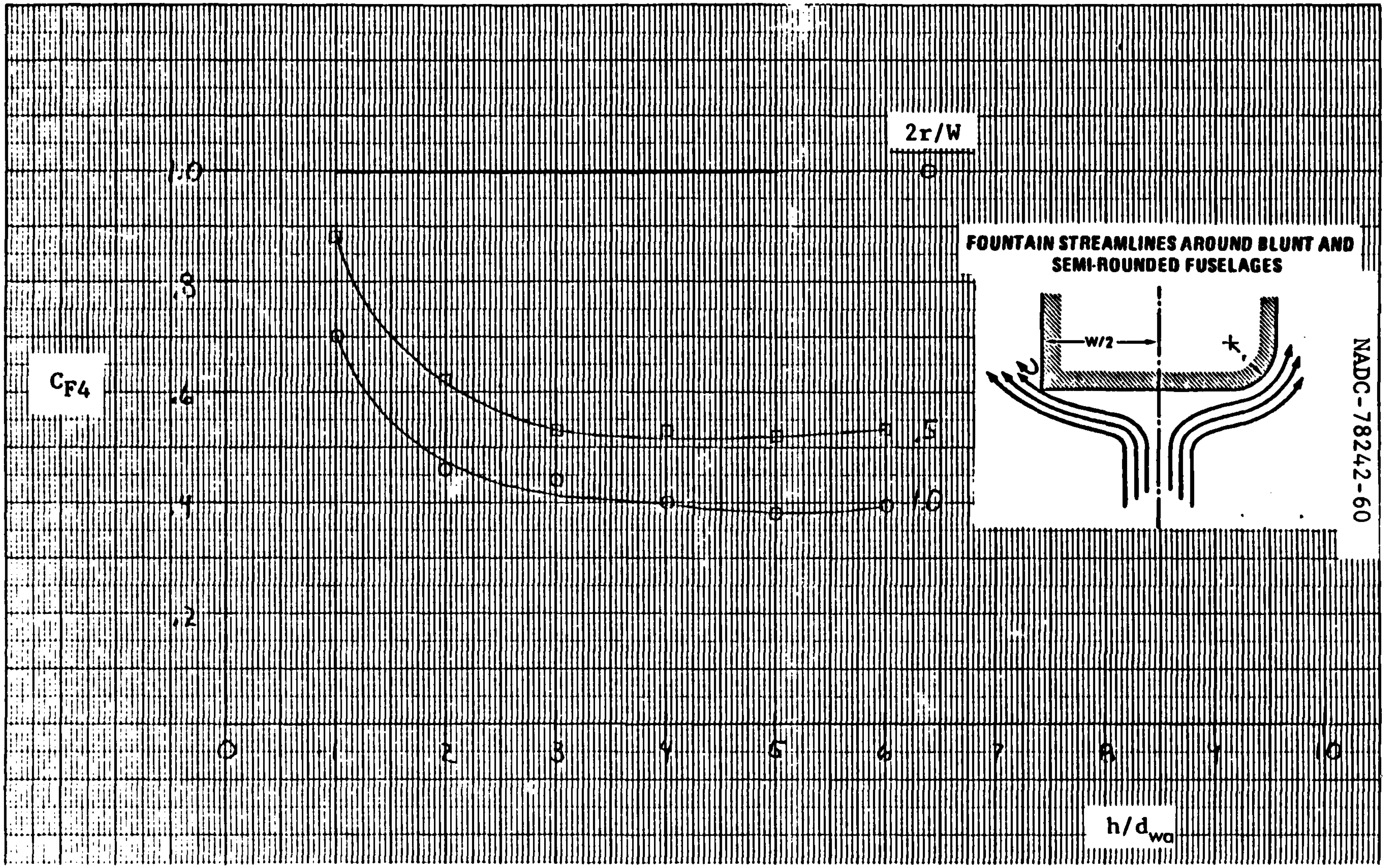

Figure 2.1-18 Effect of Planform Contour - 3 and 4 Nozzle Case

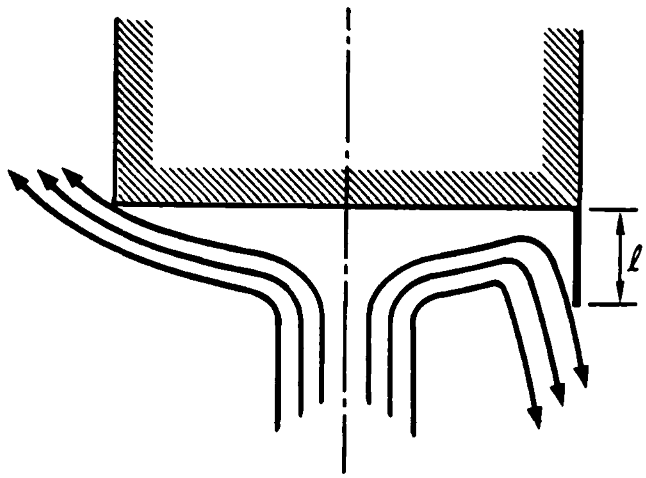

Figure 2.1-19 Fountain Streamlines Around A Blunt Fuselage and A LID

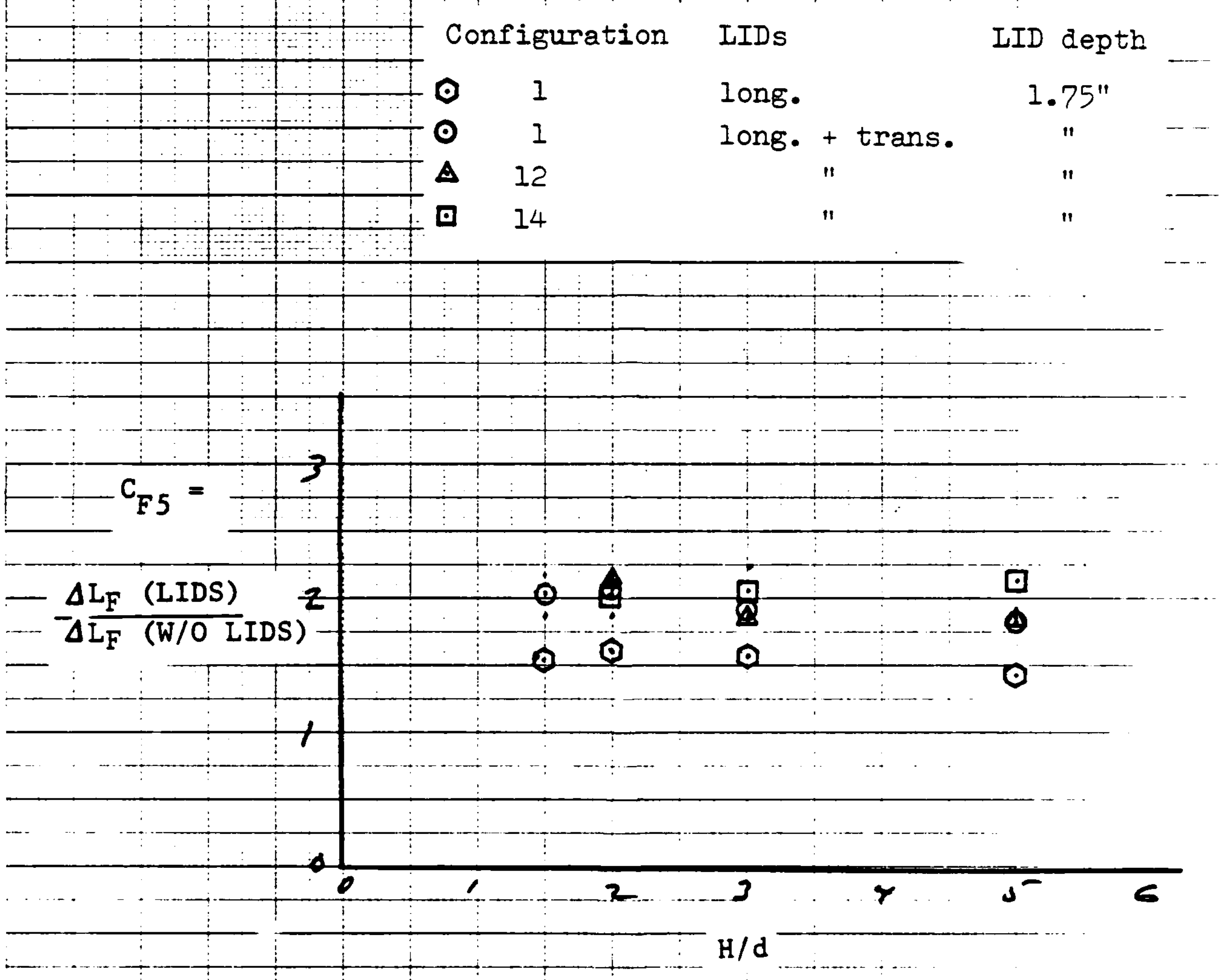

Figure 2.1-20 The Effect of LIDs On Fountain Lift

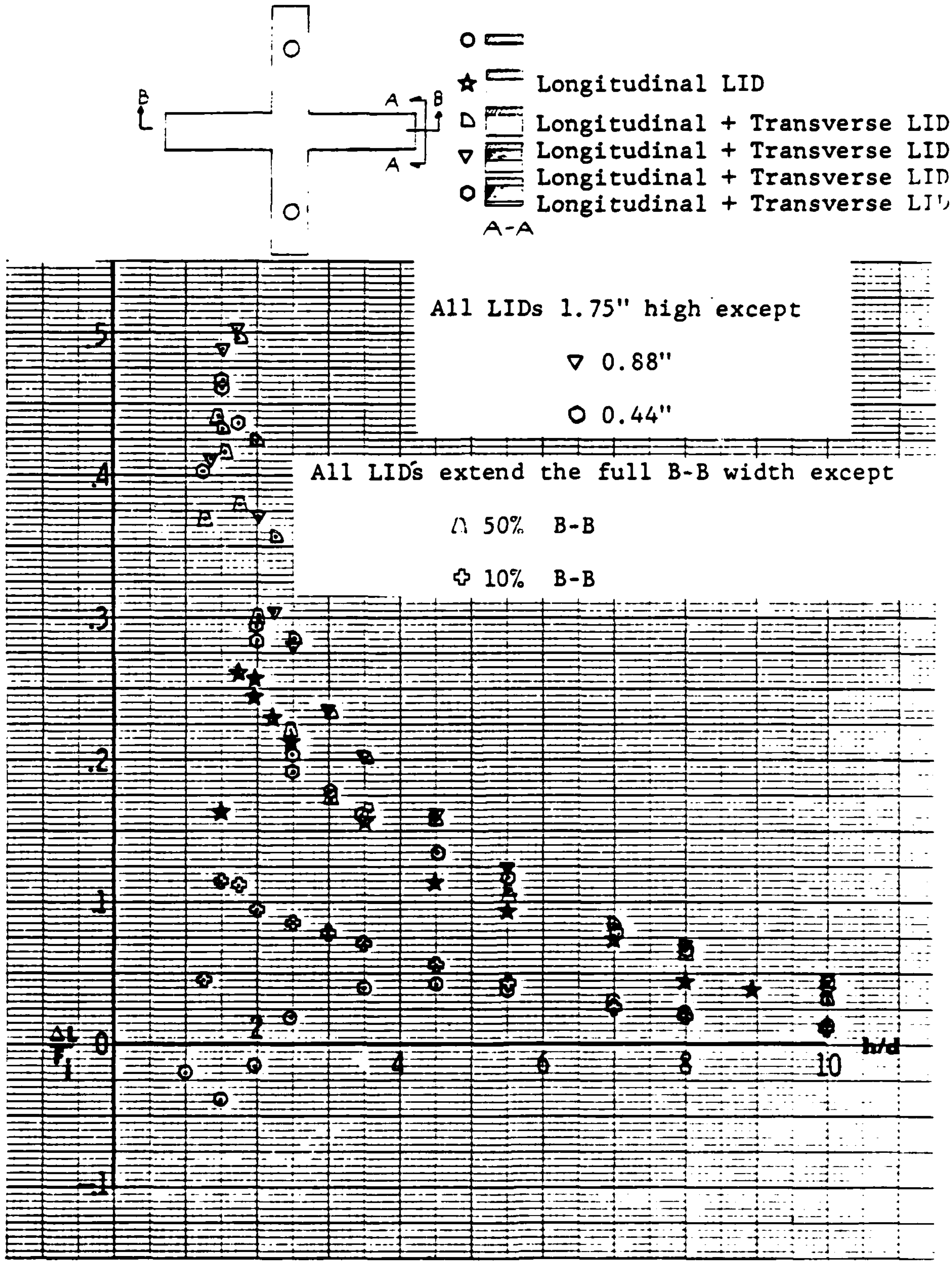

Figure 2.1-21 Configuration 1

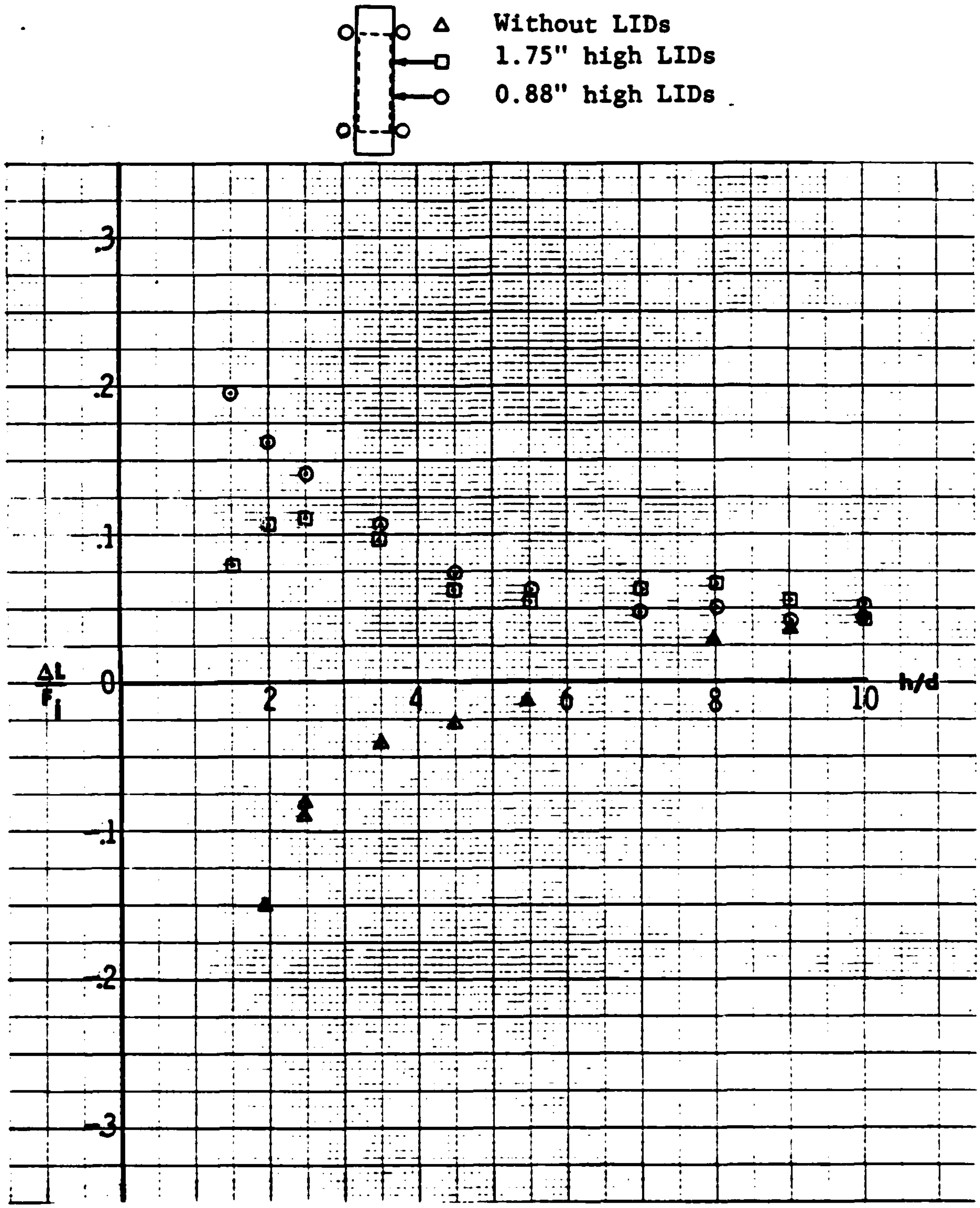

Figure 2.1-22 Configuration 15

2. LIDs should always be placed interior to the nozzles; excessively large LIDs, at low altitudes, interfere with the entrainment of ambient air to such an extent that suckdown is amplified over and above the beneficial effect of fountain lift enhancement (Figure 2.1-23).

3. In the instance where LIDs do not cover the entire planform periphery, that portion of the fountain whose lift is enhanced can be determined from geometrical considerations (see Figure 2.1-24 and Subsection 3.1).

In general, the size, shape, and extent of a LID system will be restricted by other considerations in aircraft design. Therefore, the values of C_{F5}, presented in Subsection 3.1, should be regarded as probably optimistic indicators of what can be achieved in practice.

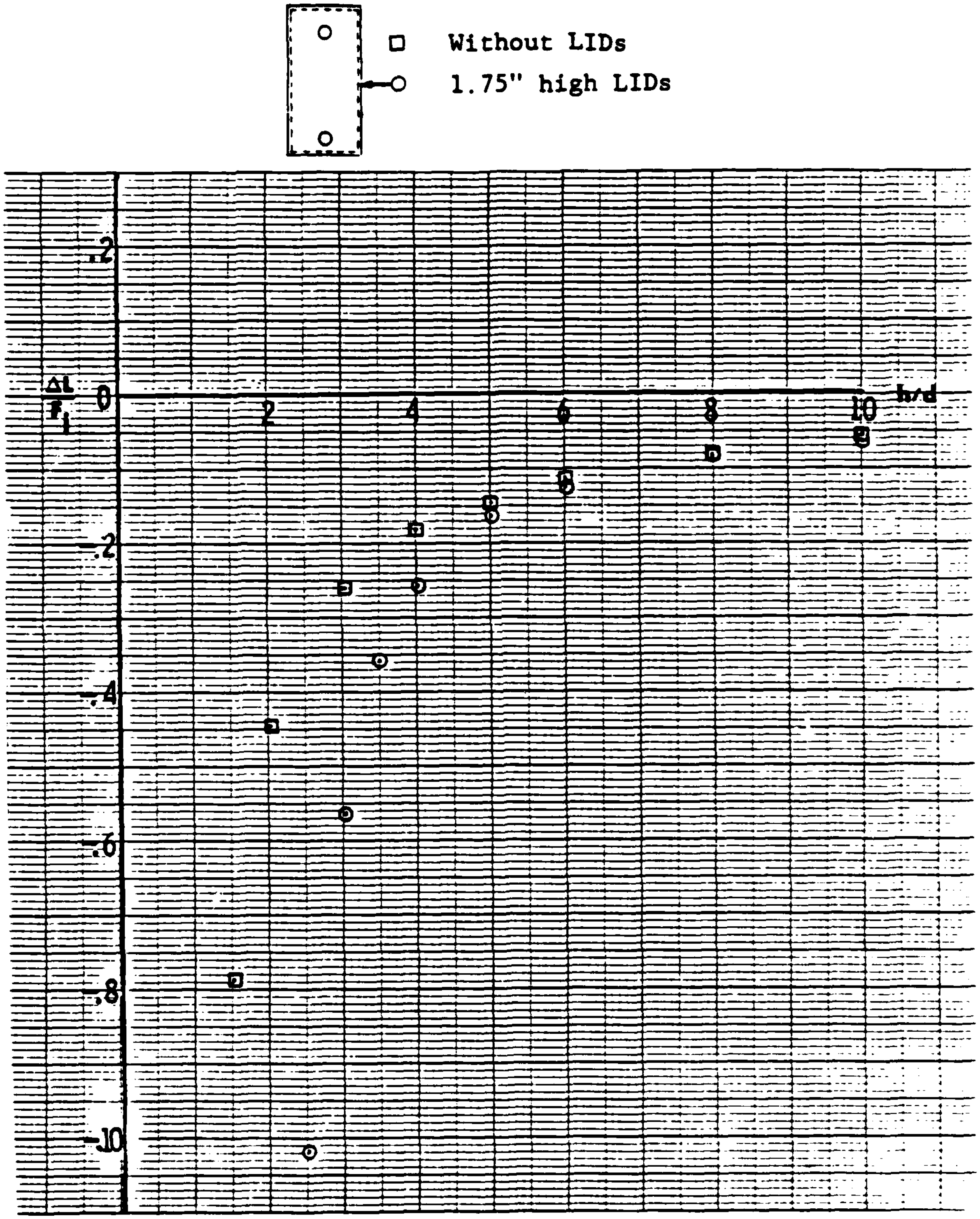

Figure 2.1-23 Configuration 22

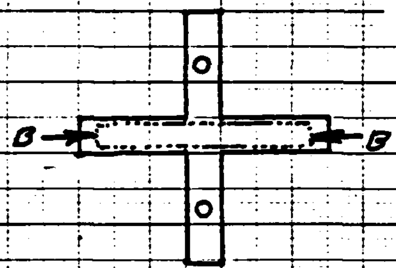

CONFIGURATION 1

LID WIDTH = 55% OF B-B: ○ $\sin\theta_{2A}/\sin\theta_2$; ○ with flag: C_{F5} ALT./C_{F5} IDEAL

LID WIDTH = 10% OF B-B: △ $\sin\theta_{2A}/\sin\theta_2$; △ with flag: C_{F5} ALT./C_{F5} IDEAL

$\frac{\sin\theta_{2A}}{\sin\theta_2}$ OR $\frac{C_{F5_{ACTUAL}}}{C_{F5_{IDEAL}}}$

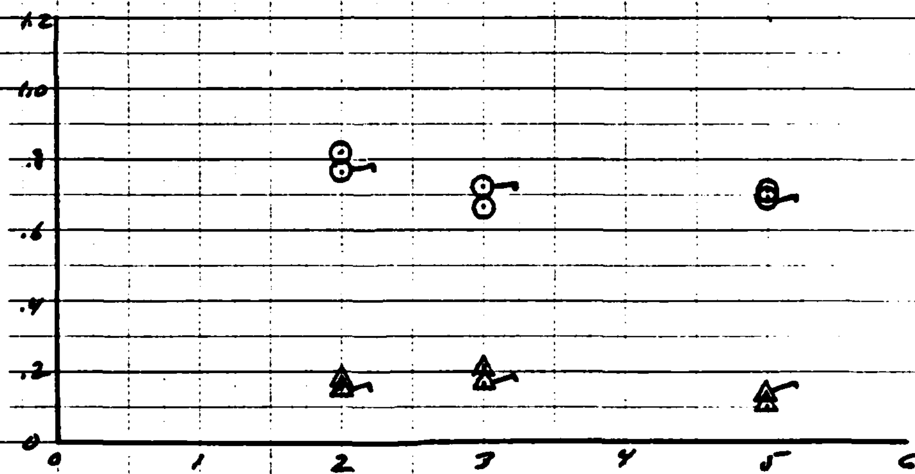

H/d

Figure 2.1-24 Effect of LID Length On C_{F5}

3. INTRODUCTION TO METHODOLOGY

The General Dynamics input into the V/STOL Ground Effects Handbook has been assembled as a reference document to serve as an aid in predicting induced lift of V/STOL aircraft in hover. The various correlations are derived from empirical methods and are intended to cover the hover flight conditions of current V/STOL aircraft. The methodology has been developed as a prediction technique in the preliminary design environment and is considered accurate to ±1% of the total lift. This section covers the effects of various nozzle and planform configurations, up to four nozzles.

3.1 METHODOLOGY

3.1.1 Induced Lift, $\Delta L/F_j$

The induced lift during hover can be separated into two parts, as shown in Equation (3.1-1).

$$\Delta L/F_j = \Delta L_s/F_j + \Delta L_F/F_j \tag{3.1-1}$$

The first, $\Delta L_s/F_j$, is the suckdown generated by the ambient air that is accelerated toward the aircraft because of entrainment by the exhaust flows, creating a low pressure field under the aircraft and, consequently, a downward force on the planform. The second effect, $\Delta L_F/F_j$, is the buoyant force derived from the impact (if any) of the fountain jet formed by a multiple-nozzle configuration upon the planform.

The basic fountain strength is determined for a two-dimensional flat plate planform which is then corrected for the effects of planform contour and Lift Improvement Devices (LIDs), if necessary.

3.1.2 Tabulation

The various components of induced lift are tabulated in Figure 3.1-1. The four main blocks of the table are

I. Suckdown

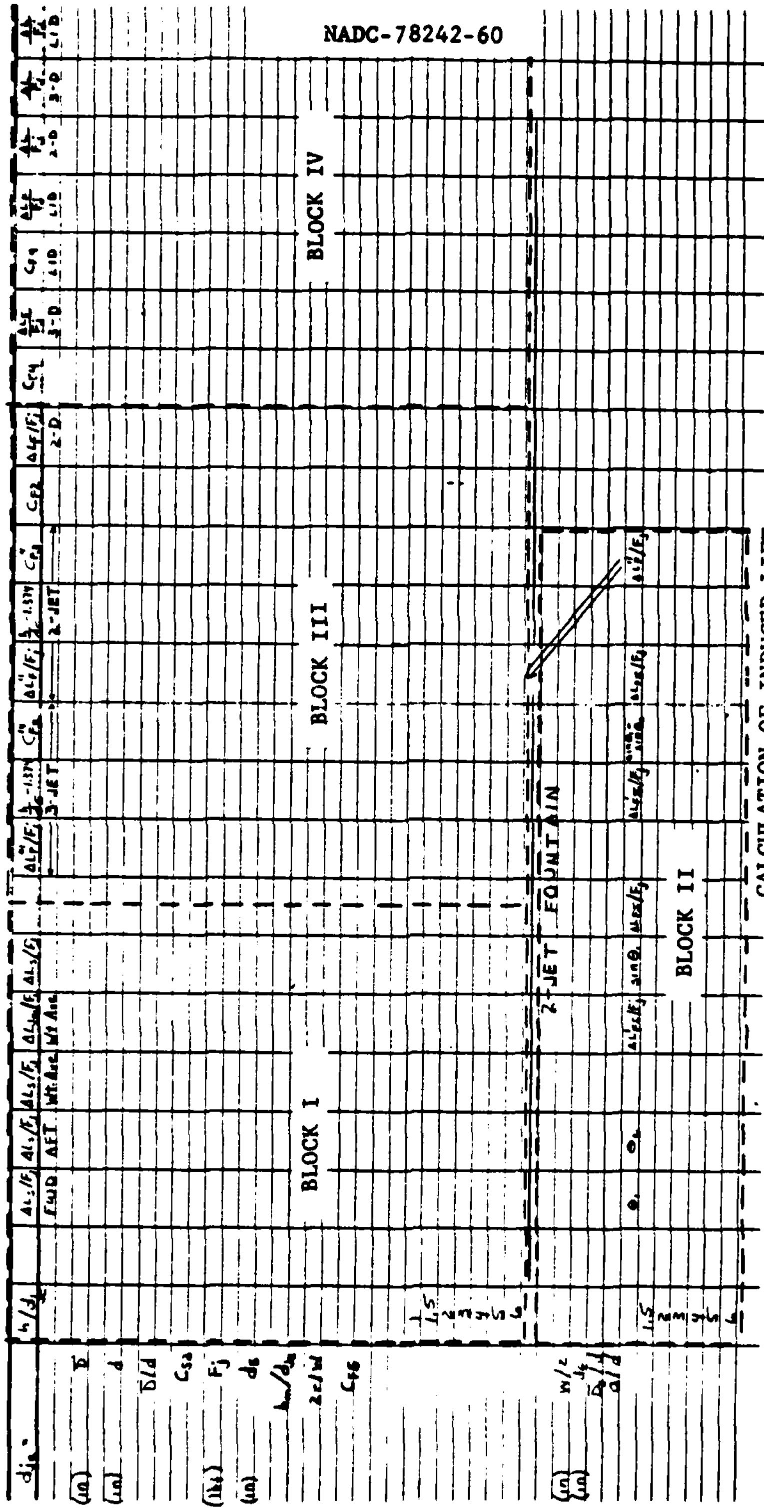

FIGURE 3.1-1
CALCULATION OF INDUCED LIFT

II. 2-Jet Fountain

III. Fountain Lift

IV. Contour and LID effects.

The general arrangement of the table should follow a vertical setup for computing each column as a function of planform height above the ground. This may be done in various ways. As depicted in the example table, a common reference height is listed in nozzle diameters. Because many configurations have multiple nozzles (that are not always equal in diameter), the approach used here is to normalize altitude by equivalent single nozzle diameter, d_{je}. However, there are two additional normalizing diameters that are used in the methodology, namely, the individual nozzle diameter, d, (used in suckdown calculations) and the thrust weighted diameter, d_{wa}, (Subsection 3.1.3, used in fountain lift calculations). It is necessary to use extreme care in setting up a tabulation sheet to reflect the equivalencies between the various altitude normalizations.

A listing of the necessary variables of the problem should be placed on the table for quick reference. The authors have listed those items of primary need on the example table, though more could be added depending on the specific configuration under study.

The first block is rather straightforward and similar in most configurations. The suckdown will be calculated individually for each nozzle along with the free-air suckdown, $\Delta L_{s\infty}/F_j$. Both Blocks II and III set up methods for calculating fountain lift. Block II accounts for the effects of a two-jet fountain. This section is separated from Block III because of the inherent differences in the method for computing the two-jet fountain strength. Block III will be the most difficult to set up since a four-jet configuration can produce the fountain characteristics of a three-jet or two-jet configuration when the planform reaches a height of jet-merging for nozzles that are in close proximity. Therefore, Block III will normally be set up for more than one fountain computation, since the jets can ultimately merge to form a two-jet fountain that must be calculated in Block II. Block IV accounts for the differences in induced lift from the two-dimensional, clean planform. Here, the effects of planform contour and LIDs are incorporated into the basic fountain effects.

The introduction of a high-wing aircraft or other non-coplanar configuration presents additional difficulties in the computation of induced lift on a hovering V/STOL aircraft. Figure 3.1-2, depicts such a planform at two altitudes above the ground - one measured to wing height (h_w) and a different height to fuselage base (h_f). The method of computation for both nozzle suckdown ($\Delta L_S/F_j$) and fountain lift ($\Delta L_F/F_j$) is affected by this type of configuration. This causes the problem tabulation to be expanded to a two-phase setup, whereby, the calculations for fuselage suckdown and fountain lift use h_f whereas the wing planform uses h_w for its computations of suckdown and fountain lift. These values of suckdown and fountain lift can then be summed; due care must be exercised in the summations to reference the induced forces at the correct planform altitude being used in the tabulation.

3.1.3 Suckdown

The equations, parameters, and methods for computing nozzle suckdown are described below:

<u>Equations</u>

$$\left[\frac{\Delta L_S - \Delta L_{S\infty}}{F_j}\right]_i = -\left[A\left(\frac{\bar{D}_i}{d_i}\right) + B\right] C_{S_i} \left[\frac{h}{\bar{D}_i - d_i}\right]^C \qquad (3.1\text{-}2)$$

where for a rectangular planform

A = 0.00125
B = 0.0185
C = -1.59

and for a triangular planform

A = 0.0072
B = -0.0166
C = -1.28

and

i = nozzle of interest

$$\left[\frac{\Delta L_{S\infty}}{F_j}\right]_i = 0.0667\left(\frac{d_i}{\bar{D}_i} - 0.420\right) \qquad (3.1\text{-}3)$$

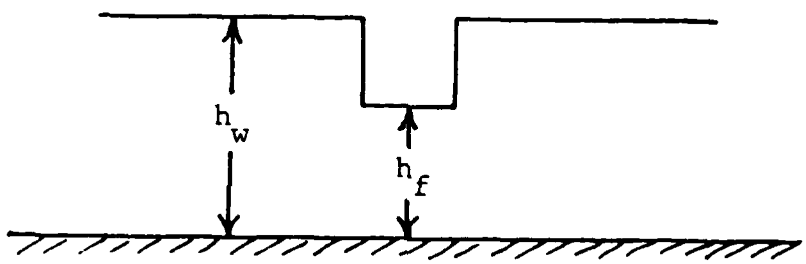

Figure 3.1-2 Non-Coplanar Planform

Parameters

d_i nozzle diameter of ith nozzle

d_{je} equivalent single nozzle diameter, $= \left[\sum_{i=1}^{n} d_i^{\,2} \right]^{\frac{1}{2}}$

d_{wa} average nozzle diameter of n nozzles,

$$= \left[\sum_{i=1}^{n} d_i (F_j)_i \right] / \left[\sum_{i=1}^{n} (F_j)_i \right]$$

$\bar{D}_i$ effective mean diameter,

$$= \left[\frac{2}{\pi} \sum_{K=1}^{m} \frac{s_k}{r_k} \right] - d_i - \frac{\pi}{4} \sum_{i=2}^{n} \frac{d_i^{\,2}}{r_i}$$

where

1. The incremental area and its associated radius from the nozzle are s_k and r_k, respectively (see Figure 3.1-3).
2. The individual nozzle diameter (second term) need only be subtracted if d_i falls on the planform.
3. Subsequent effective nozzle diameters (third term) need only be subtracted if they fail on the planform.
4. The entire planform is covered by m elements.

$\bar{D}_{wa}$ thrust weighted average of effective mean diameters,

$$= \left[\sum_{i=1}^{n} \bar{D}_i (F_j)_i \right] / \left[\sum_{i=1}^{n} (F_j)_i \right]$$

Suckdown Extrapolation Coefficient

$$C_s = C_{s1} \cdot C_{s2} \qquad (3.1\text{-}4)$$

where

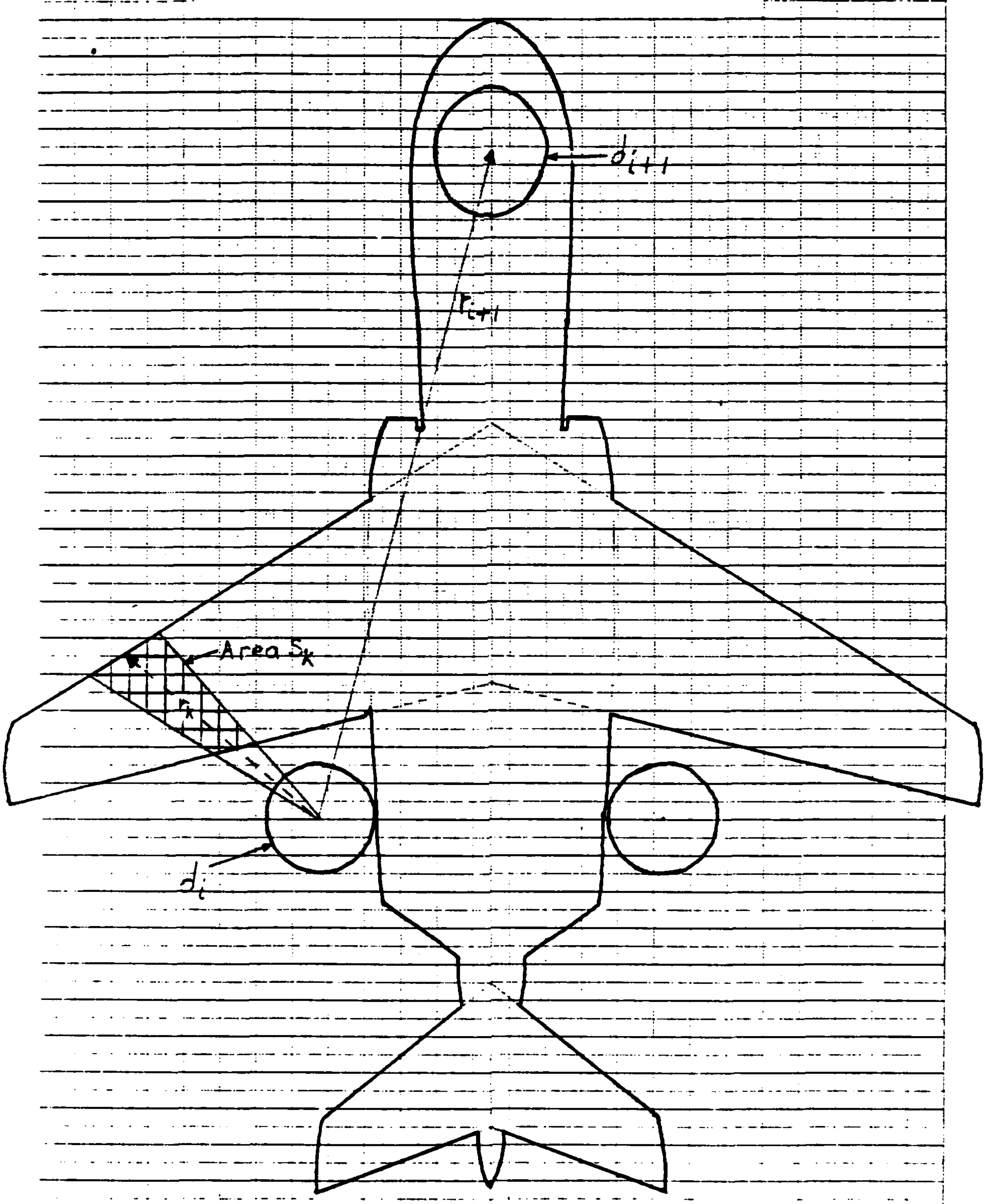

Figure 3.1-3 Calculation of $\bar{D}_i$

C_{S1} = 1.0, reserved for scale effects

C_{S2} = effect of nozzle pressure ratio

$$= 1.173 - 0.2495 \ln(NPR), \quad NPR \leq 2.0 \tag{3.1-5a}$$

$$= 1.061 - .0889 \ln(NPR), \quad NPR \geq 2.0 \tag{3.1-5b}$$

(C_{S2} can be obtained graphically from Figure 3.1-4)

The suckdown associated with each nozzle of the aircraft is calculated from Equation 3.1-2 and then listed in Block I of the tabulation. Because of its small magnitude, the free-air suckdown of the aircraft can be calculated from Equation 3.1-3 for each individual nozzle from $d_i/\bar{D}_i$ or for the total aircraft from $d_{wa}/\bar{D}_{wa}$. The total suckdown of the aircraft is then the sum of the thrust-weighted average of individual nozzle suckdown and free-air suckdown, i.e.,

$$\Delta L_s/F_j = \left[(\Delta L_s - \Delta L_{s\infty})/F_j\right]_{wa} + \left[\Delta L_{s\infty}/F_j\right]_{wa} \tag{3.1-6a}$$

For the calculation of suckdown on a non-coplanar planform it is necessary to find $(\Delta L_s/F_j)_{wing}$ using $\bar{D}_{wing}$ and h_w where $\bar{D}_w$ is determined for the exposed wing area only. Likewise, the value of $(\Delta L_s/F_j)_{fuselage}$ is determined by use of $\bar{D}_{fuselage}$ and h_f. So that,

$$\Delta L_s/F_j = (\Delta L_s/F_j)_{wing} + (\Delta L_s/F_j)_{fuselage} \tag{3.1-6b}$$

at each planform reference altitude of interest.

3.1.4 Fountain Effects

The equations, parameters, and methods for computing fountain lift are described below:

<u>Equations</u>

$$\Delta L_F/F_j = C_{F2}\left[(\Delta L_F^{II}/F_j) \cdot C_{F3}^{II} + (\Delta L_F^{III}/F_j) \cdot C_{F3}^{III} + (\Delta L_F^{IV}/F_j) \cdot C_{F3}^{IV}\right] \tag{3.1-7}$$

where ^{II} designates two-jet, and so on

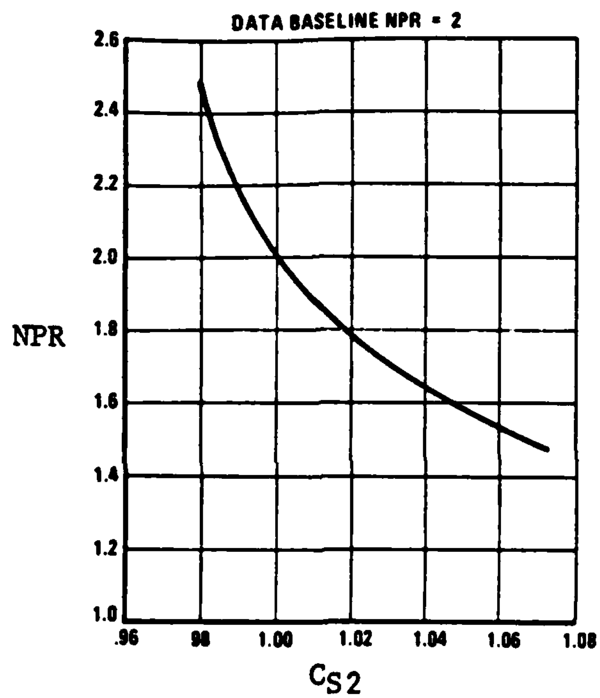

Figure 3.1-4 NPR Extrapolation Coefficient

$$\Delta L_F^{II}/F_j = \Delta L_{FI}/F_j + \Delta L_{FII}/F_j \tag{3.1-8}$$

where

$$\Delta L_{FI}/F_j = (\Delta L^{1}_{FI}/F_j) \cdot \sin \theta, \tag{3.1-9a}$$

$$\Delta L_{FII}/F_j = (\Delta L^{1}_{FII}/F_j) \cdot (\sin \theta_2 - \sin \theta_1) \tag{3.1-9b}$$

<u>Parameters</u>

- θ local angle that the fountain jet impinges on planform, $= \tan^{-1}\left[\frac{w/2}{d_f + h}\right]$
- W_1 width of fuselage for fore and aft jets or wing root chord for latterally spaced jets.
- W_2 wing span for fore and aft jets or fuselage width for laterally spaced jets.
- d_f distance from two-jet stagnation line to center of nozzle
- $\bar{D}$ effective mean diameter of jet on fuselage alone
- d_E distance between nozzles (near edge to near edge)
- h_m height of jet merging, $= 1.374\ d_E$

<u>Fountain Extrapolation Coefficients</u>

$$C_F = C_{F1} \cdot C_{F2} \cdot C_{F3} \cdot C_{F4} \cdot C_{F5} \tag{3.1-10}$$

where

$C_{F1} = 1.0$, reserved for scale effects

C_{F2} effect of nozzle pressure ratio,

$$= 0.736 \ln(NPR) + 0.481, \quad NPR \leq 2.0 \tag{3.1-11a}$$
$$= 0.035 \ln(NPR) + 0.930, \quad NPR \geq 2.0 \tag{3.1-11b}$$

(C_{F2} can be obtained graphically from Figure 3.1-5)

NPR ≤ 2 $\quad C_{F2} = 0.736 \ln(NPR) + 0.481$

NPR ≥ 2 $\quad C_{F2} = 0.035 \ln(NPR) + 0.930$

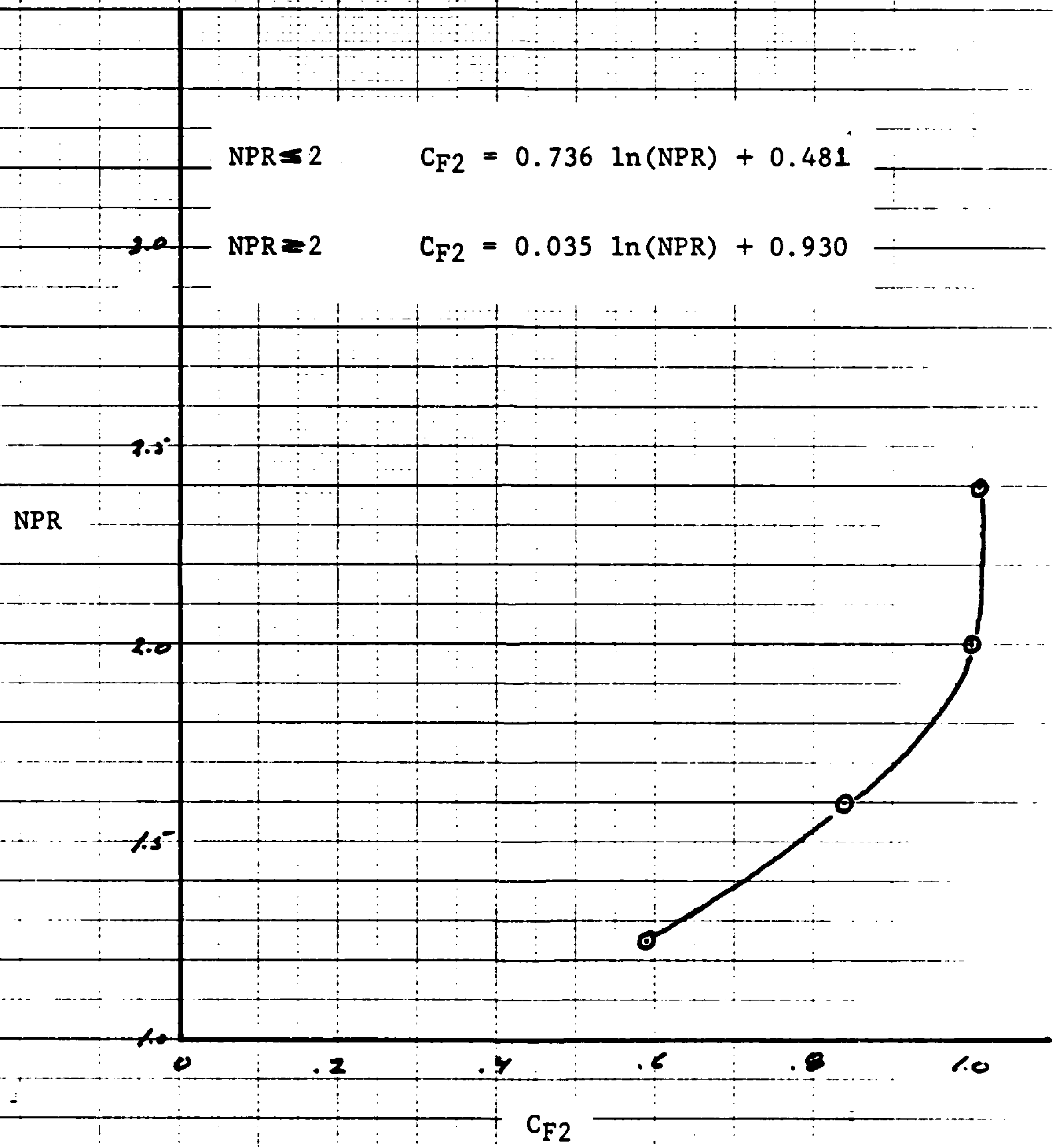

Figure 3.1-5

NPR Extrapolation Coefficient

C_{F3} effect of jet merging, obtained empirically from Figure 3.1-6

C_{F4} effect of planform contour, obtained empirically from

Figure 3.1-7 (three or more jets)
Figure 3.1-8 (two-jet fountain)

C_{F5} effect of Lift Improvement Devices (LIDs),

= 1.0, without LIDs
= 1.5, longitudinal LIDs
= 2.0, longitudinal and transverse LIDs

A non-coplanar planform will require additional calculation to accurately represent the fountain lift if the fountain impacts both non-coplanar portions of the planform. The fountain effects on the wing, $(\Delta L_F/F_j)_{wing}$, must be computed with $\bar{D}_{wing}$ and h_w as was performed in the suckdown calculations for non-coplanar planforms. Also, $(\Delta L_F/F_j)_{fuselage}$ will depend upon $\bar{D}_{fuselage}$ and h_f.

Because the two-jet fountain lift calculation breaks out the wing and fuselage areas, it is more detailed than the three- or four-jet cases. Therefore, it can be used as a guide for tabulation. As in suckdown,

$$\Delta L_F/F_j = (\Delta L_F/F_j)_{wing} + (\Delta L_F/F_j)_{fuselage} \qquad (3.1\text{-}12)$$

3.1.4.1 Multi-Nozzle Fountain

The buoyant force produced by the fountain jet of a multi-nozzle configuration has been quantified by empirical means. Figures 3.1-9 through 3.1-12 provide the basic data of fountain lift for two-, three-, and 4-nozzle configurations. As stated in the tabulation section of this method, it is usually necessary to determine fountain lift for more than one type of fountain due to jet merging with any given configuration.

The altitude (h) used for fountain buoyancy calculations is the distance from the ground to the lowest point on the planform that the fountain impacts.

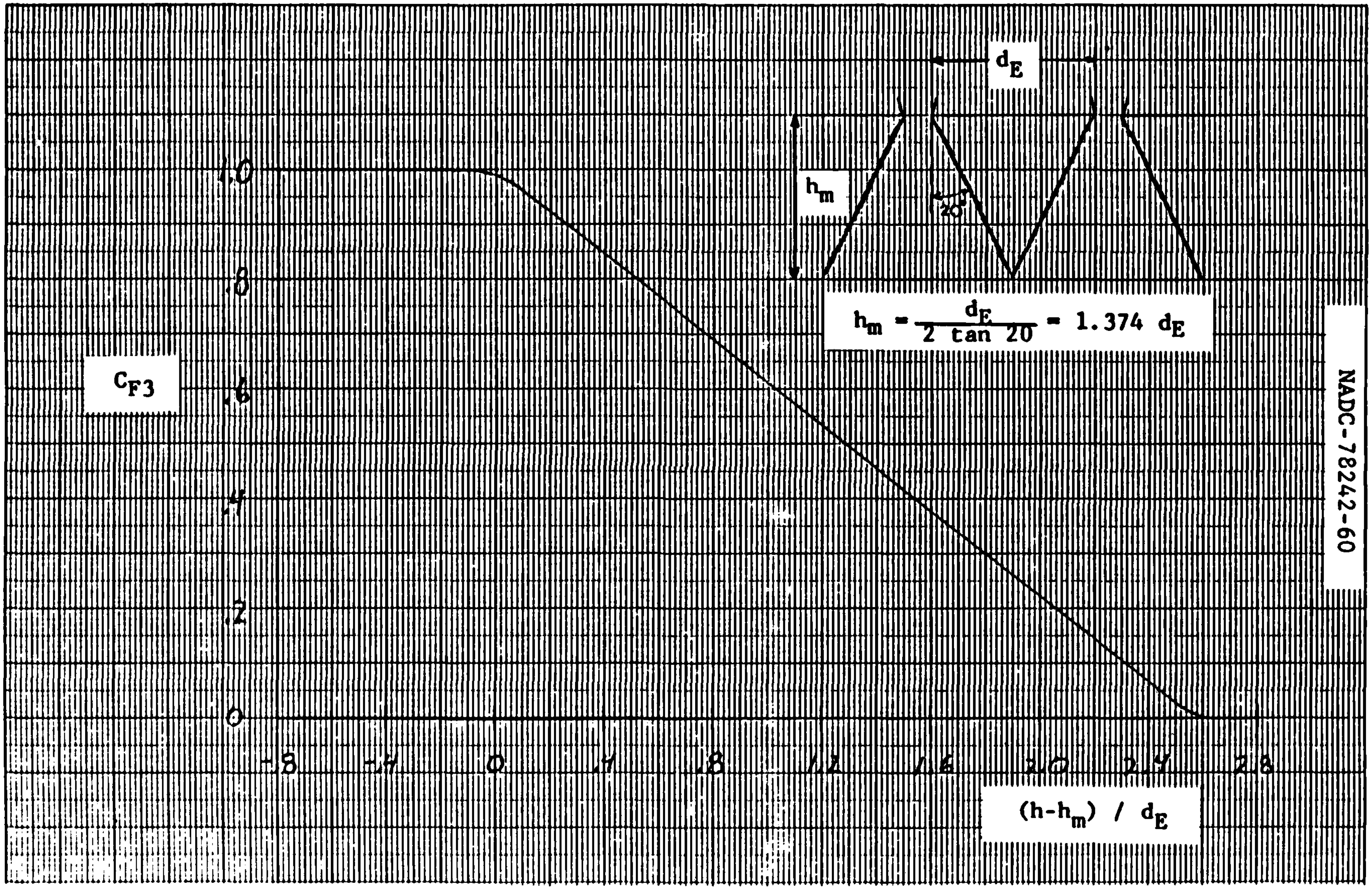

Figure 3.1-6   Effect of Jet Merging On Fountain Lift

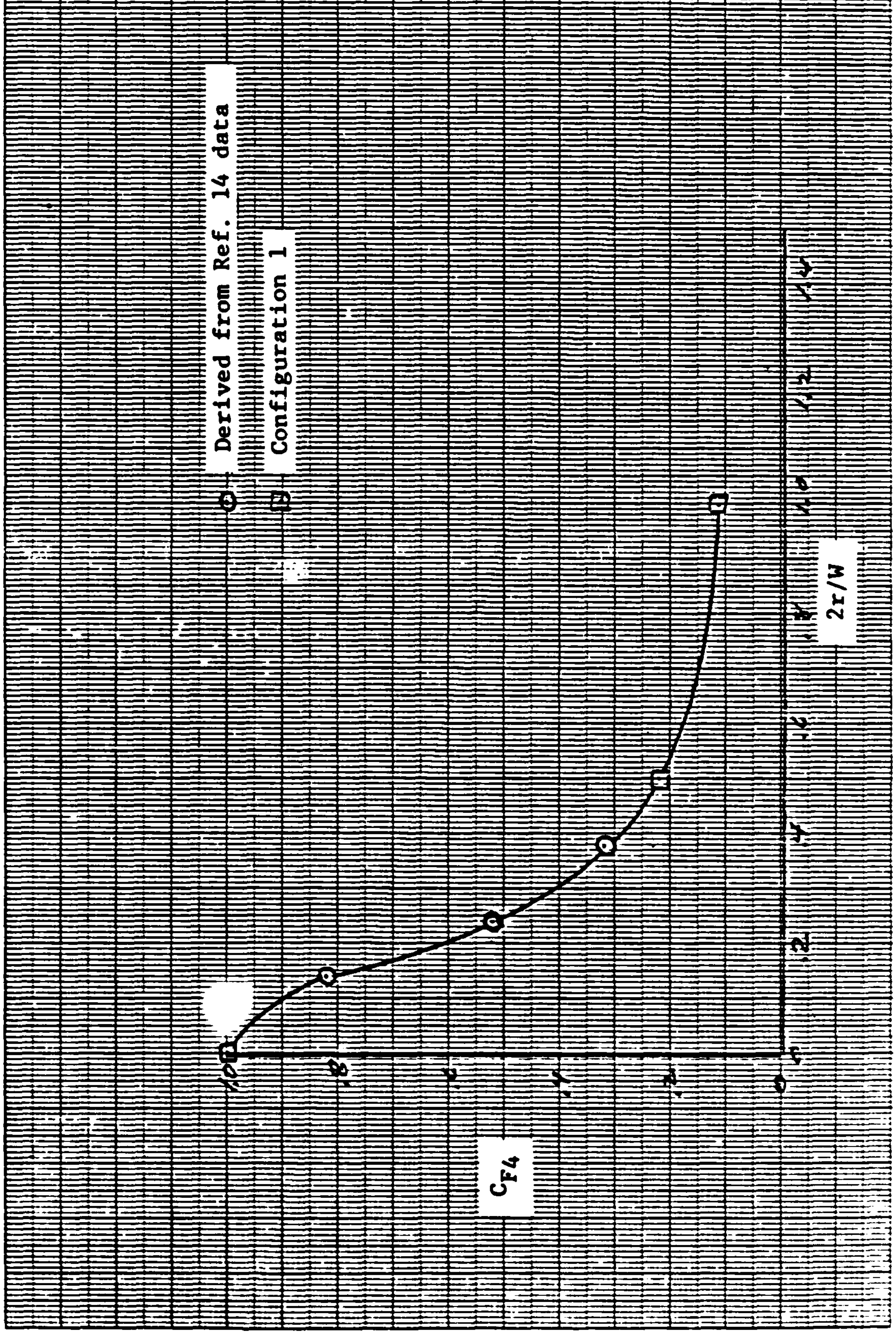

Figure 3.1-7 Effect of Planform Contour - 2 Nozzle Case

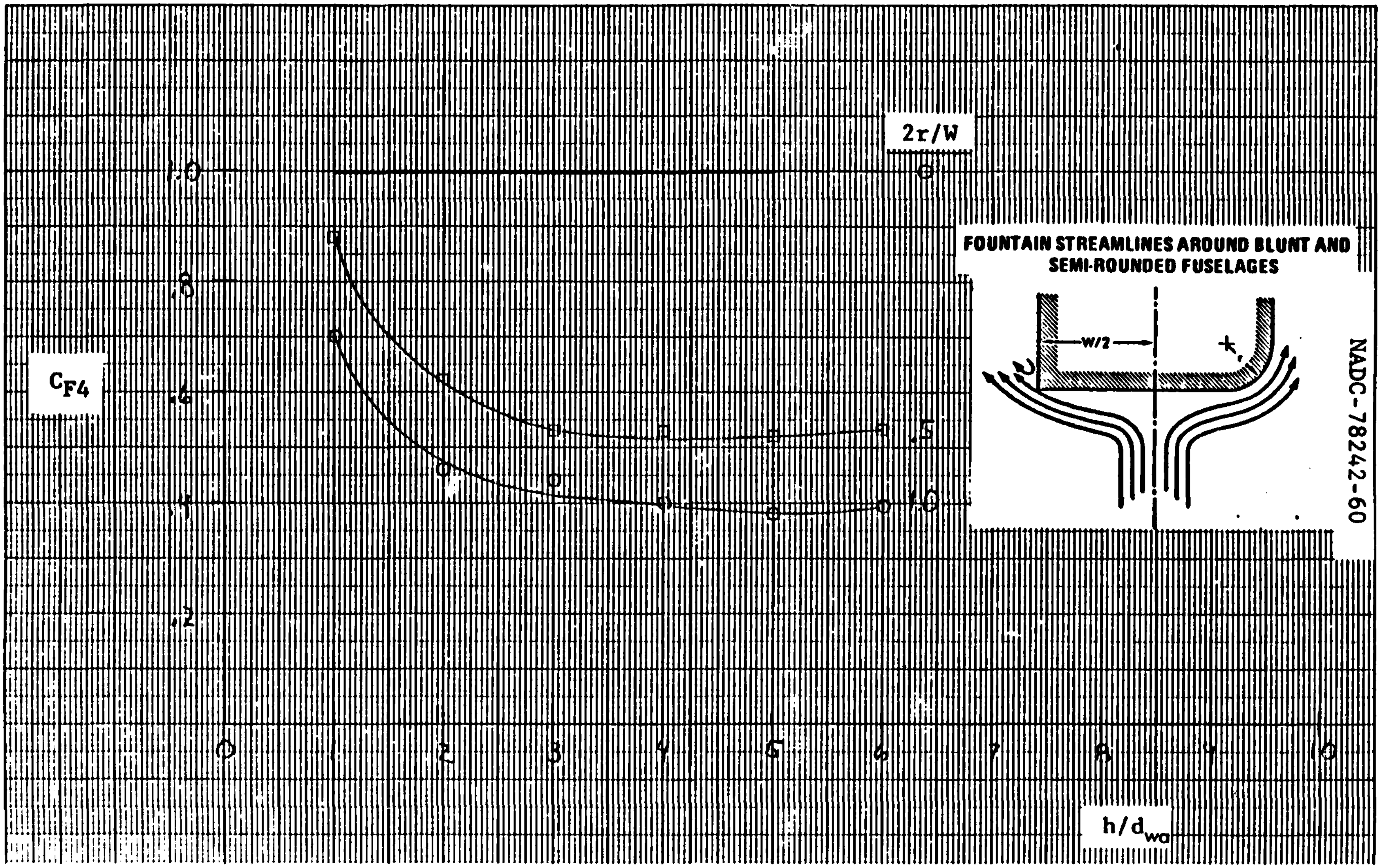

Figure 3.1-8 Effect of Planform Contour - 3 and 4 Nozzle Case

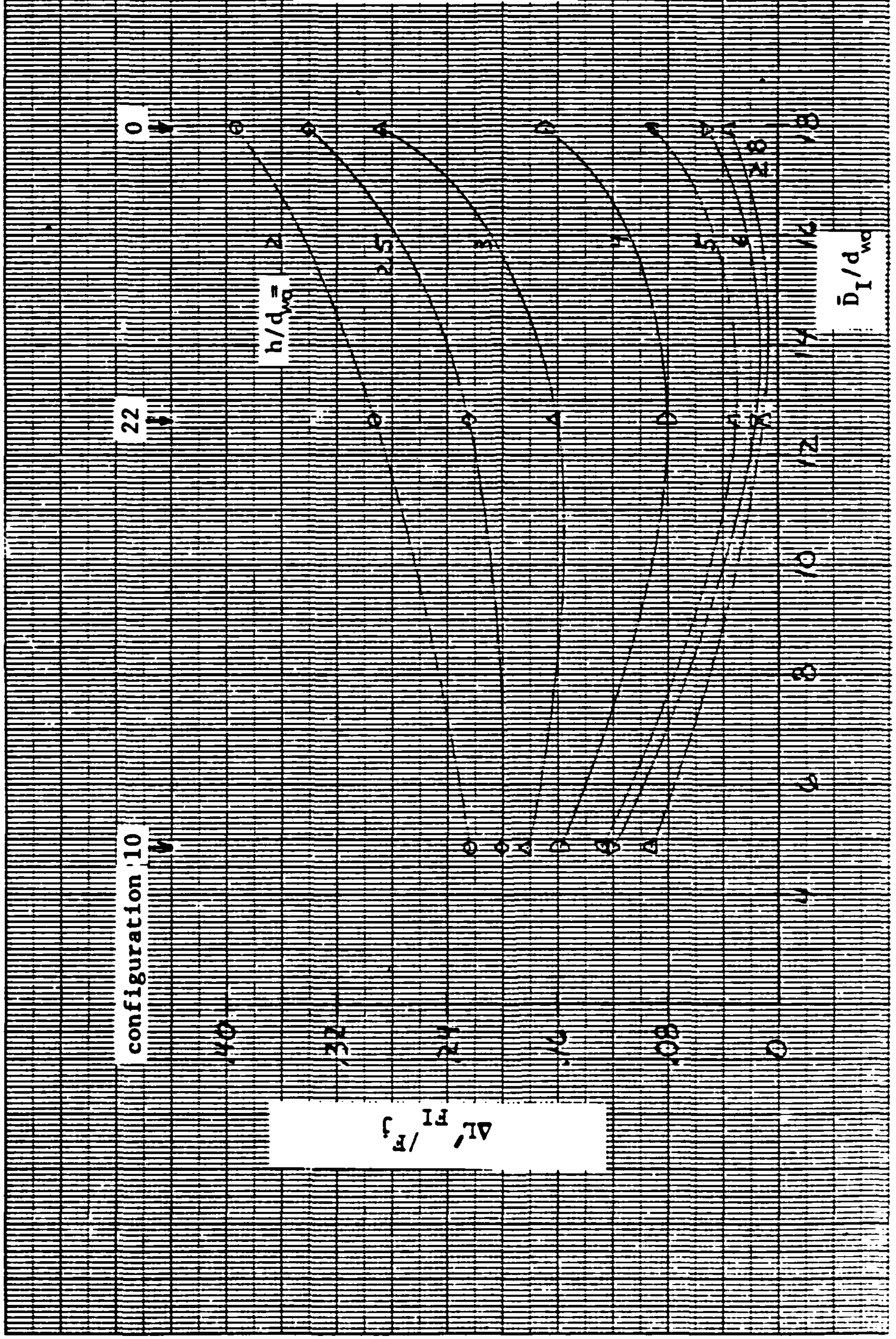

Figure 3.1-9 Fountain Lift, 2-Jet, Central Area

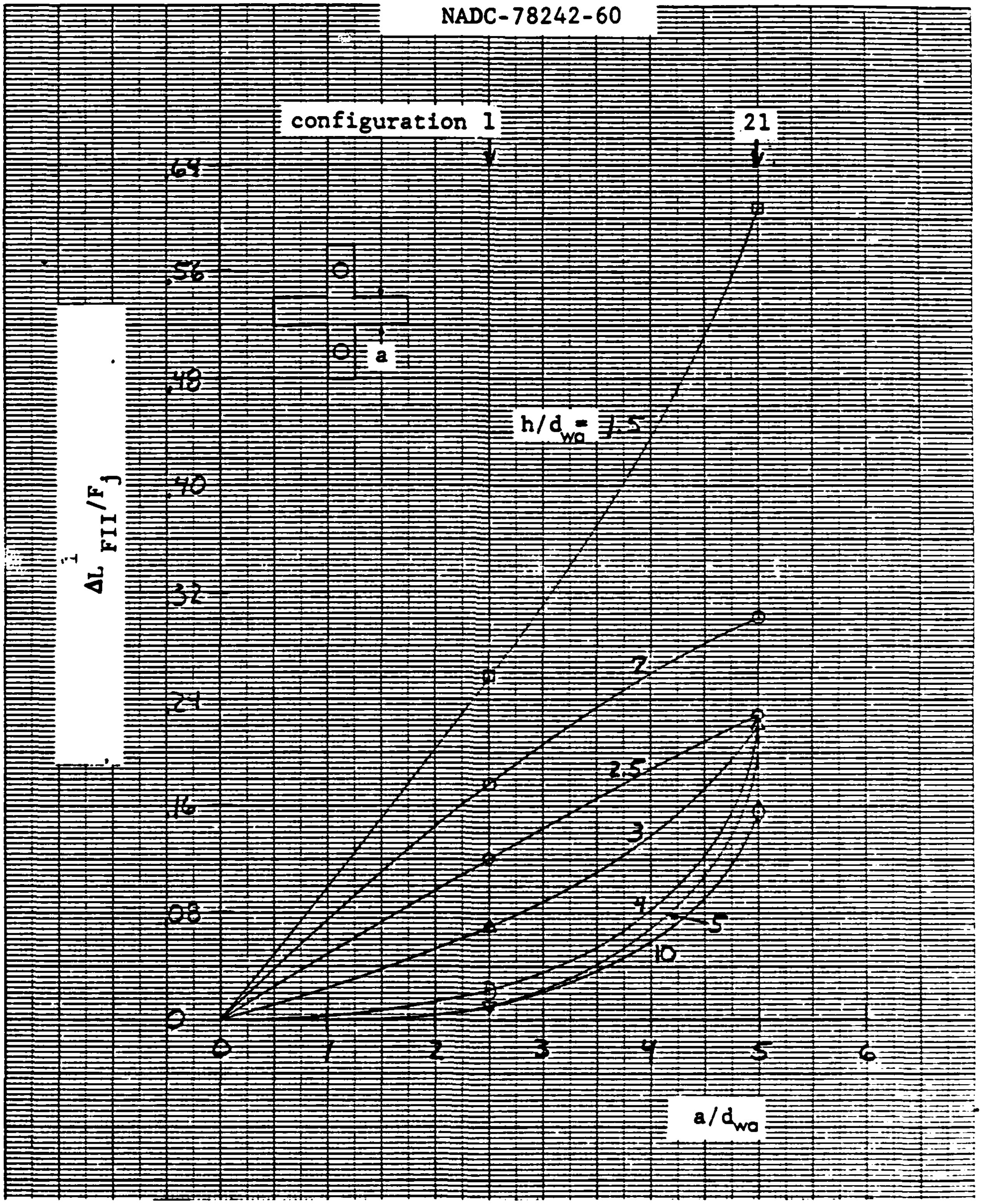

Figure 3.1-10 Fountain Lift, 2-Jet, Peripheral Area

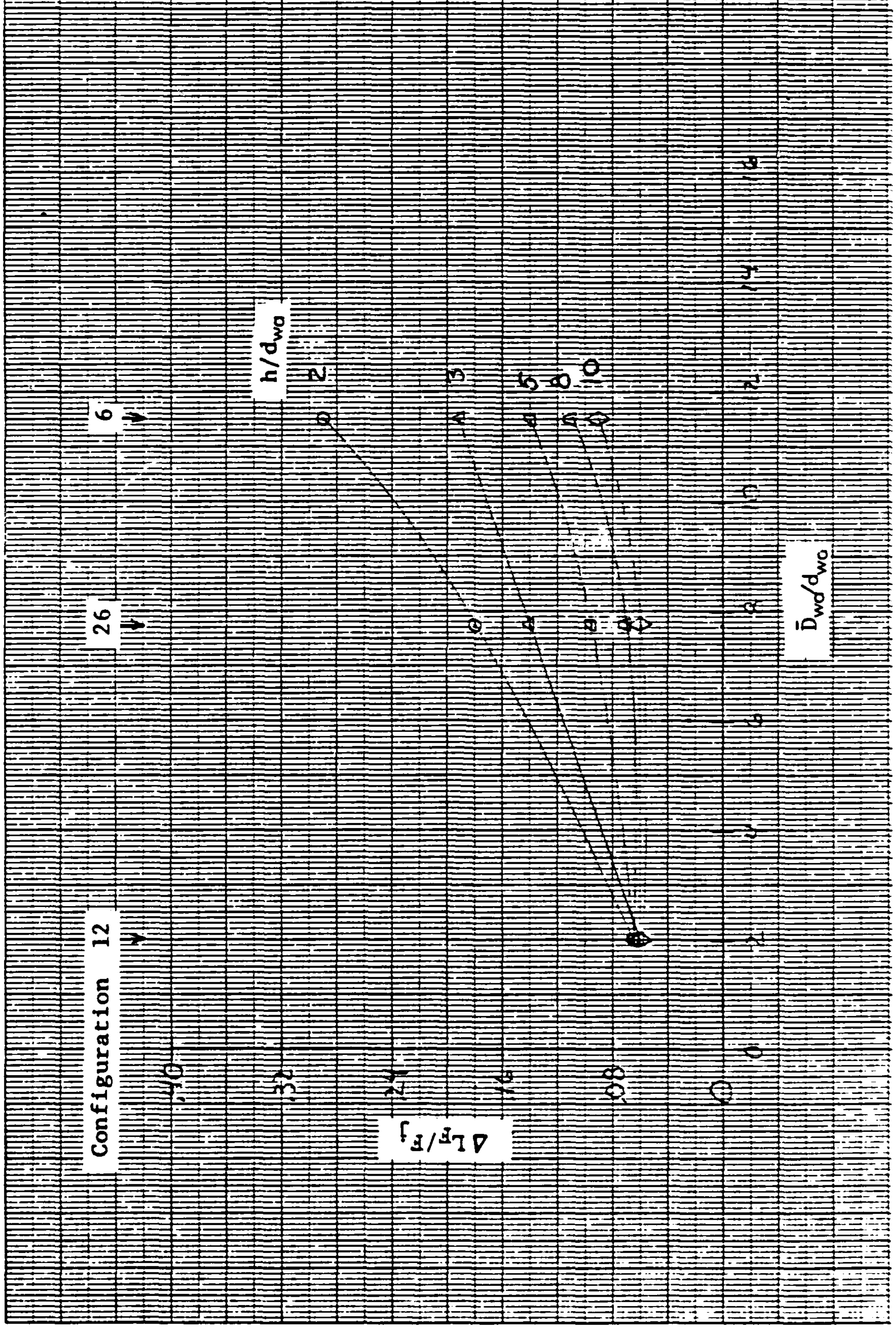

Figure 3.1-11 Fountain Lift - 3-Jet Configuration

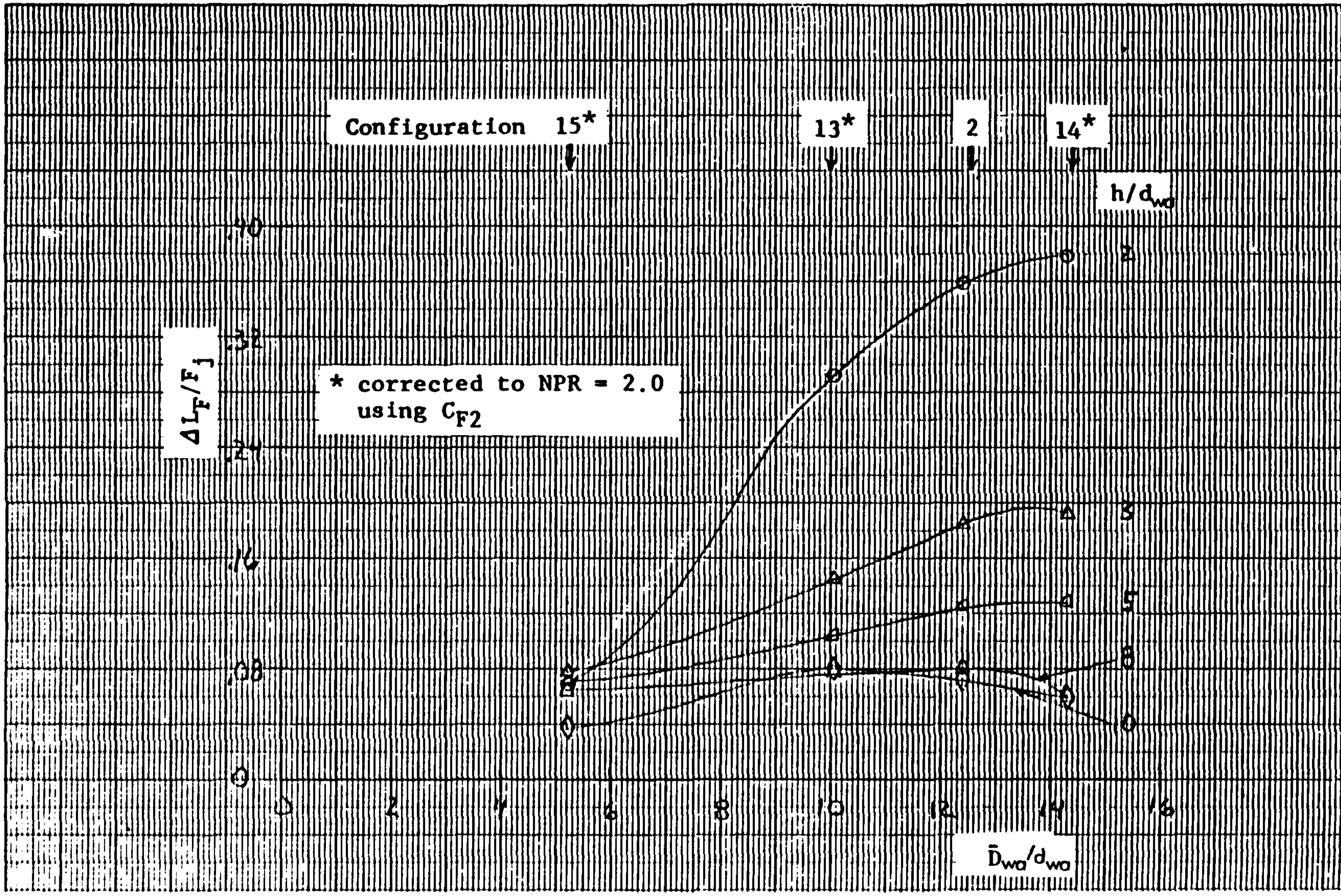

Figure 3.1-12 Fountain Lift - 4-Jet Configuration

3.1.4.2 Two-Jet Fountain

The lift for this type of fountain is calculated in Block II of the tabulation accounting system. The two-jet fountain is determined differently from the three- or four-jet cases because of its unique structure. The stagnation line formed between the two jets will impinge on the aircraft planform in a manner unlike the more centrally concentrated three- and four-jet fountains. The fountain effect on the central planform, $\Delta L_{FI}/F_j$, must be added to the fountain formed on the peripheral section, $\Delta L_{FII}/F_j$ (Figure 3.1-13). Thus, the two-jet fountain buoyancy is

$$\Delta L_F^{II}/F_j = \Delta L_{FI}/F_j + \Delta L_{FII}/F_j \tag{3.1-13}$$

Two-Jet Fountain, $\Delta L_{FI}/F_j$

Figure 3.1-9 presents the fountain lift acting on the aircraft fuselage or wing (depending on nozzle location) in the two-jet case. $\Delta L^1_{FI}/F_j$ can be found for various planform heights (h/d) as a function of $\bar{D}_I/d_{wa}$, where $\bar{D}_I$ is the mean effective diameter of each nozzle on the entire planform central area, averaged by thrust.

The fountain lift generated on the central area is then

$$\Delta L_{FI}/F_j = (\Delta L^1{}_{FI}/F_j) \cdot \sin \theta_1 \tag{3.1-9a}$$

where

$$\theta_1 = \tan^{-1}\left(\frac{W_1/2}{d_f + h}\right) \tag{3.1-14}$$

For a non-symmetric central area (Figure 3.1-14b), the two-jet fountain buoyancy becomes

$$\Delta L_{FI}/F_j = \frac{1}{2} (\Delta L^1{}_{FI}/F_j) (\sin \theta_1' + \sin \theta_1'') \tag{3.1-15}$$

Two-Jet Fountain, $\Delta L_{FII}/F_j$

The fountain lift attained on the peripheral area is shown in Figure 3.1-10. $\Delta L^1{}_{FII}/F_j$ is indexed by use of the parameter a/d_{wa}, where a is the average planform width that is perpendicular to the stagnation line (Figure 3.1-15).

θ_1 is taken from Equation 3.1-14 and

TWO-JET FOUNTAIN $\Delta L_F/F_j$

Fuselage Mounted Engines

SEPARATE PLANFORM INTO CENTRAL AND PERIPHERAL AREAS
(I & II, RESPECTIVELY)

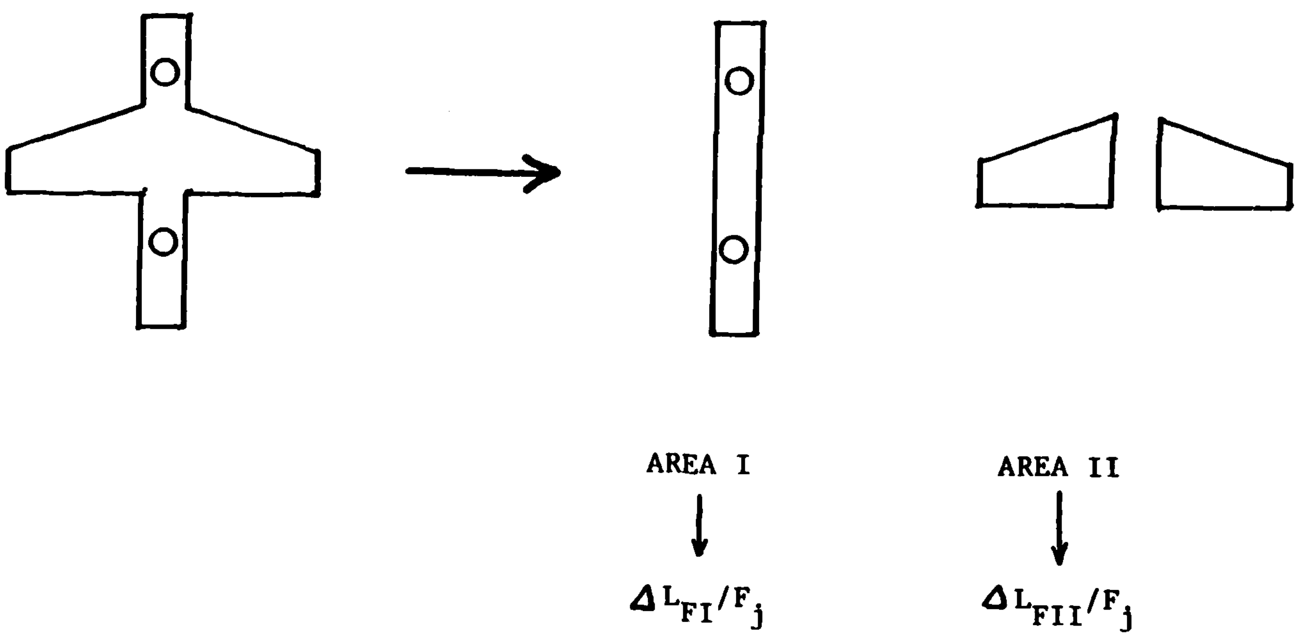

Figure 3.1-13a Two-Jet Fountain $\Delta L_F/F_j$

TWO-JET FOUNTAIN $\Delta L_F/F_j$

Wing Mounted Engines

SEPARATE PLANFORM INTO CENTRAL AND PERIPHERAL AREAS
(I & II, RESPECTIVELY)

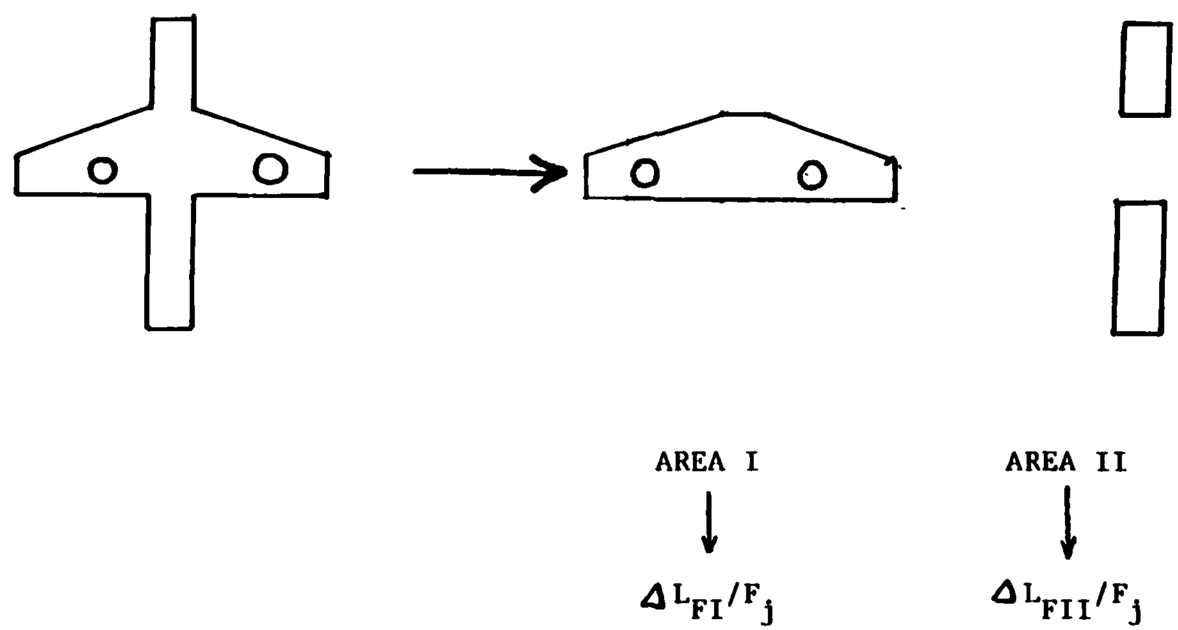

Figure 3.1-13b Two-Jet Fountain $\Delta L_F/F_j$

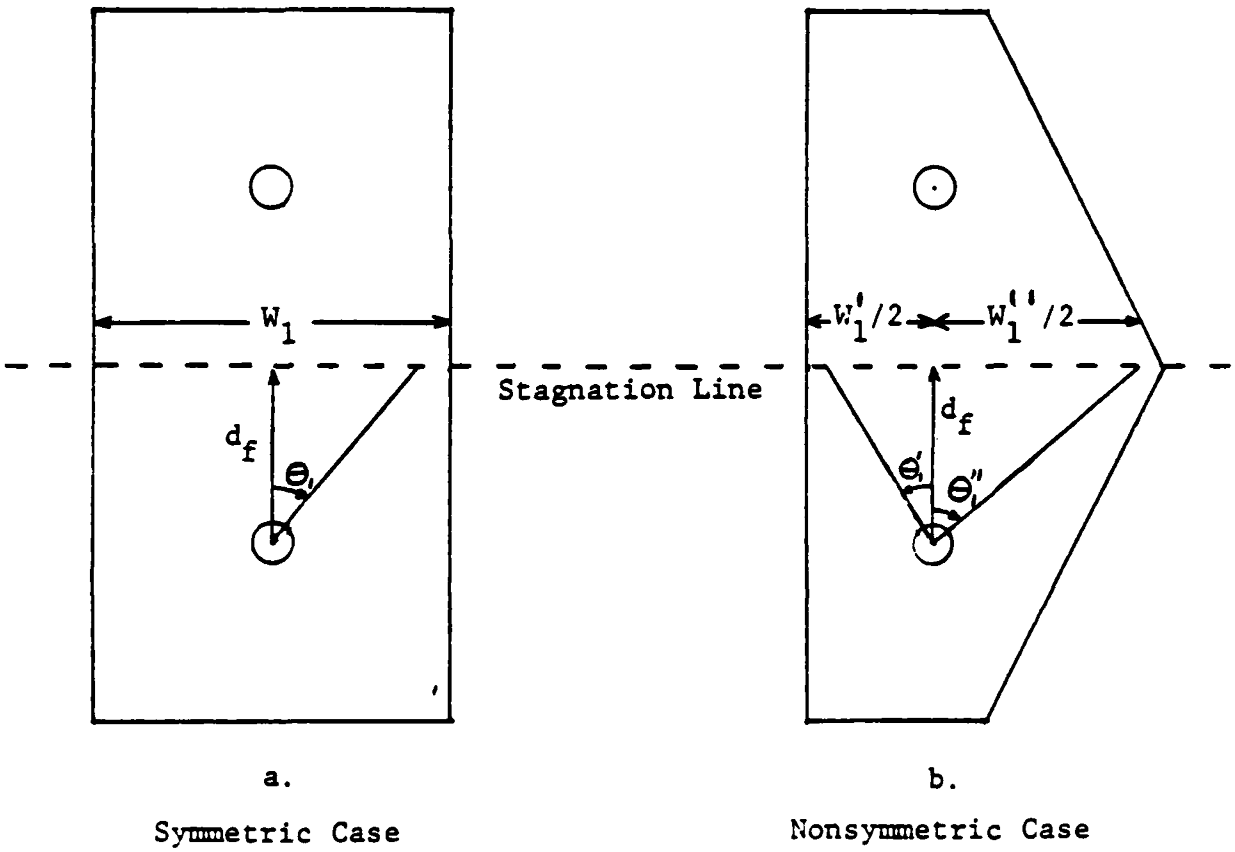

Figure 3.1-14 Two-Jet Fountain (Central Area)

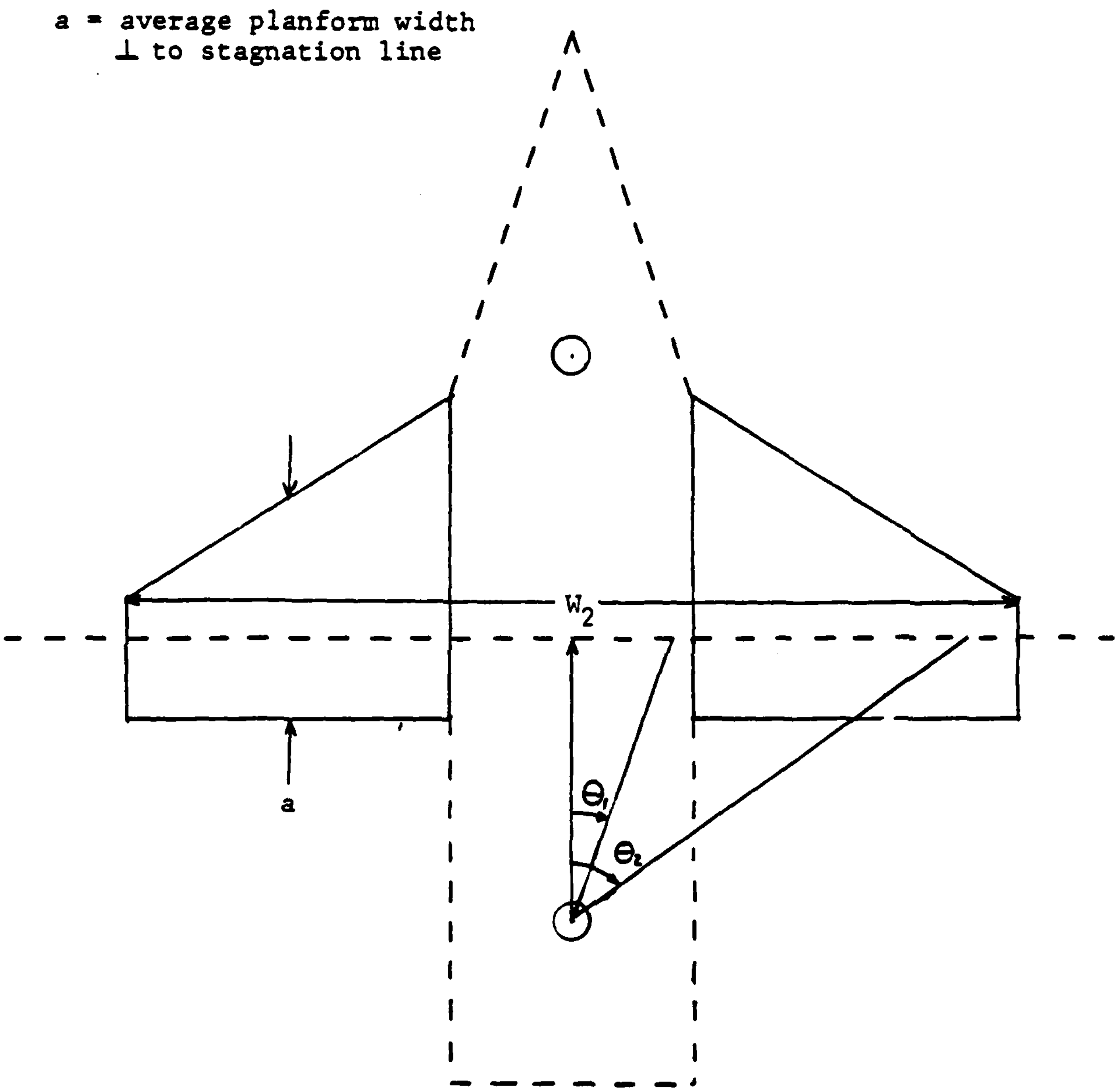

Figure 3.1-15 Two-Jet Fountain (Peripheral Area)

$$\theta_2 = \tan^{-1}\left[\frac{W_2/2}{d_f + h}\right]$$

This produces a fountain lift due to the peripheral area

$$\Delta L_{FII}/F_j = (\Delta L^1{}_{FII}/F_j) \cdot (\sin\theta_2 - \sin\theta_1) \qquad (3.1\text{-}9b)$$

For a non-symmetric case,

$$\Delta L_{FII}/F_j = \frac{1}{2}\left[(\Delta L^1{}_{FII}/F_j) \cdot (\sin\theta_2' - \sin\theta_1') + (\Delta L^1_{FII}/F_j) \cdot (\sin\theta_2'' - \sin\theta_1'')\right] \qquad (3.1\text{-}16)$$

3.1.4.3 Three- And Four-Nozzle Fountain

For a three- or four-nozzle configuration, the fountain strength is a function of the effective mean diameter over the average nozzle diameter ($\bar{D}_{wa}/d_{wa}$). By indexing Figure 3.1-11 or 3.1-12 with the appropriate value of $\bar{D}_{wa}/d_{wa}$ from Subsection 3.1.3, $\Delta L_F/F_j$ of $\Delta L_F/F_j$ can be extracted at various planform heights (h/d_{wa}).

3.1.4.4 Fountain Extrapolation Coefficients C_{F2} and C_{F3}

The coefficients for fountain extrapolation must be considered to fully represent the true fountain lift of the configuration under study.

As shown in Equation 3.1-7, the correction for nozzle pressure ratio, C_{F2}, must be determined for each nozzle and then weight averaged by thrust to give a composite C_{F2}.

$$C_{F2} = \left[\sum_{i=1}^{n} (C_{F2})_i (F_j)_i\right] / \left[\sum_{i=1}^{n} (F_j)_i\right] \qquad (3.1\text{-}17)$$

The values of C_{F2} for each nozzle can be determined through Figure 3.1-5 or Equation 3.1-11.

When the altitude of a hovering aircraft increases, the jet dispersion will cause merging of indivisual jets with other jets and, hence, a change in the fountain character. To account for this fountain characteristic, it is necessary to include in Equation 3.1-7 the fountain merging coefficient, C_{F3}, for each fountain type.

C_{F3} is determined for all fountain types and at each planform altitude from Figure 3.1-6 by indexing the parameter $(\frac{h}{d_E} - 1.374)$, where d_E is the distance between merging nozzles. At any particular planform height, a multiplicity of fountain types could occur where a four-nozzle fountain, by merging, becomes a three-jet fountain. At the altitude that jet merging commences, the merging coefficient of the four-nozzle fountain, C_{F3}^{IV}, will have a value less than unity and, as altitude increases, decrease to zero. In this regime, the next merging coefficient, C_{F3}^{III}, will have a value

$$C_{F3}^{III} = 1 - C_{F3}^{IV} \qquad (3.1\text{-}18a)$$

at each particular altitude of interest. Similarly, C_{F3}^{III} will become a driving function for C_{F3}^{II} when an altitude is reached to cause the three-jet case to merge into two jets, i.e.,

$$C_{F3}^{II} = 1 - C_{F3}^{III} \qquad (3.1\text{-}18b)$$

at these particular planform altitudes. Finally, a point will be reached when the aircraft planform exceeds the height of total jet merging and fountain breakdown, where it can be seen that the summation of jet merging coefficients will be less than unity because the only merging coefficient remaining is C_{F3} and its value will be less than one. A tabular example is shown in Figure 3.1-16.

3.1.5 Induced Lift

3.1.5.1 Two-Dimensional Induced Lift

Once the values of C_{F2} and C_{F3} have been determined, it is possible to calculate the fountain buoyancy of a two-dimensional planform by use of Equation 3.1-7. The two-dimensional fountain lift can then be sumed with the planformed suckdown in order to compute the induced lift of the configuration

$$(\Delta L/F_j)_{2-D} = (\Delta L_F/F_j)_{2-D} + \Delta L_s/F_j \qquad (3.1\text{-}19)$$

h/d_{wa}	C''''_{F3}	C'''_{F3}	C''_{F3}	ΣC_{F3}	NOTE
1	1	0	0	1	
2	1	0	0	1	
3	.7	.3	0	1	1
4	.4	.6	0	1	
5	0	1	0	1	2
6	0	.5	.5	1	3
7	0	0	1	1	4
8	0	0	1	1	
9	0	0	.3	.3	5
10	0	0	0	0	6

NOTES:

1. Two of the four jets begin to merge, starting a three-jet fountain.
2. Merging of two jets complete; fountain is a three-jet fountain.
3. Two remaining jets begin to merge, starting a two-jet fountain.
4. Completion of merging of two jets; fountain is now a two-jet fountain.
5. Merging of all the jets begins, reducing fountain lift.
6. Merging complete; fountain lift eliminated.

Figure 3.1-16. Example of Jet Merging Process

3.1.5.2 Fountain Extrapolation Coefficients C_{F4} And C_{F5}

It is necessary to correct the two-dimensional fountain lift for effects of planform contour and LIDS by using C_{F4} and C_{F5}. The effect of planform contour is determined by the use of Figures 3.1-7 and 3.1-8. Both figures use the contour parameter 2r/W as the index of the fountain lift effect on a rounded surface, C_{F4}. Figure 3.1-7 covers the planform roundness coefficient, C_{F4}, of a three- or four-jet fountain; whereas, Figure 3.1-8 must be used to determine C_{F4} for the case of a two-jet fountain. The roundness extrapolation coefficient must be determined uniquely at each planform altitude and then used to correct the two-dimensional fountain strength to a three-dimensional effect. That is, the fountain character (two-jet, three-jet ....) must be known to determine whether Figure 3.1-7 or 3.1-8 will be used for C_{F4} at each height of computation. The three-dimensional induced lift then becomes

$$(\Delta L\ /F_j)_{3-D} = C_{F4}\ (\Delta L_F/F_j)_{2-D} + \Delta L_s/F_j \qquad (3.1\text{-}20)$$

where LIDs are used, C_{F4} = 1.0 except for the special case given by Equation 3.1-23. The presence of LIDs will increase fountain buoyancy and must be considered through the fountain extrapolation coefficient, C_{F5}. For the general case of fully enclosed longitudinal and transverse LIDs (Figure 3.1-17 a and b), the value of C_{F5} is 2.0, as opposed to the configuration without LIDs where C_{F5} = 1.0. A configuration with only longitudinal LIDs (Figure 3.1-17c) uses C_{F5} = 1.5. The maximum benefit obtained from the LIDs mentioned above will occur only when the LID captures the entire fountain that impinges on the planform. Loss in the theoretical lift improvement of an LID occurs when the device does not fully span the planform width as depicted in Figure 3.1-17 a and b. Figure 3.1-17a shows a two-jet fountain which has a LID that only subtends an angle θ_L on the fuselage. The fountain extrapolation coefficient must be decreased in this case by

$$C_{F5} = 1 + (C_{F5}-1)\ \frac{\sin\theta_1}{\sin\theta_2} \qquad (3.1\text{-}21)$$

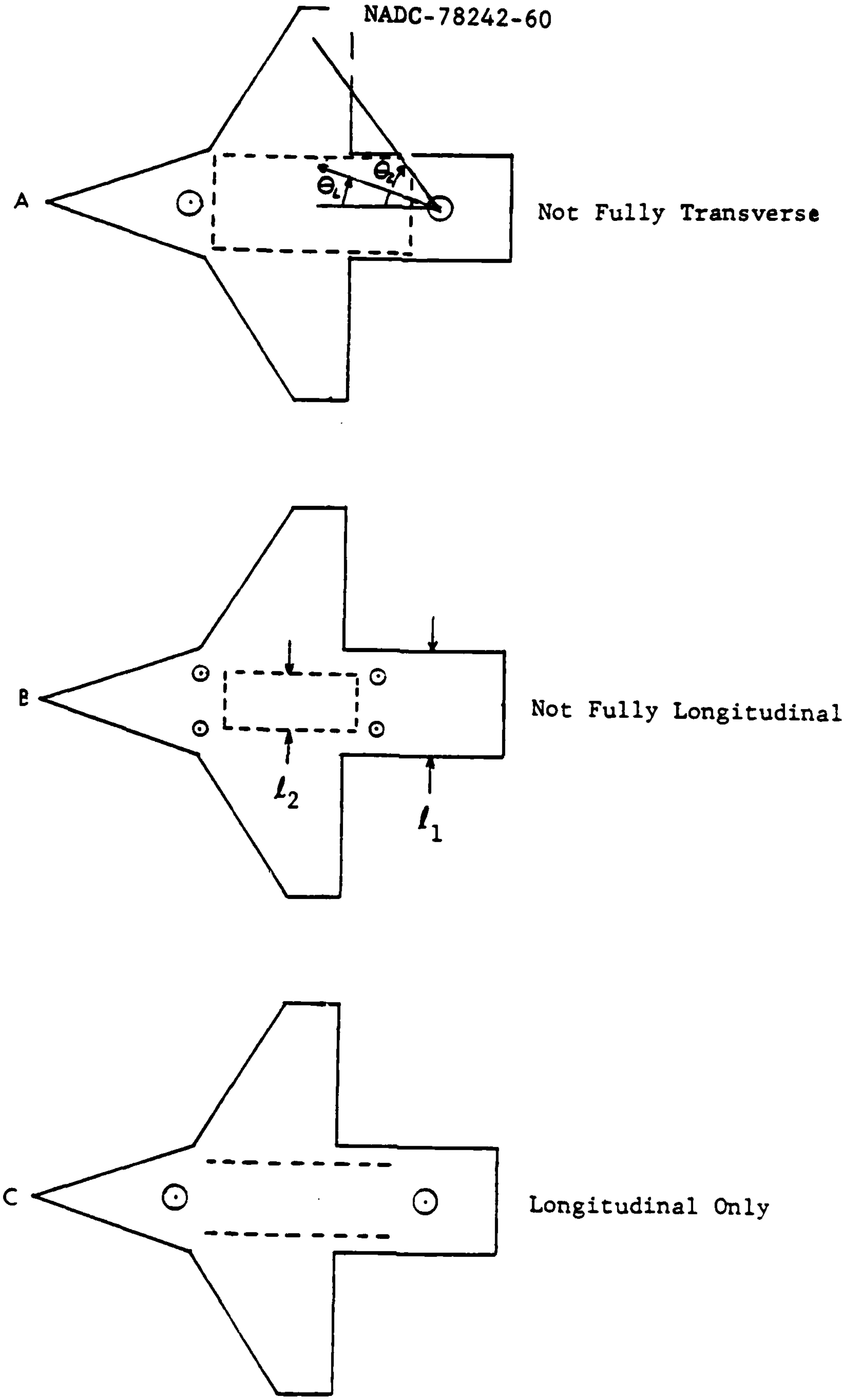

Figure 3.1-17 C_{F5} - LIDs, Special Situations

For a three- or four-jet fountain (Figure 3.1-17 b, a decreased LID size leads to the relationship:

$$C_{F5} = 1 + (C_{F5}-1)\ \frac{\ell_2}{\ell_1} \qquad (3.1\text{-}22)$$

where (ℓ_2/ℓ_1) is the ratio of LID width to fuselage width.

An additional fountain lift factor must be considered when using LIDs. The loss of lift due to planform contour (C_{F4}) does not occur in the area covered by the LID. Therefore, if the LIDs do not subtend the entire planform, the new coefficient for planform roundness becomes

$$C_{F4} = C_{F4} + (1-C_{F4})\ \frac{\ell_2}{\ell_1} \qquad (3.1\text{-}23)$$

The induced lift for a configuration with a LID now becomes

$$(\Delta L/F_j)_{LID} = C_{F4} \cdot C_{F5} \cdot (\Delta L_F/F_j)_{2\text{-}D} + \Delta L_s/F_j \qquad (3.1\text{-}24)$$

3.2 SAMPLE CALCULATION FOR A SUBSONIC VSTOL AIRCRAFT

3.2.1 Suckdown

The most difficult step toward the computation of suckdown is the calculation of $\bar{D}$ for each nozzle, because it must be performed graphically, as per Section 3.1.3. The effective mean diameter also influences the determination of fountain strength which expands the importance of $\bar{D}$. A McDonnell-Douglas Subsonic V/STOL configuration is analyzed in this section with the following values of $\bar{D}_i$ graphically determined:

$$\bar{D}_1 = 7.044 \text{ in}$$

$$\bar{D}_2 = \bar{D}_3 = 9.843 \text{ in}$$

It is also necessary to use a single $\bar{D}$ for later computations. This is calculated as a thrust-weighted average.

$$\bar{D}_{wa} = \frac{(7.044)F_{j1} + 2\ (9.843)\ F_{j2,3}}{F_{j1} + F_{j2} + F_{j3}} = 8.910$$

which is $\bar{D}_{wa} = (\bar{D}_1 + \bar{D}_2 + \bar{D}_3)/3$

since $F_{j1} = F_{j2} = F_{j3} = 58.51\ lb_f$

The suckdown portion of the induced lift calculation is shown in Block I (Figure 3.2-1) of the problem tabulation. Total aircraft suckdown must be computed individually for each nozzle of the aircraft, and the appropriate coefficients must be used for the rectangular or triangular form of the equation listed in Subsection 3.1.3. Most trapezoidal shapes produce results that correlate well with test data. This is accomplished by use of the rectangular form of Equation 3.1-2; therefore, the subsonic V/STOL configuration in this section is analyzed with the rectangular form. In order to use Equation 3.1-2,

$$\frac{\Delta L_s - \Delta L_{s\infty}}{F_j} = -(0.00125(\bar{D}/d) + 0.0185)\ C_s \left(\frac{h}{\bar{D}-d}\right)^{-1.59}$$

for the computation of suckdown, it is first necessary to list the following parameters:

$d_1 = d_2 = d_3 = 2.323$ in

$d_{je} = (3(2.323^2))^{\frac{1}{2}} = 4.024$ in

$$d_{wa} = \frac{d_1F_{j1} + d_2F_{j2} + d_3F_{j3}}{F_{j1} + F_{j2} + F_{j3}} = 2.323 \text{ in}$$

$NPR_1 = NPR_2 = NPR_3 = 1.50$

$(C_{S2})_1 = (C_{S2})_2 = (C_{S2})_3 = 1.173 - 0.2495\ \ln(1.5) = 1.0718$

Then suckdown can be computed as a function of planform height and $\bar{D}_i$,

TABULATION SHE

d_{je} = 4.024 in	$\frac{h}{d_{je}}$		$\left(\frac{\Delta L_s}{F_j}\right)_{fwd}$	$\left(\frac{\Delta L_s}{F_j}\right)_{aft}$	$\left(\frac{\Delta L_s}{F_j}\right)_{W.A.}$	$\left(\frac{\Delta L_{jet}}{F_j}\right)_{WA}$		$\frac{\Delta L_s}{F_j}$	
$\bar{D}$ (in)			7.044	4.843	8.110				
d (in)			2.323	2.323	2.323				
$\bar{D}/d$			3.032	4.237	3.836	3.836			
C_{s_2}			1.0718	1.0718					
F_j (lb)			58.52	58.52					
	1		-.031	.069	.056	.011		-.067	
	1.5		-.016	.036	.029			-.040	
	2		-.010	.023	.019			-.030	
	3		-.005	.012	.010			-.021	
	4		-.003	.008	.006			-.017	
	5		-.002	.005	.004			-.015	
	6		-.002	.004	.003			-.014	

CALCULATION OF SUCKDOWN

SUBSONIC VSTOL -- 3 NOZZLE CONFIGURATION

W.A. = Weighted Average

FIGURE 3.2-1

$$\frac{\Delta L_s - \Delta L_{s\infty}}{F_j} = -(.00125\ \frac{\bar{D}_i}{2.323} + .0185)\ 1.0718$$

$$\cdot \left\{\frac{(h/d_{je}).4.024}{\bar{D}_i - 2.323}\right\}^{-1.59}$$

which results in

$$\left(\frac{\Delta L_s - \Delta L_{s\infty}}{F_j}\right)_1 = -.031$$

$$\left(\frac{\Delta L_s - \Delta L_{s\infty}}{F_j}\right)_{2,3} = -.069$$

at $h/d_{je} = 1$.

As before, the weighted average becomes

$$\left(\frac{\Delta L_s - \Delta L_{s\infty}}{F_j}\right)_{wa} = \frac{-.031 + 2(-.069)}{3} = -.056$$

Since

$$\frac{\bar{D}_{wa}}{d_{wa}} = \frac{8.910}{2.323} = 3.836$$

it is possible to compute the free-air suckdown with Equation 3.1-3.

$$\frac{\Delta L_{s\infty}}{F_j}_{wa} = \left[0.0667\left(\frac{1}{3.836}\right) - 0.420\right] = -.011$$

Then

$$\frac{\Delta L_s}{F_j} = \left(\frac{\Delta L_s - \Delta L_{s\infty}}{F_j}\right)_{wa} + \left(\frac{\Delta L_{s\infty}}{F_j}\right)_{wa}$$

$$= 0.056 \ -.011 = 0.067$$

at $h/d_{je} = 1$.

Figure 3.2-1a is a comparison of the predicted suckdown of the forward nozzle of this configuration plotted against actual test data.

3.2.2 Fountain Lift

3.2.2.1 Two-Jet Fountain

Although this is a three-jet configuration, the two aft jets begin to merge at a rather low altitude, namely

$$h_m = 1.374\ d_E = 7.00 \text{ inches}$$

$$h_m/d_{je} = 1.74.$$

Therefore, this configuration will behave as two-jet model for a significant extent of altitude and, consequently, two-jet fountain lift must be calculated.

Block II (Figure 3.2-2) of the tabulation sheet presents the approach to this calculation. The width of the fuselage and span are measured as

$$W_1 = 5.24 \text{ in} \qquad \text{(fuselage)}$$
$$W_2 = 21.66 \text{ in} \qquad \text{(span)}$$

The distance between forward and aft nozzle centerlines is 14.56 inches; locating the stagnation line equidistant from the nozzles gives

$$d_f = 7.28 \text{ in}$$

This allows for the computation of θ_1 and θ_2 at each planform height, as described in Subsection 3.1.4.

$$\theta_1 = \tan^{-1} \frac{2.62}{1.5\ (4.024) + 7.28} = 11.13 \text{ degrees}$$

$$\theta_2 = \tan^{-1} \frac{10.83}{1.5\ (4.024) + 7.28} = 39.12 \text{ degrees}$$

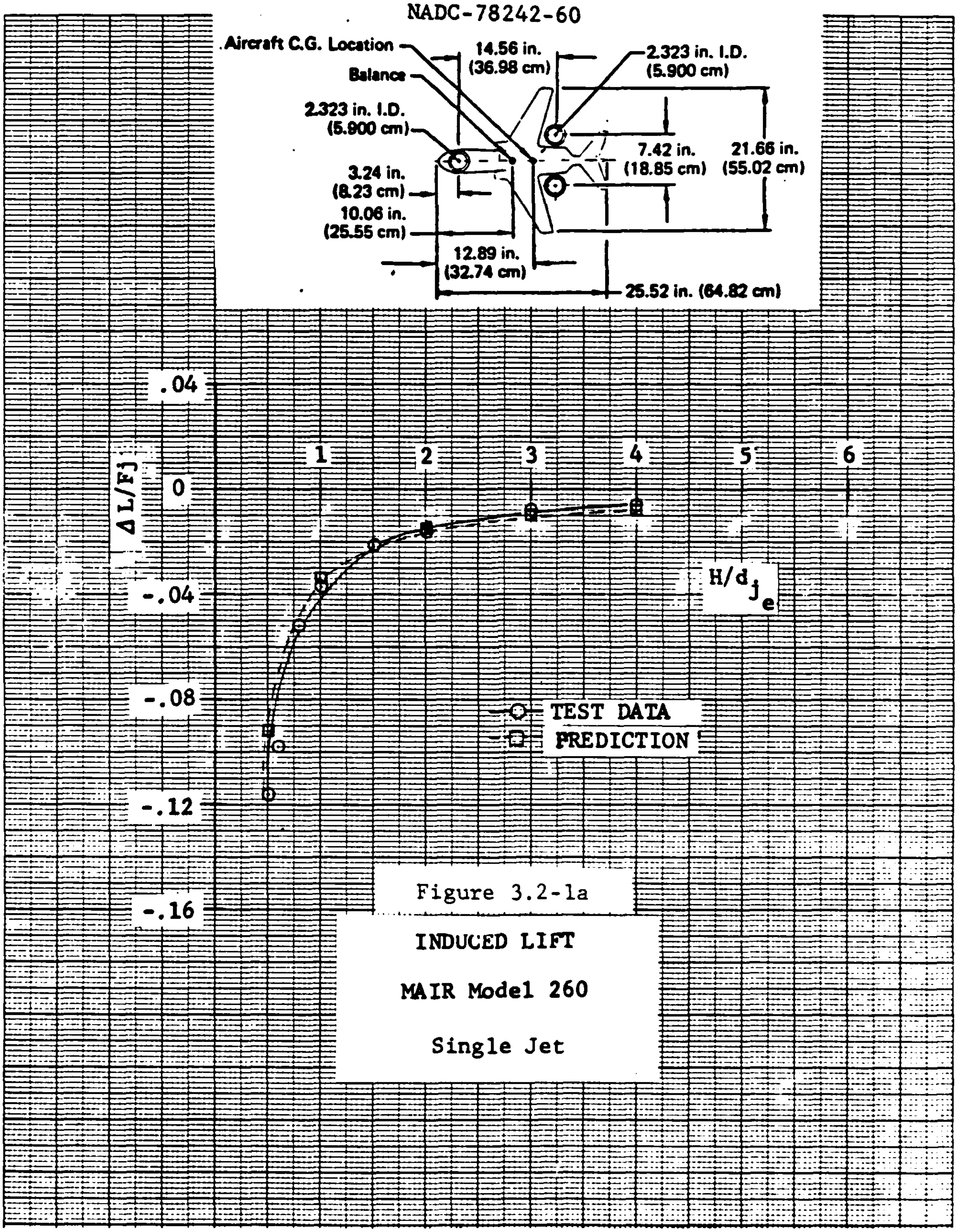

Figure 3.2-1a

INDUCED LIFT

MAIR Model 260

Single Jet

TABULATION SHEET

d_{je} [illegible]	$\frac{h}{d_{je}}$	θ_1	θ_2		$\frac{\Delta L'_{LI}}{F_j}$	$\sin\theta_1$	$\frac{\Delta L_{FI}}{F_j}$	$\frac{\Delta L'_{FII}}{F_j}$	$\sin\theta_2 - \sin\theta_1$	$\frac{\Delta L_{fII}}{F_j}$		$\frac{\Delta L''_F}{F_j}$	
W/2 (in)		2.62	10.83										
d_f (in)		7.28	7.28										
$\bar{D}_x/d_{ave}$					2.342								
a/d_{ave}								1.387					
	1.5	11.13	39.12		.204	.193	.039	.057	.438	.025		.064	
	2	9.70	35.24		.204	.168	.034	.016	.409	.007		.041	
	3	7.71	29.23		.178	.134	.024	.002	.354	.001		.025	
	4	6.40	25.86		.149	.111	.017	.001	.309	0		.017	
	5	5.46	21.57		.117	.095	.011	.001	.272	0		.011	
	6	4.77	19.02		.084	.083	.007	.001	.243	0		.007	

CALCULATION OF 2-NOZZLE FOUNTAIN

SUBSONIC VSTOL -- 3 NOZZLE CONFIGURATION

$\bar{D}_x = 5.490$ in $a = 3.223$ in

FIGURE 3.2-2

During the graphical determination of $\bar{D}$ for the configuration under study, it is necessary to measure the value of $\bar{D}_I$. Also required is the measurement of the mean chord of the exposed wing. For this subsonic V/STOL

$$\bar{D}_I = 5.440 \text{ in}$$
$$\bar{D}_I/d_{wa} = 2.342$$
$$a = 3.223 \text{ in}$$

and

$$a/d_{wa} = 1.387$$

The parameters listed above will then be used to determine the two-jet fountain lift of the fuselage and wings (Figures 3.1-9 bis and 3.1-10 bis).

At h/d = 2,

$$\Delta L^1_{FI}/F_j = 0.210$$
$$\Delta L^1_{FII}/F_j = 0.10.$$

Once the values of $\Delta L^1_{FI}/F_j$ and $\Delta L^1_{FII}/F_j$ are found at various h/d, it is possible to cross plot these values against h/d_{je} (which is used in this sample calculation to be consistent with Ref. 13). The cross plotted values have been extracted at evan values of h/d_{je} and listed in Block II of the problem tabulation. The next step in the computation is to incorporate the subtended angles for the fuselage and wing areas, i.e.,

$$\Delta L_{FI}/F_j = 0.204 \sin 11.13 \text{ degrees} = .039$$
$$\Delta L_{FII}/F_j = 0.057 (\sin 39.12 \text{ degrees} - \sin 11.13 \text{ degrees}) = .025$$

at $h/d_{je} = 1.5$.

Thus, the two-jet fountain lift is

$$\Delta L^{II}_F/F_j = 0.039 + 0.025 = 0.064$$

at $h/d_{je} = 1.5$

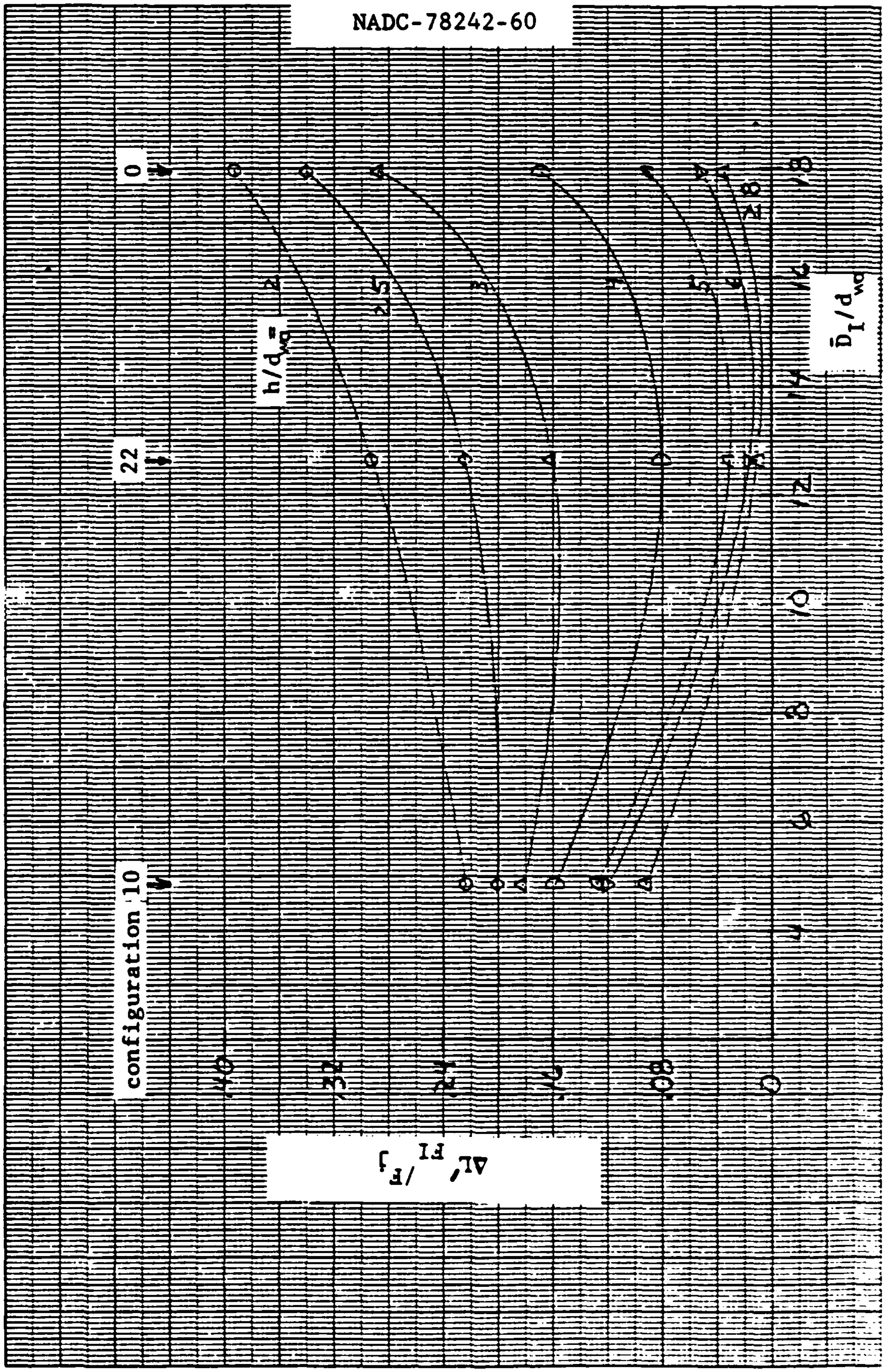

Figure 3.1-9 bis. Fountain Lift, 2-Jet, Central Area

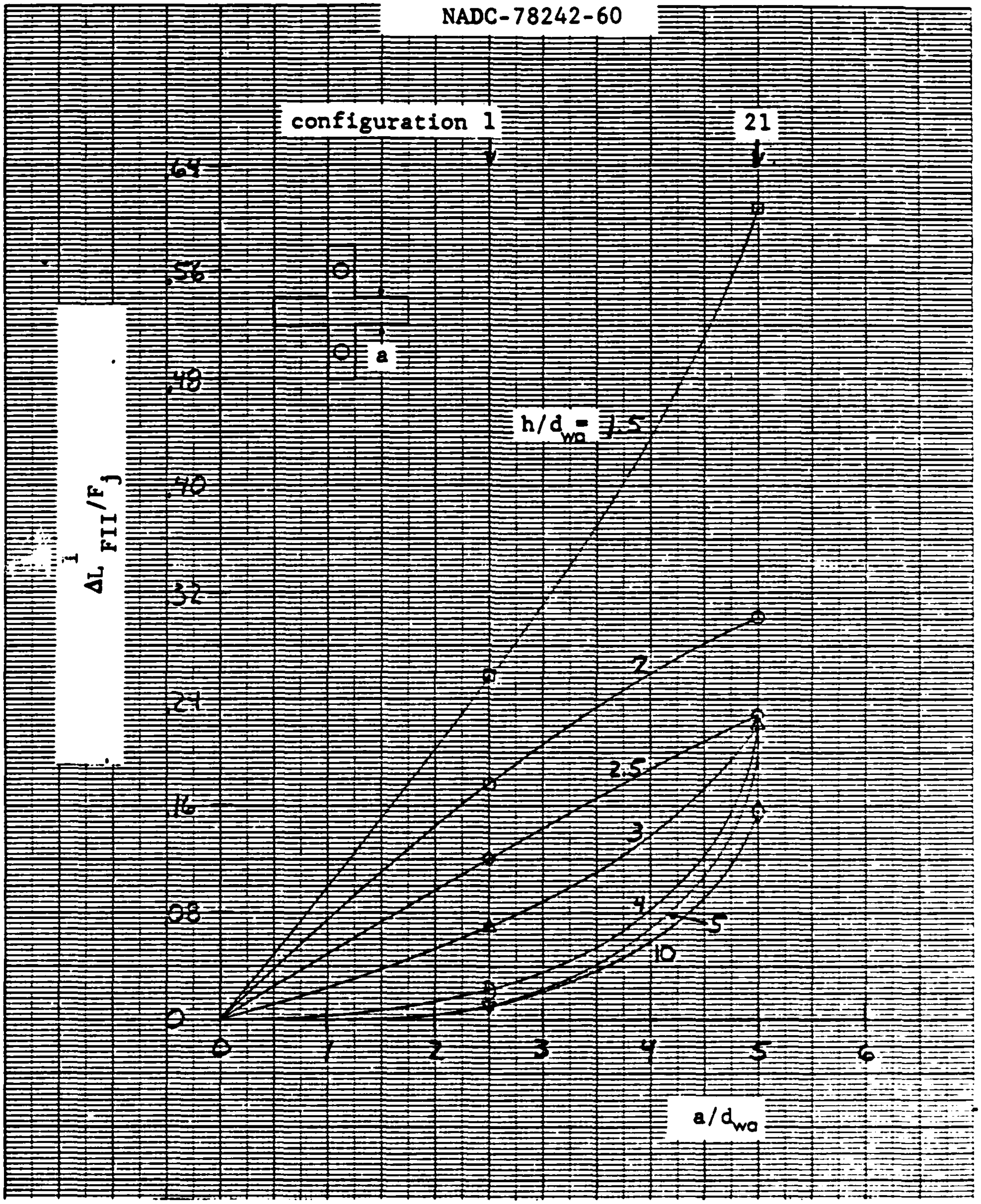

Figure 3.1-10 bis. Fountain Lift, 2-Jet, Peripheral Area

3.2.2.2 Three-Jet Fountain

This subsonic V/STOL possesses a three-jet fountain at altitudes close to ground proximity. The fountain lift for this condition can be taken directly from Figure 3.1-11 bis by indexing $\bar{D}_{wa}/d_{wa}$, which was calculated in Subsection 3.2.1.

Since

$$\bar{D}_{wa}/d_{wa} = 3.836$$

$$\Delta L_F^{III}/F_j = 0.098$$

at $h/d_{je} = 2$

Once again, the values of $\Delta L_F^{III}/F_j$ must be cross-plotted versus h/d_{je} which produces the results in Block III (Figure 3.2-3) of the problem tabulation.

3.2.2.3 Fountain Extrapolation Coefficients C_{F2} And C_{F3}

The extrapolation coefficient for NPR, C_{F2}, must be included in the fountain lift computation to obtain proper correlation of results since the subsonic V/STOL has NPRs other than the baseline 2.0. With all three nozzles having NPR = 1.5, we have from Subsection 3.1.4

$$C_{F2} = 0.736 \ln(1.5) + 0.481 = 0.779$$

Additionally, the fountain extrapolation coefficient for jet-merging, C_{F3}, must be determined as a function of planform height. Figure 3.1-6 bis is an empirical formulation of the jet-merging coefficient, C_{F3}. The three-jet fountain of the subsonic V/STOL merges into a two-jet fountain because of the close proximity of the two aft nozzles, d_E = 5.10 inches. Further, the forward jet will eventually merge with the aft jets. In the first case, $h_m/d_{je} = 1.74$, and

$$\frac{h}{d_e} - 1.374 = \frac{1(4.024)}{5.10} - 1.374 = -0.585$$

at $h/d_{je} = 1$, which yields $C_{F3}^{III} = 1.0$ from Figure 3.1-6 bis. Further values of C_{F3}^{III} are shown in Block III of the tabulation sheet. It is noted that the strength of the two-jet

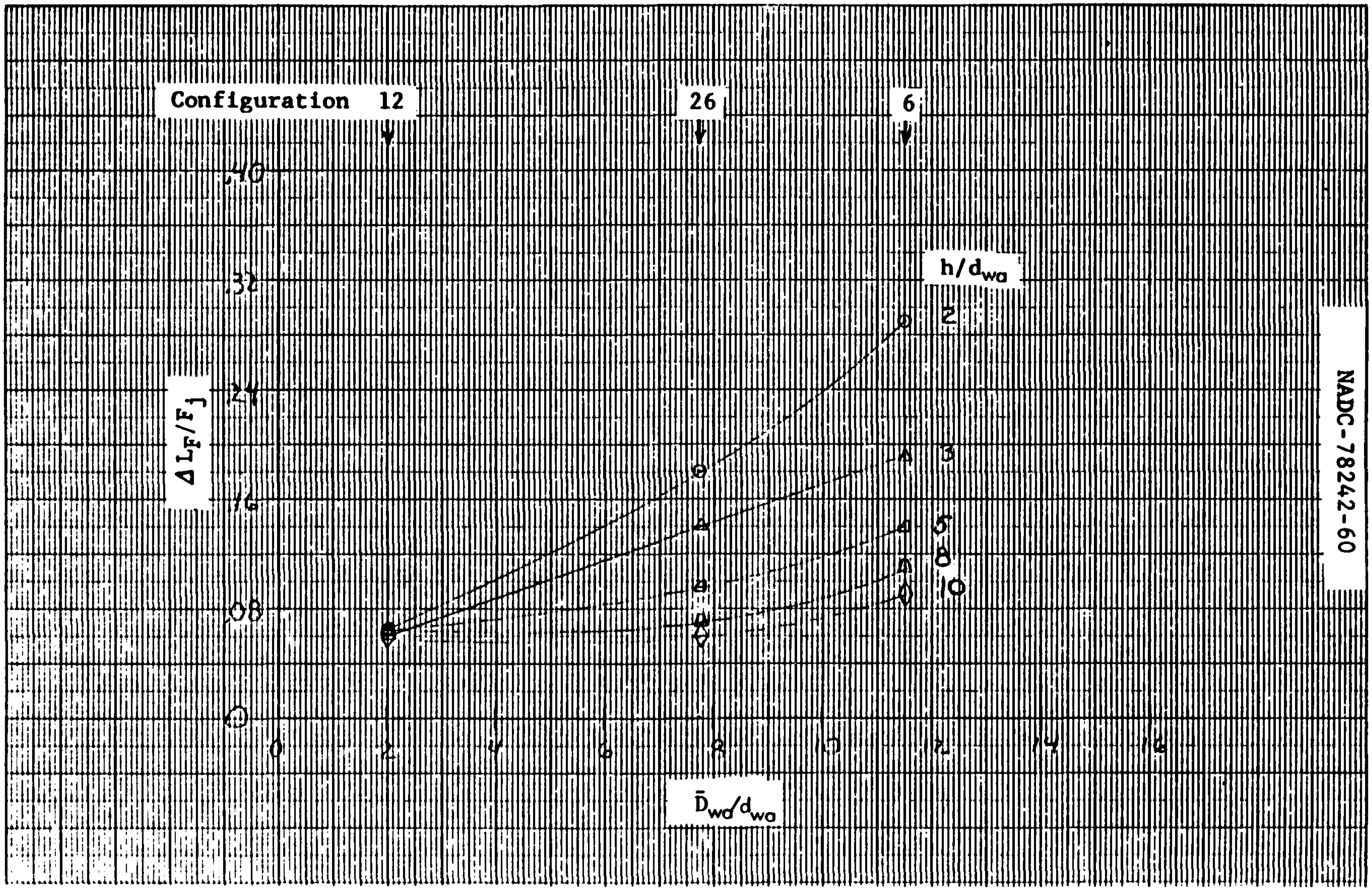

Figure 3.1-11 bis. Fountain Lift - 3-Jet Configuration

TABULATION SHEET

$d_{je} =$ 4.074	$\frac{h}{d_{je}}$	$\frac{\Delta L_F'''}{F_J}$	$\frac{h}{d_E}$-1.374	C_{F_3}'''	$\frac{\Delta L_F''}{F_j}$	$\frac{h}{d_E}$-1.374	C_{F_3}''		C_{F_L}		$\frac{\Delta L_F}{F_j}$	
$\bar{D}_{HA}$ (in)		8.410										
$\bar{D}_{HA}/d_{ave}$		3.836										
d_E (in)			5.047			12.257						
h_m/d_{je}		1.740			4.178							
	1	.130	-.585	1	—	—	0		.779		.101	
	1.5	.088	.190	1	.064	—	0				.069	
	2	.081	.205	.922	.041	—	.078				.061	
	3	.072	.414	.611	.025	-.387	.389				.042	
	4	.065	1.784	.305	.017	-.051	.695				.025	
	5	—	2.573	0	.011	.270	.895				.008	
	6	—	[illegible]	0	.007	.599	.766				.004	

CALCULATION OF FOUNTAIN LIFT

SUBSONIC VSTOL -- 3 NOZZLE CONFIGURATION

FIGURE 3.2-3

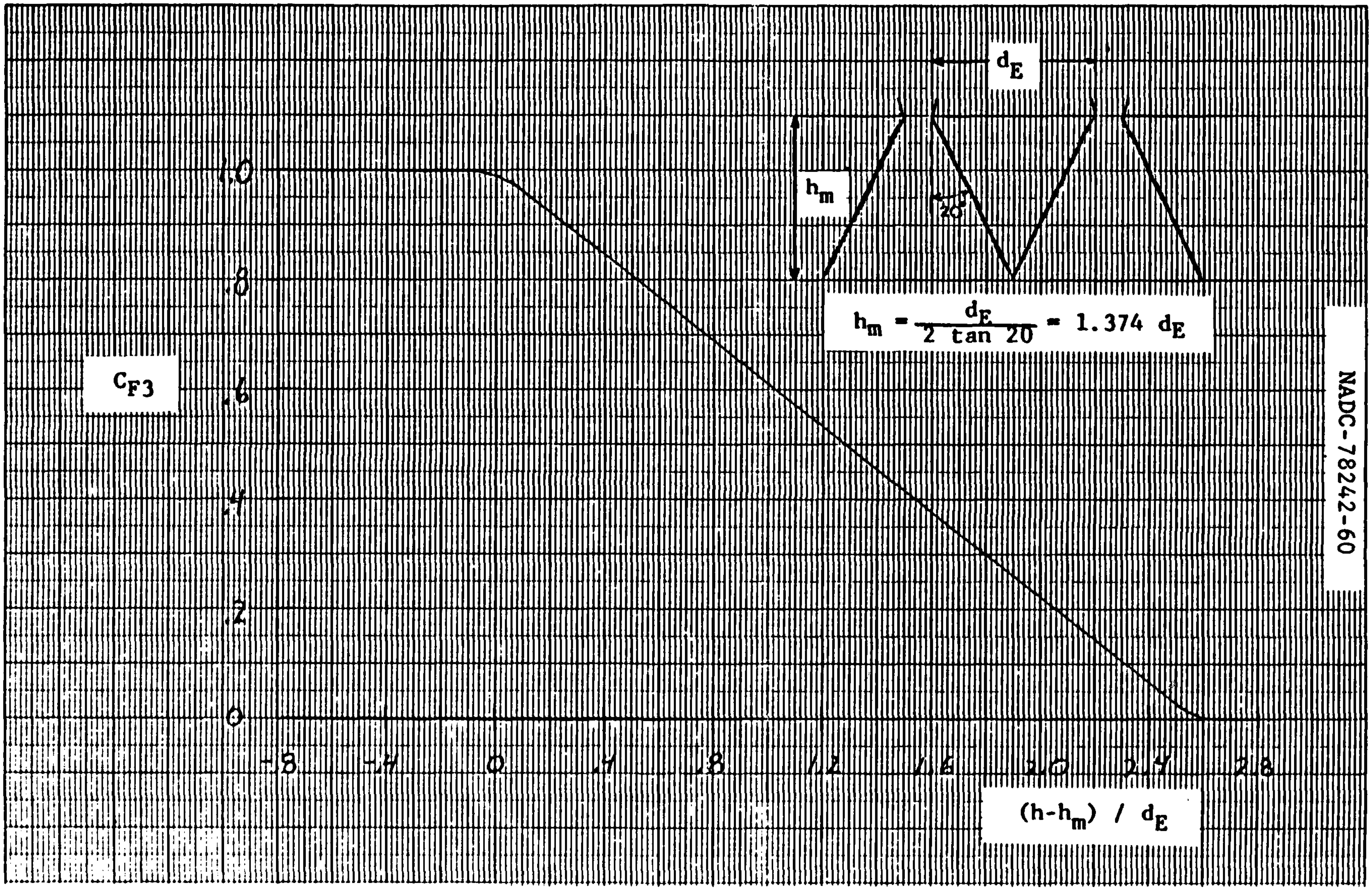

Figure 3.1-6 bis. Effect of Jet Merging On Fountain Lift

fountain is $C_{F3}^{II} = (1-C_{F3}^{III})$ until the three-jet fountain dissipates at $h/d_{je} = 5$. The merging of the forward and aft jets occurs at $h_m/d_{je} = 4.178$ which results in

$$\frac{h}{d_E} - 1.374 = \frac{5(4.024)}{12.237} - 1.374 = 0.270$$

at $h/d_{je} = 5$. The corresponding jet-merging coefficient from Figure 3.1-6 bis becomes $C_{F3}^{II} = 0.895$.

3.2.2.4 <u>Subsonic V/STOL Fountain Lift</u>

The preceding calculations from Blocks II and III are incorporated into Equation 3.1-7 bis to determine total fountain lift of the two-dimensional model considered. At a planform height of $h/d_{je} = 1.5$ we have,

$$\Delta L_F/F_j = 0.779 \left[(.088)\,1.000 + (.064)\ \ .000\right]$$
$$= 0.069$$

The complete computation of fountain lift is listed in Block III of the problem tabulation.

3.2.3 Induced Lift

3.2.3.1 <u>Two-Dimensional Induced Lift</u>

Once the suckdown and fountain lift have been computed, it is possible to determine the induced lift of a two-dimensional flat-plate configuration (Block IV, Figure 3.2-4). Equation 3.1-1 may now be used to relate the total induced lift on the aircraft planform. At $h/d_{je} = 1$, we have

$$(\Delta L/F_j)_{2\text{-}D} = -0.067 + 0.101 = 0.034$$

Figure 3.2-5 presents the predicted induced lift from the preceding calculations compared with test data of the same configuration.

3.2.3.2 <u>Fountain Extrapolation Coefficients C_{F4} and C_{F5}</u>

To incorporate the effect of planform contour into the fountain lift predictions of the subsonic V/STOL

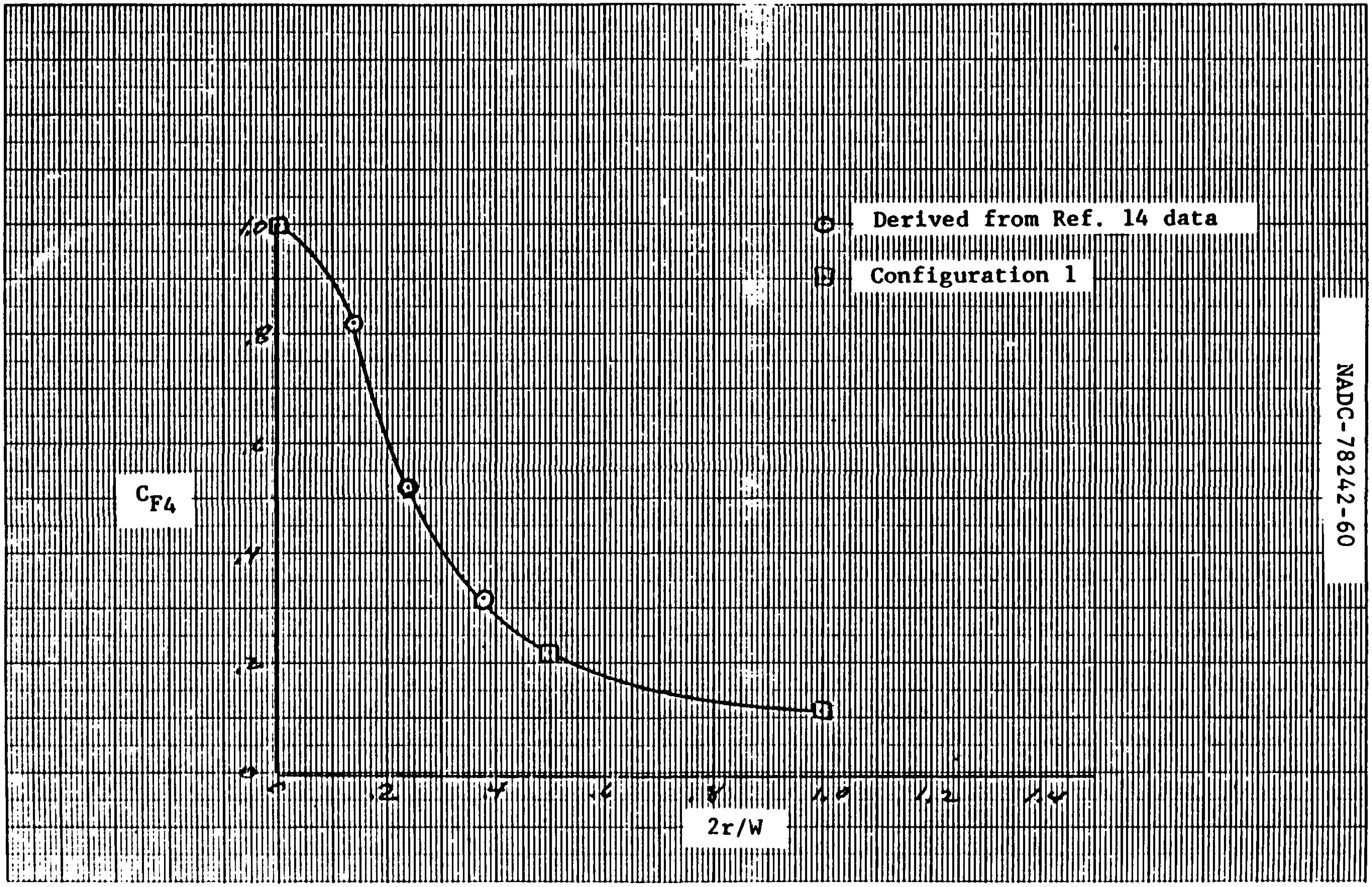

Figure 3.1-7 bis. Effect of Planform Contour - 2 Nozzle Case

TABULATION SHEET

d_{je} = 4.024 in	$\frac{h}{d_{je}}$	$\frac{\Delta L_F}{F_j}$ 2-D	C_{F4}	$\frac{\Delta L_F}{F_j}$ 3-D	C_{F4} LID	C_{F5}	$\frac{\Delta L_F}{F_j}$ LID	$\frac{\Delta L}{F_j}$ 2-D	$\frac{\Delta L}{F_j}$ 3-D	$\frac{\Delta L}{F_j}$ LID
Lr/W			0.5							
	1	.101	.660	.067	.830	1.385	.116	.034	.000	.049
	1.5	.069	.555	.038	.778	↓	.074	.029	-.002	.034
	2	.061	.517	.032	.759	↓	.064	.031	.002	.034
	3	.042	.315*	.013	.657	1.271*	.035	.021	-.008	.014
	4	.025	.220	.006	.610	1.157	.018	.008	-.011	.001
	5	.008	.220	.002	.610	1.149	.006	-.007	-.013	-.009
	6	.004	.220	.001	.610	1.140	.003	-.010	-.013	-.011

* AVERAGE OF 3- AND 2- JET VALUES DUE TO BEING ~1/2 WAY THROUGH MERGING

CALCULATION OF INDUCED LIFT

SUBSONIC VSTOL -- 3 NOZZLE CONFIGURATION

FIGURE 3.2-4

AD-A082 688 GENERAL DYNAMICS CORP FORT WORTH TX FORT WORTH DIV F/G 20/4
V/STOL PROPULSION-INDUCED AERODYNAMICS HOVER CALCULATION METHOD--ETC(U)
FEB 80 W H FOLEY, J A SANSONE N62269-79-C-0212

UNCLASSIFIED NADC-78242-60 NL

2 OF 2
AD A082688

END
DATE FILMED
4-80
DTIC

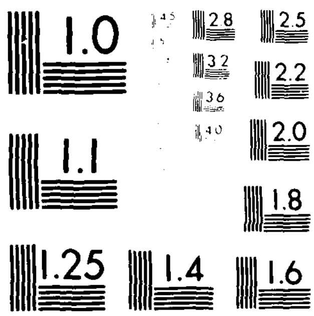

MICROCOPY RESOLUTION TEST CHART

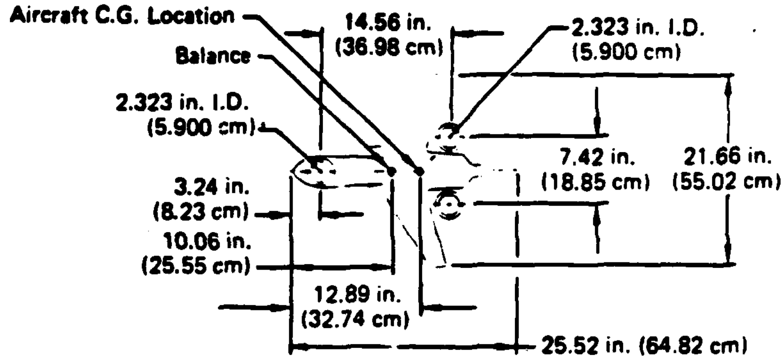

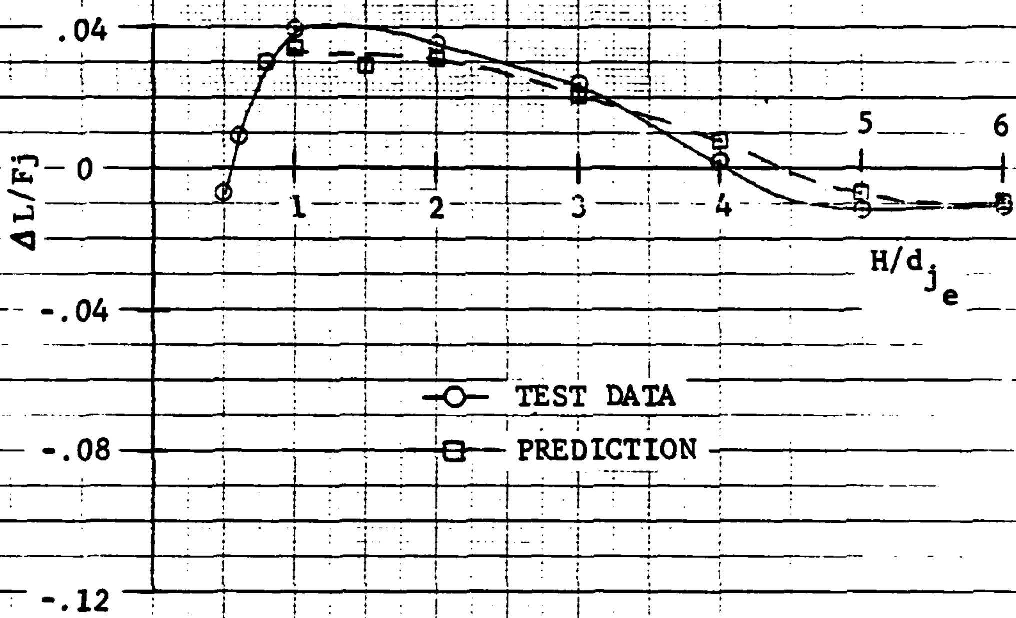

Figure 3.2-5 Induced Lift

MAIR Model 260

Flat Plate Planform - 3 Jet

configuration, it is necessary to compute the planform contour parameter 2r/W. As depicted in Figure 3.1-7 bis, the radius of curvature, r, and fuselage width, w, must be measured. For the subsonic V/STOL

$$r = 1.3 \text{ in}$$
$$w = 5.24 \text{ in}$$

and

$$2r/w = 0.5$$

which is used to index Figure 3.1-7 bis to determine the three-jet fountain extrapolation coefficient for planform contour. As noted in Subsection 3.2.2.3, the three-jet fountain dissipates at a planform height of $h/d_{je} = 4.178$. Above this height, it becomes necessary to determine C_{F4} from Figure 3.1-8 bis which produces

$$C_{F4} = 0.220$$

The values of C_{F4} are listed in Block IV and used to correct the fountain lift of Block III for planform contour, such that

$$(\Delta L_F/F_j)_{3\text{-}D} = C_{F4}\ (\Delta L_F/F_j)_{2\text{-}D}$$
$$= 0.101\ (.660) = 0.067$$

which results in

$$(\Delta L/F_j)_{3\text{-}D} = -.067 + .067 = 0.0$$

at $h/d_{je} = 1$.

Figure 3.2-6 compares the predictions of these computations with actual test data.

To cover the effect of LIDs on the fountain strength, it is first necessary to determine the new coefficient for planform roundness, C_{F4}. The width of the LID and fuselage are

$$\ell_2 = W_{LID} = 2.70 \text{ in}$$

$$\ell_1 = W_{fuselage} = 5.24 \text{ in}$$

Thus, the value of C_{F4} at $h/d_{je} = 1$ becomes

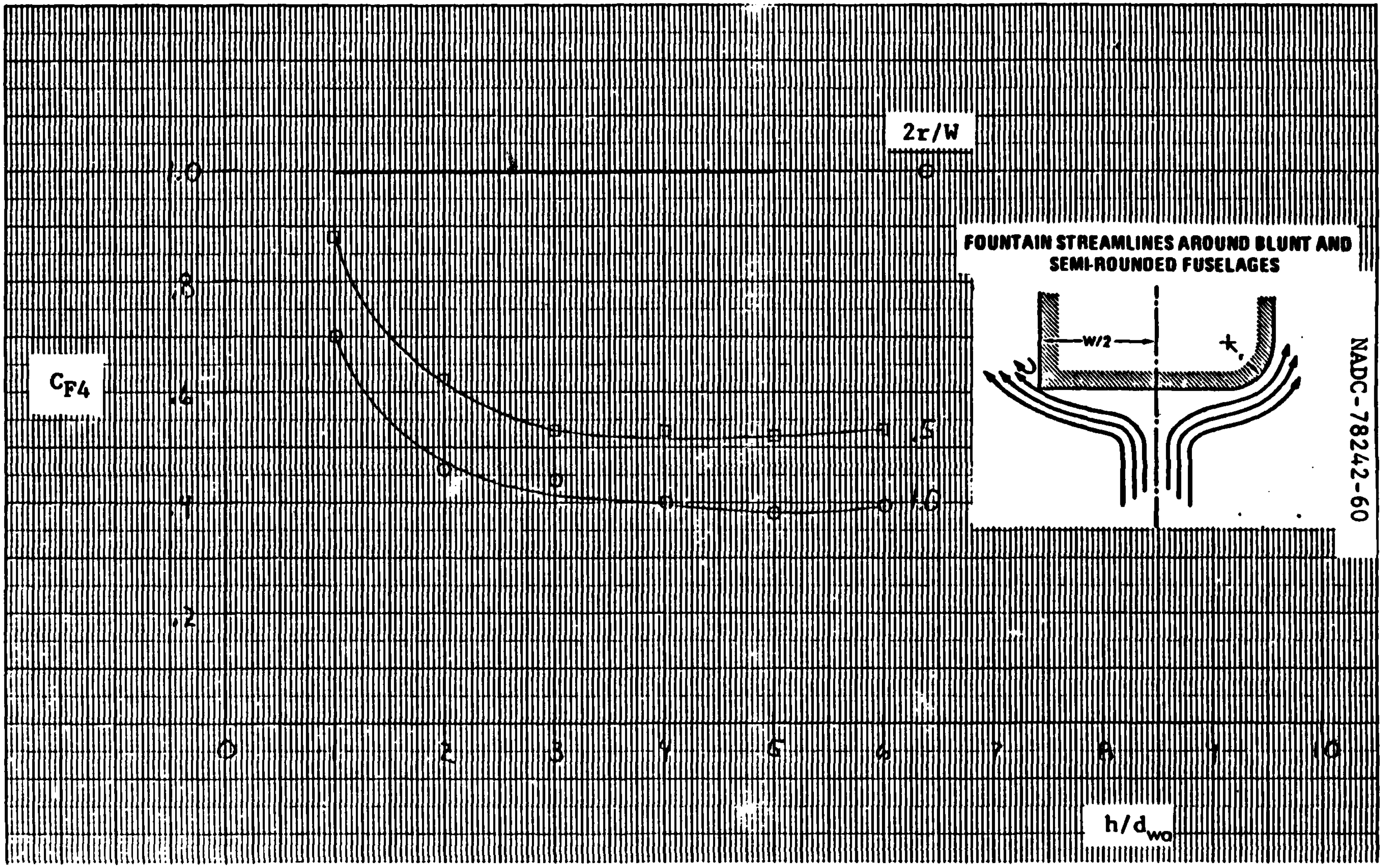

Figure 3.1-8 bis. Effect of Planform Contour - 3 and 4 Nozzle Case

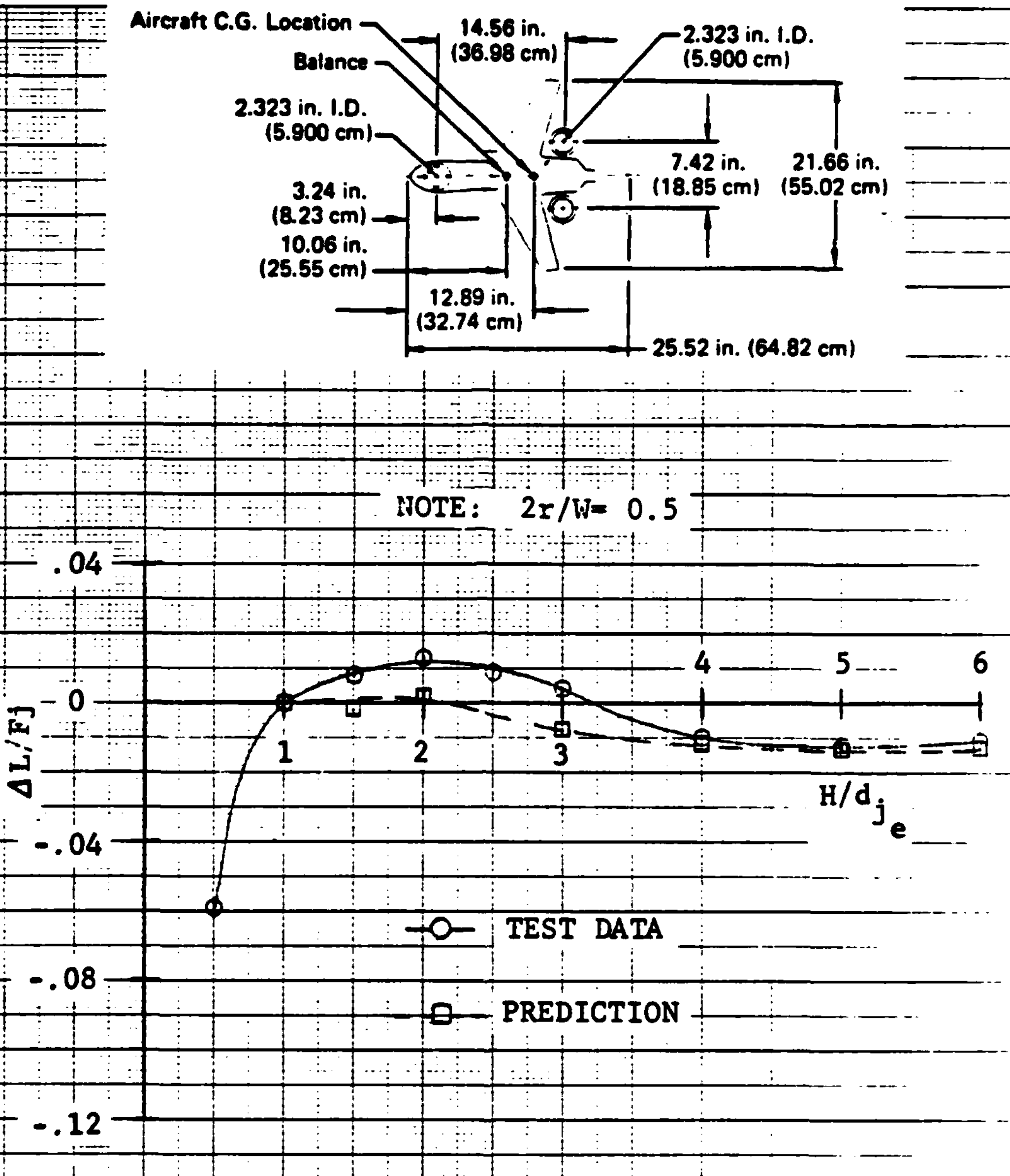

Figure 3.2-6 Induced Lift

MAIR Model 260

Fully Contoured Planform - 3 Jet

$$(C_{F4})_{LID} = 0.66 + \frac{2.70}{5.24}(1-0.660)$$
$$= 0.83$$

as described in Subsection 3.1.5.2.

To evaluate the effect of the LID, the value of C_{F5} must first be set at a theoretical value of 1.75 for a three-sided LID. Because the LID is not as wide as the full fuselage, the extrapolation coefficient for this LID must be modified as shown in Subsection 3.1.5.2.

$$C_{F5} = 1 + (1.75-1)\left[\frac{2.70}{5.24}\right]$$
$$= 1.385$$

for a three-jet fountain. For the case of a two-jet fountain the new coefficient is

$$C_{F5} = 1 + (1.75-1)\left[\frac{\sin 10.5 \text{ degrees}}{\sin 56 \text{ degrees}}\right]$$
$$= 1.165$$

These values for C_{F5} are shown on Block IV of the tabulation sheet and have been used in conjunction with C_{F4} to correct the two-dimensional fountain strength to account for the LID effects on induced lift. The new fountain lift for this configuration at $h/d_{je} = 1$ is

$$(\Delta L_F/F_j)_{LID} = 0.101\ (0.830)\ 1.385$$
$$= 0.116$$

so that induced lift has improved over the configuration without the LID.

$$(\Delta L/F_j) = 0.116 - 0.067 = 0.049$$

The comparison plot of predicted and actual test data for the subsonic V/STOL with LID is shown in Figure 3.2-7.

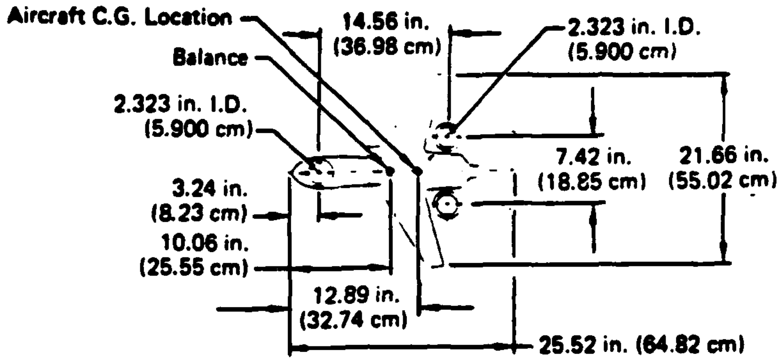

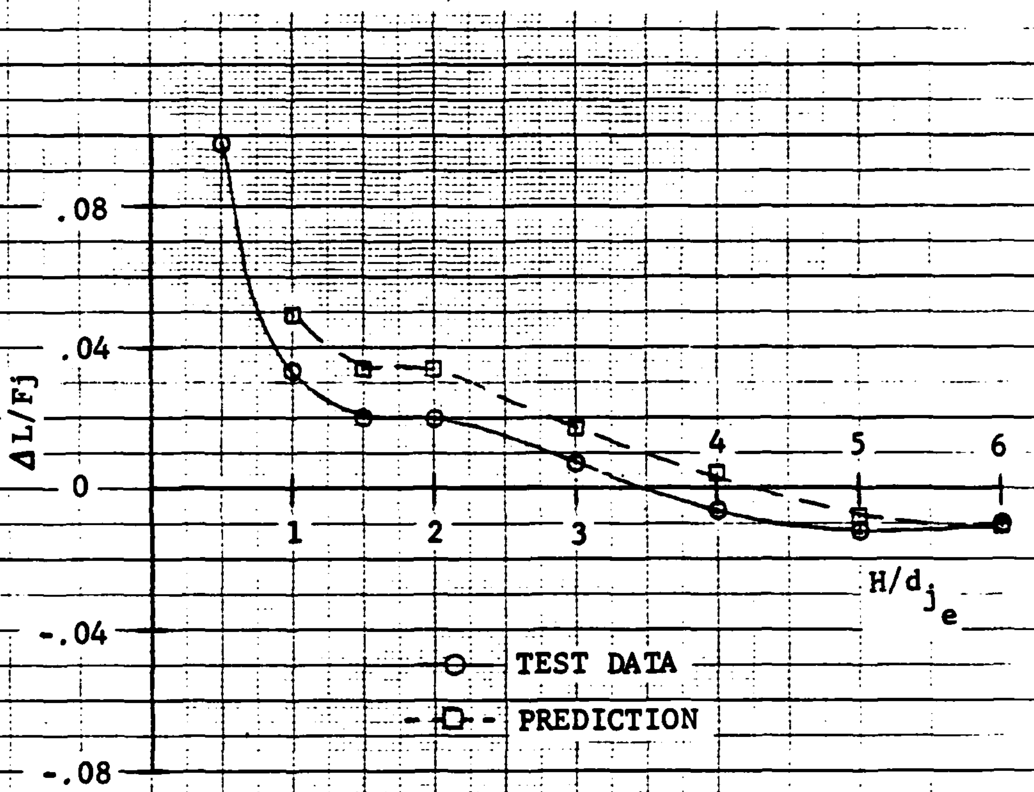

Figure 3.2-7 Induced Lift

MAIR Model 260

Fully Contoured Planform

3 Jet w/LIDs

4. CORRELATIONS

The methodology of Section 3 has been applied to several configurations taken from Refs. 13 and 14. The comparisons between the predictions and the test data are shown in Figures 4.0-1 through 4.0-10. Across the range of variables involved, the methodology appears capable of accuracies of about $\pm .01 \Delta L/F_j$.

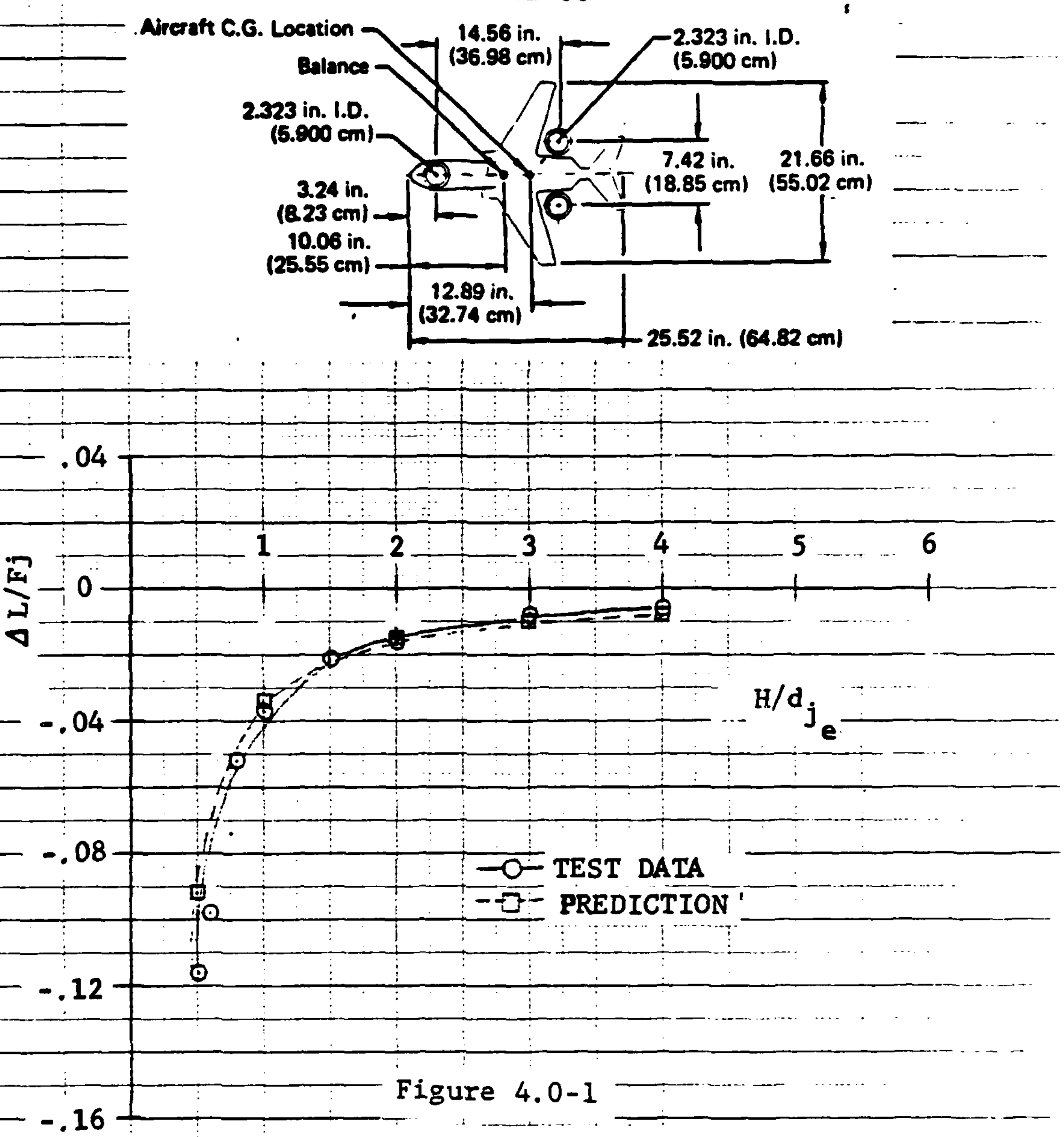

Figure 4.0-1

INDUCED LIFT

MAIR Model 260

Single Jet

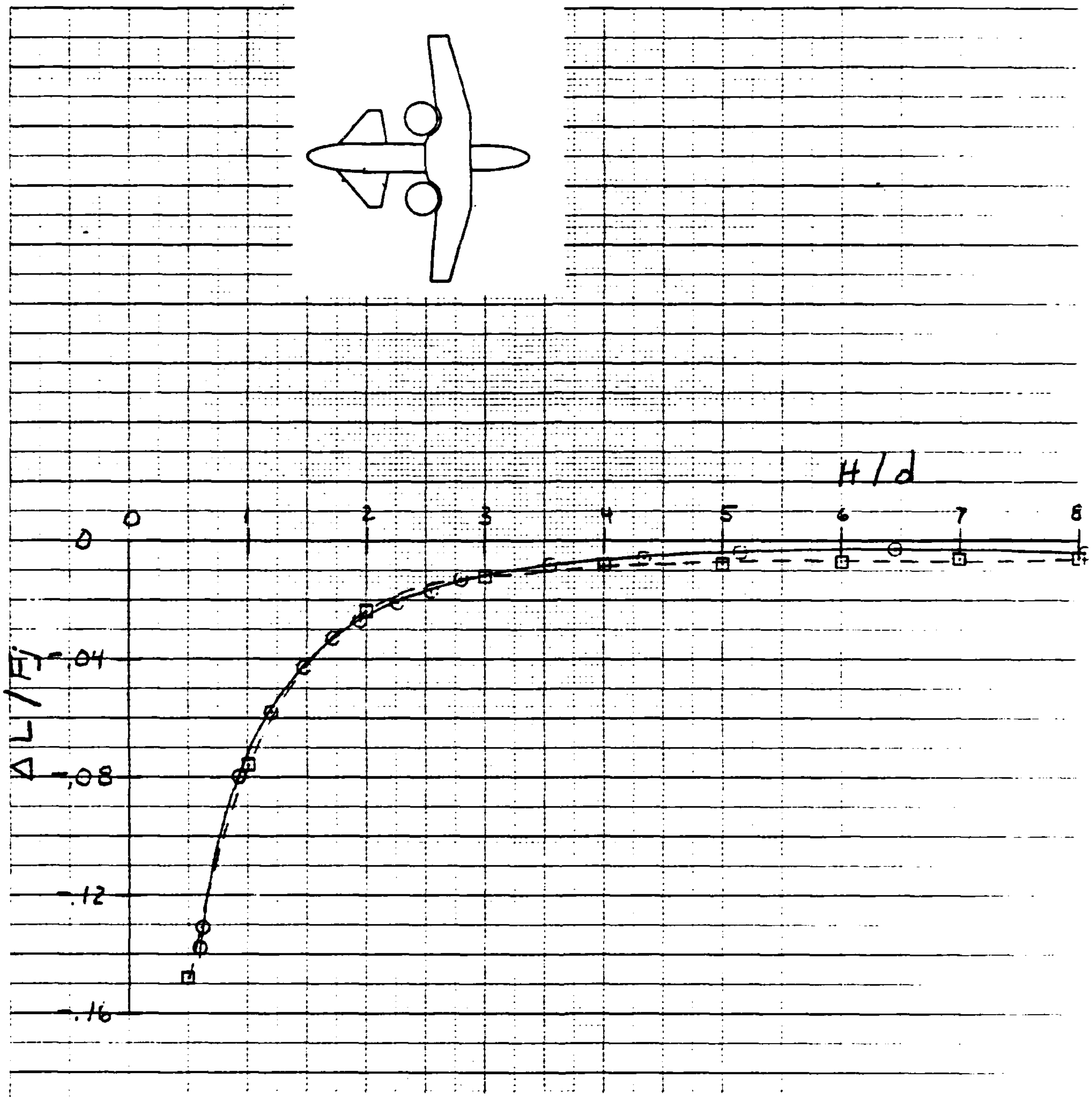

Figure 4.0-2 Induced Lift

Grumman Design 698-309

Single Jet Operation

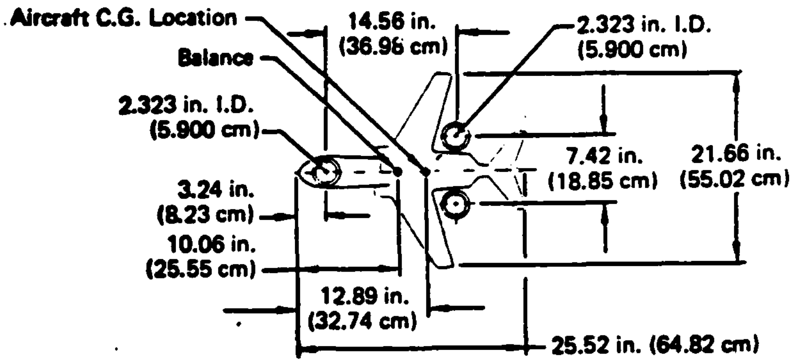

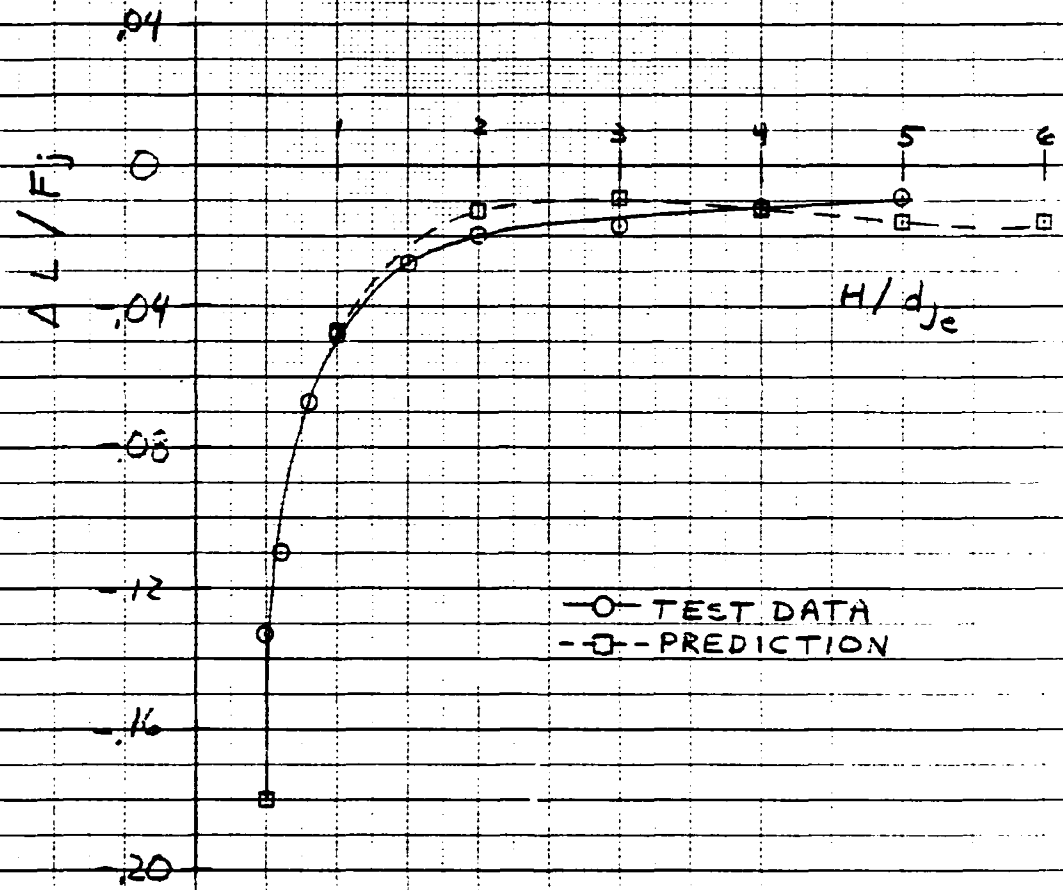

Figure 4.0-3 Induced Lift

MAIR Model 260

Fully Contoured Planform - 2 Jet

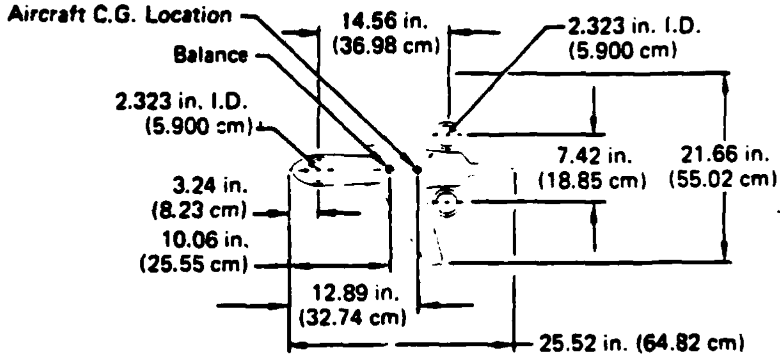

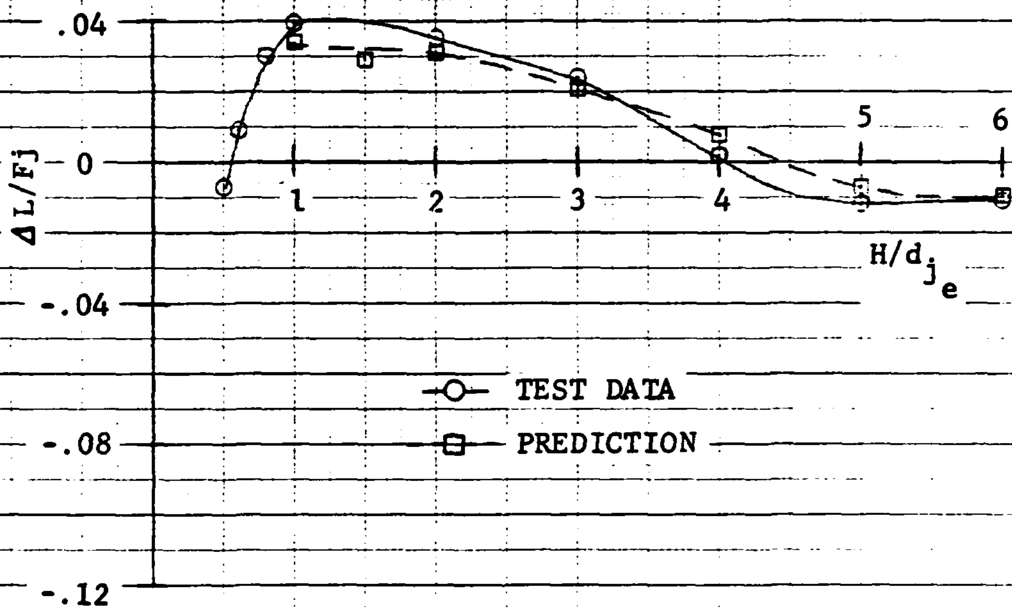

Figure 4.0-4 Induced Lift

MAIR Model 260

Flat Plate Planform - 3 Jet

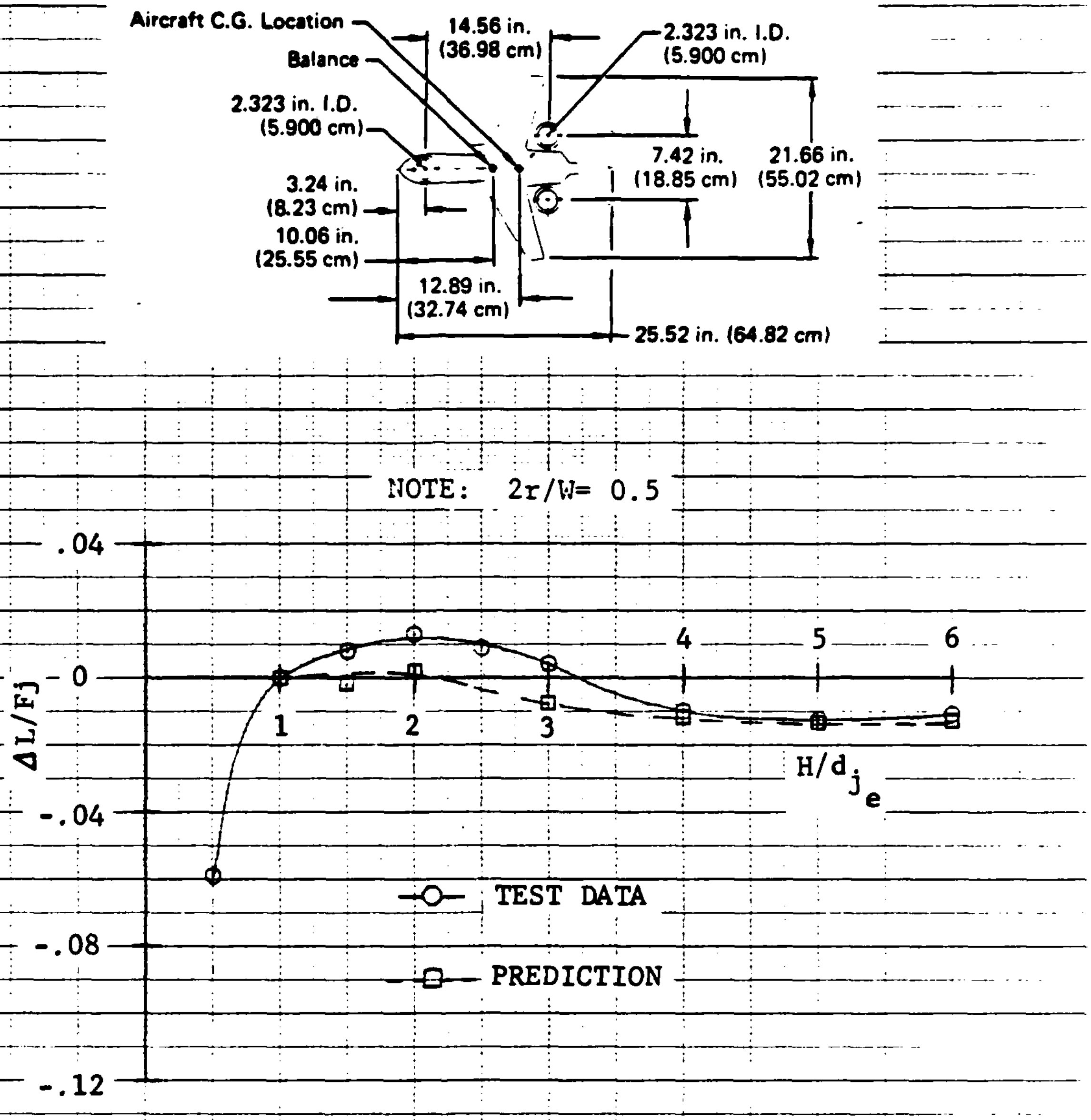

Figure 4.0-5 Induced Lift

MAIR Model 260

Fully Contoured Planform - 3 Jet

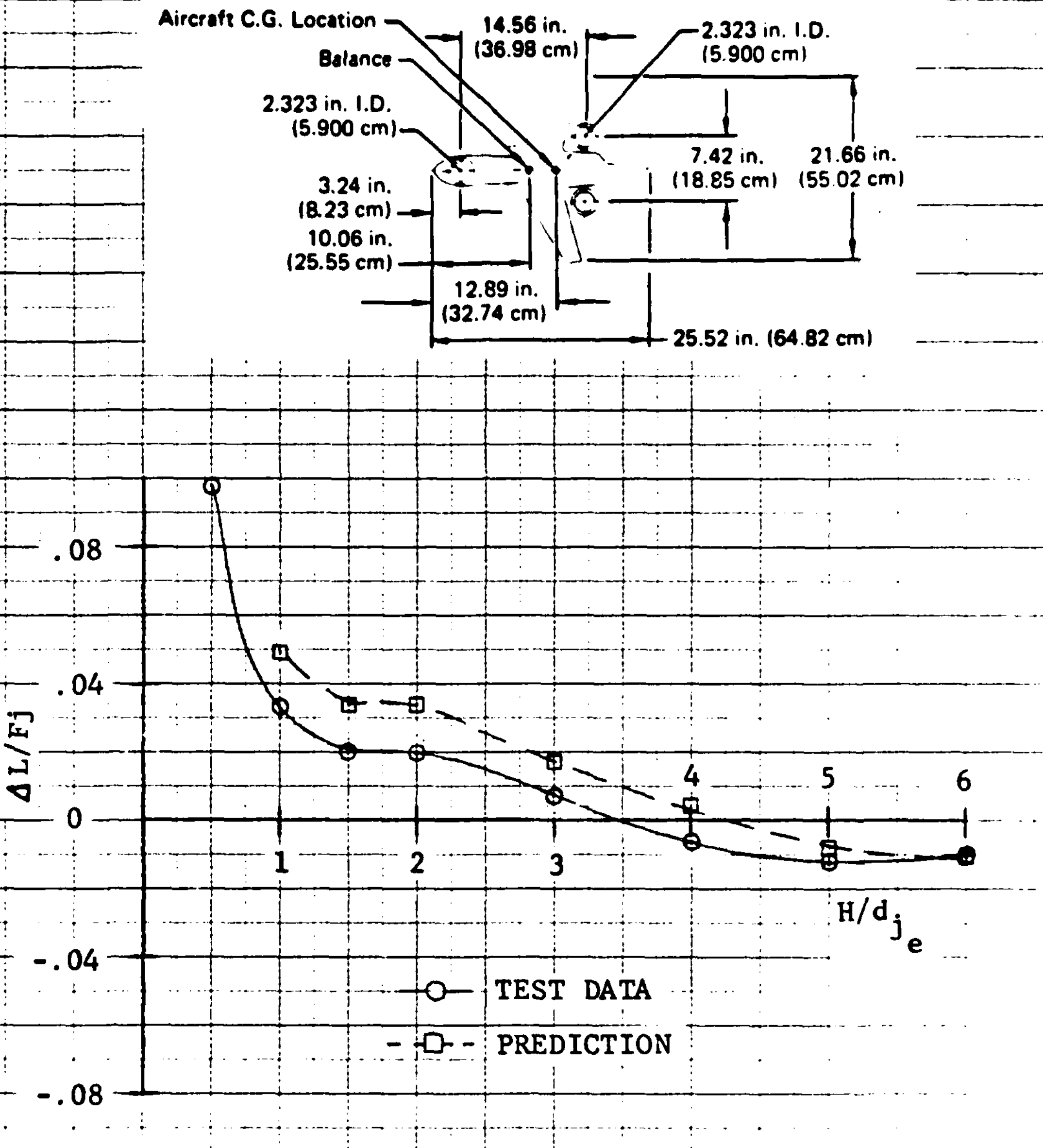

Figure 4.0-6 Induced Lift

MAIR Model 260

Fully Contoured Planform

3 Jet w/LIDs

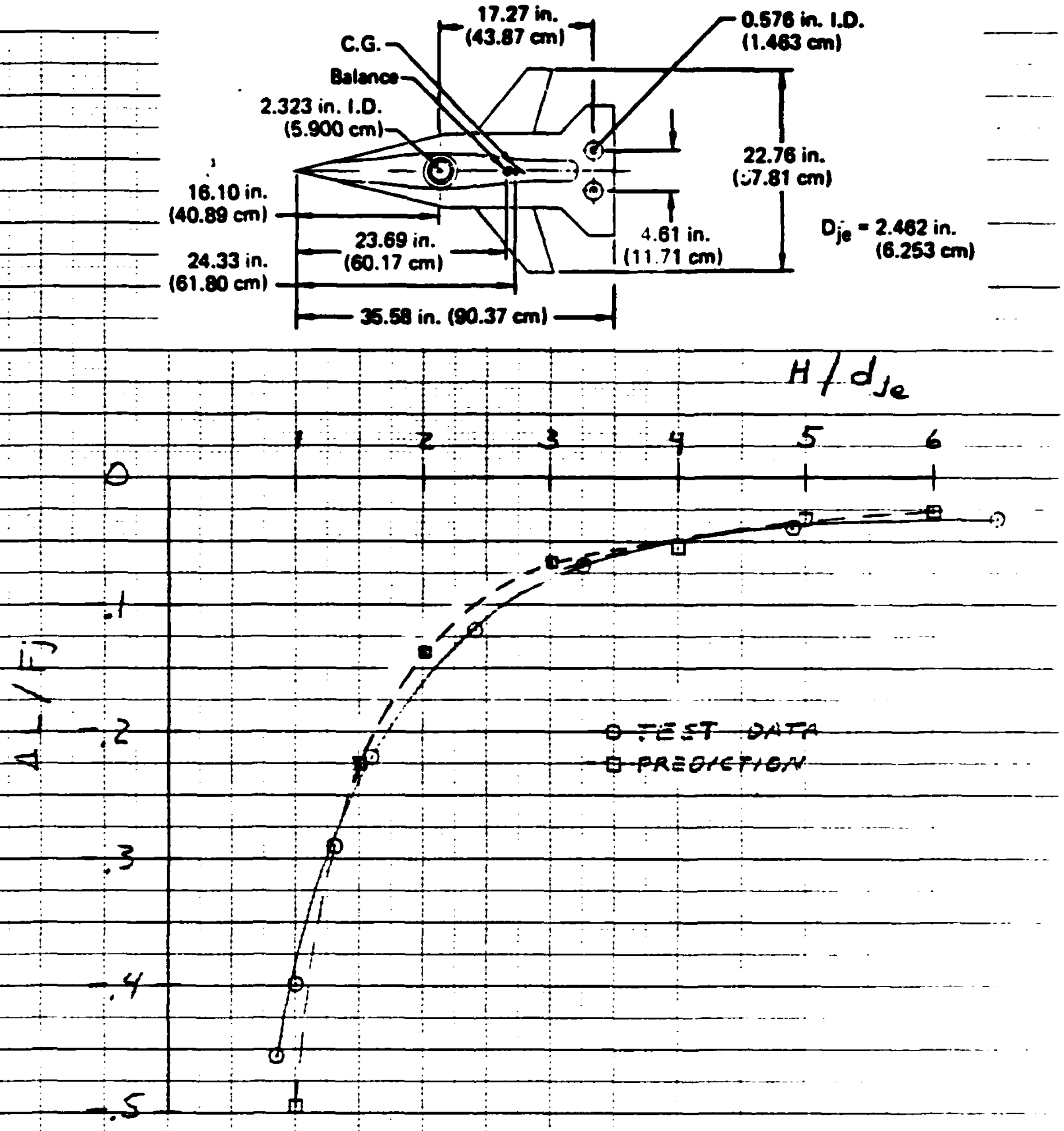

Figure 4.0-7 Induced Lift

MAIR Supersonic VSTOL

Flat Plate Planform - 3 Jet

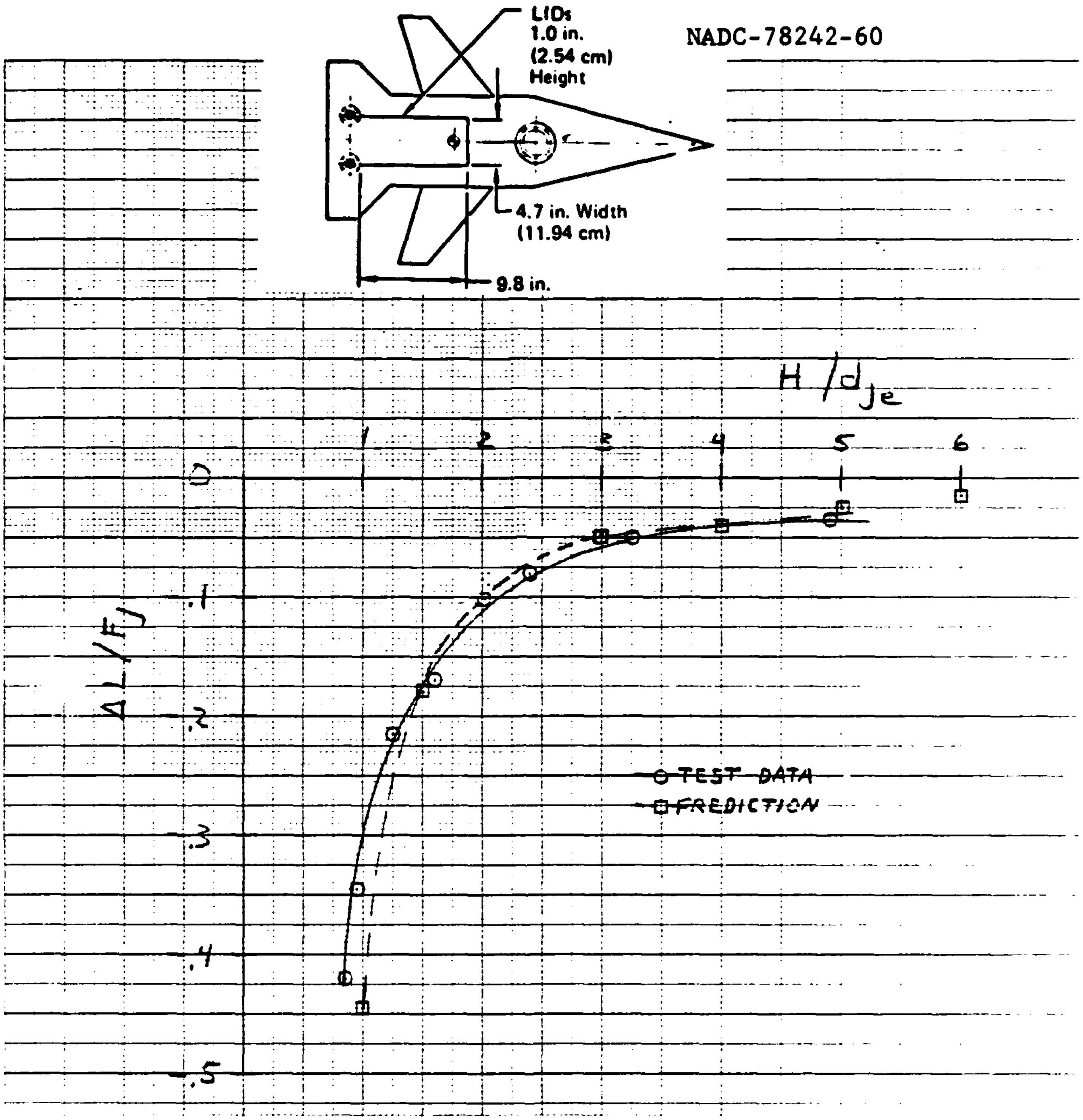

Figure 4.0-8 Induced Lift

MAIR Supersonic VSTOL

Flat Plate Planform

3 Jet with LID

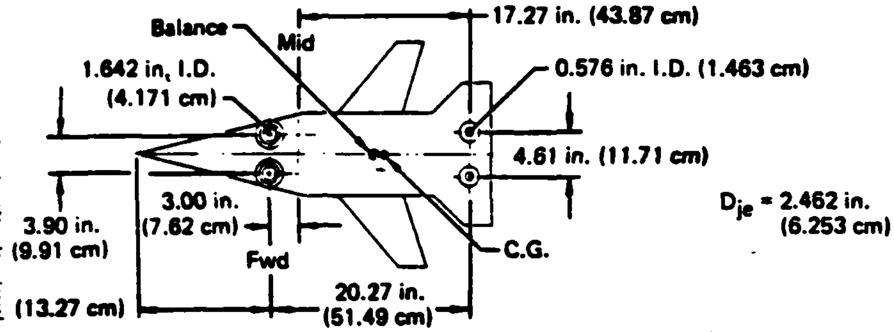

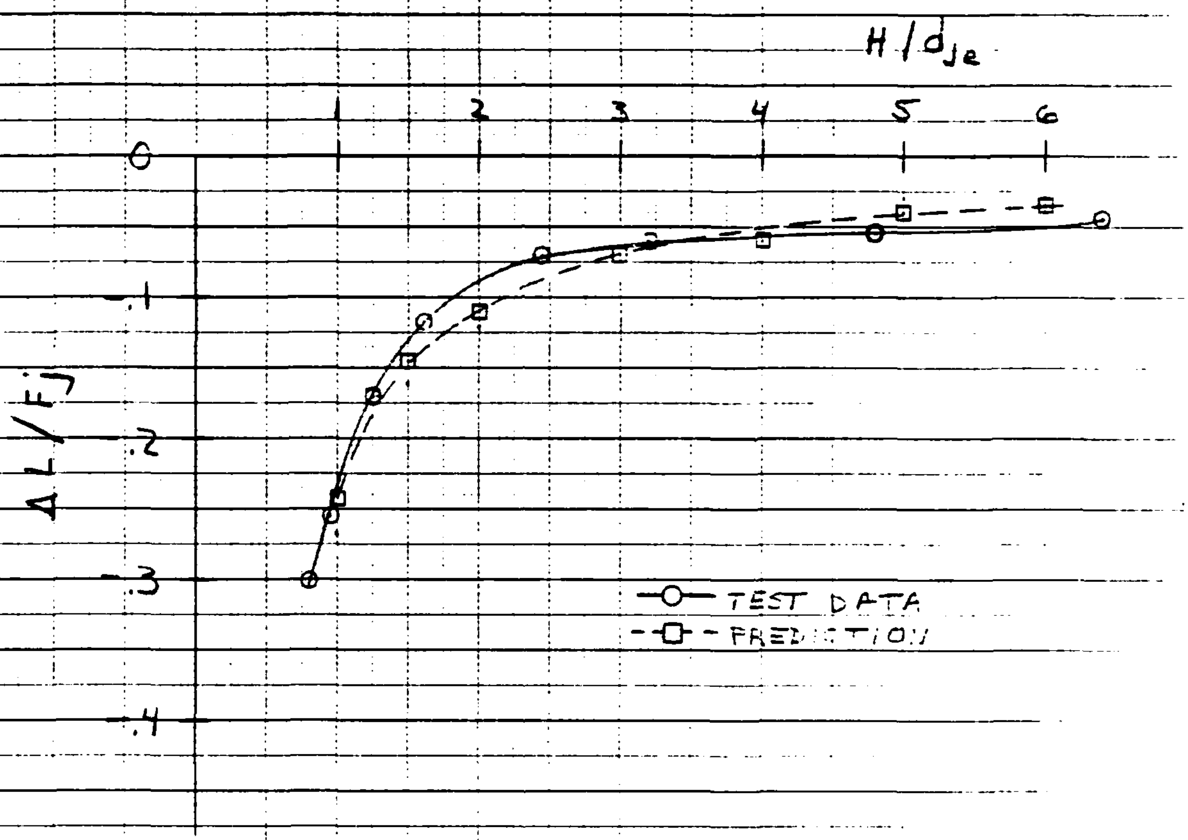

Figure 4.0-9 Induced Lift

MAIR Supersonic VSTOL

Flat Plate Planform

4 Jet

(mid-jet location)

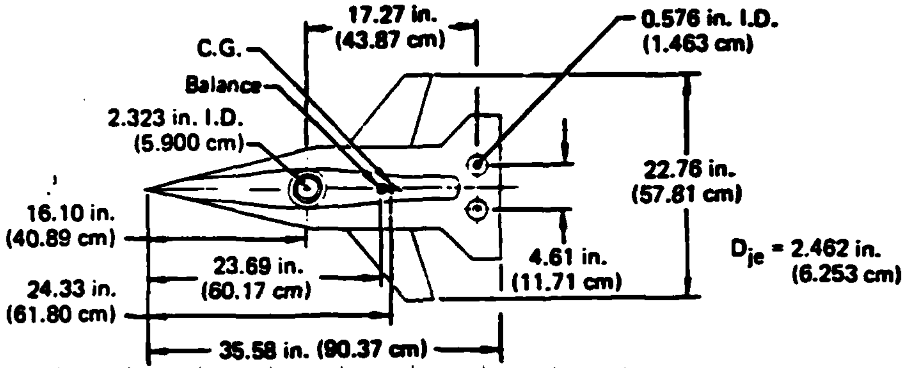

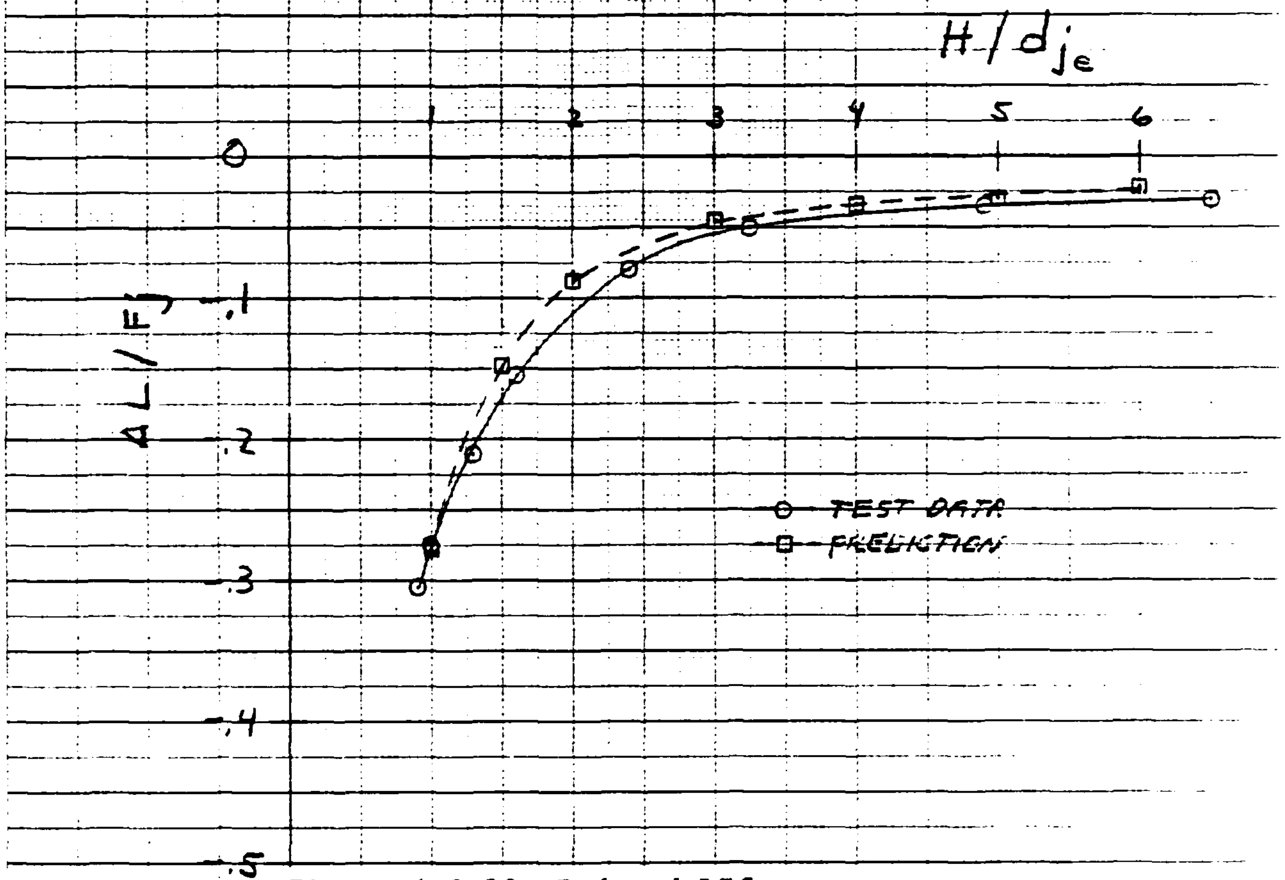

Figure 4.0-10 Induced LIft

MAIR Supersonic VSTOL

Semi-Contoured Planform

3 Jet

REFERENCES

1. Spreeman, K.P. and Sherman, I.R., Effects of Ground Proximity on the Thrust of a Simple Downward Directed Jet Beneath a Flat Surface, NACA TN 4407, 1958.

2. Davenport, E.E. and Spreeman, K.P., Thrust Characteristics of Multiple Lifting Jets in Ground Proximity, NASA TN D-513, 1960.

3. Vogler, R.D., Ground Effects on Single and Multiple Jet VTOL Models at Transition Speeds Over Stationary and Moving Ground Planes, NASA TN D-3213, 1966.

4. Wyatt, L.A., Static Tests of Ground Effect on Planforms Fitted with a Centrally Located Round Lifting Jet, Ministry of Aviation C.P. 749, 1962.

5. Kotansky, D.R., Durando, N.A., and Bristow, D.R., Jet-Induced Forces and Moments In and Out of Ground Effect, McDonnell Aircraft Company Report, June, 1977.

6. Siclari, M.J., Barche, J., and Migdal, D., V/STOL Aircraft Prediction Technique Development for Jet-Induced Lift in Hover, Grumman Aerospace Corp. PDR 623-18, April, 1975.

7. Karemaa, A., Smith, C.W., Weber, H.A., and Garner, J.E., The Aerodynamic and Thermodynamic Characteristics of Fountains and Some Far-Field Temperature Distributions, Office of Naval Research Report ONR-CR212-237-1F, July, 1978.

8. Smith, C.W. and Karemaa, A., Induced Effects of Multiple-Jet Fountains on Flat-Plate Surfaces, AIAA Paper No. 78-1516, August, 1978.

9. Kuhn, R., An Empirical Method for Estimating Jet Induced Lift Losses of V/STOL Aircraft Hovering In and Out of Ground Effect, Proceedings of the Workshop on VSTOL Aerodynamics, May, 1979.

10. Siclari, J.J., Hill, W.G., and Jenkins, R.C., Investigation of Stagnation Line and Upwash Formation, AIAA Paper No. 78-1516, August, 1978.

11. Lummus, J.R., The Criticality of Engine Exhause Simulations on VSTOL Model-Measured Ground Effects, Office of Naval Research Report No. ONR-CR212-255-1F, August, 1979.

12. Foley, W.H., Methodology for Prediction of V/STOL Propulsion Induced Forces in Ground Effect, AIAA Paper 79-1281.

13. Kamnan, J.H. and Hall, C.L., Lift System Induced Aerodynamics of V/STOL Aircraft in a Moving Deck Environment, McDonnel Aircraft Company Report No. NADC-77-107-30, September, 1978.

14. Wohllebe, E.A. and Migdal, D., Some Basic Test Results of V/STOL Jet-Induced Lift Effect in Hover, AIAA Paper No. 79-0339, January, 1979.

15. Gentry, G.L. and Margason, R.J., Jet-Induced Lift Losses on VTOL Configurations Hovering In and Out of Ground Effect, NASA TN D-3166, 1966.

APPENDIX A - FORCE DATA

A complete set of force balance data obtained during this program is contained on Figures A-1 through A-14.

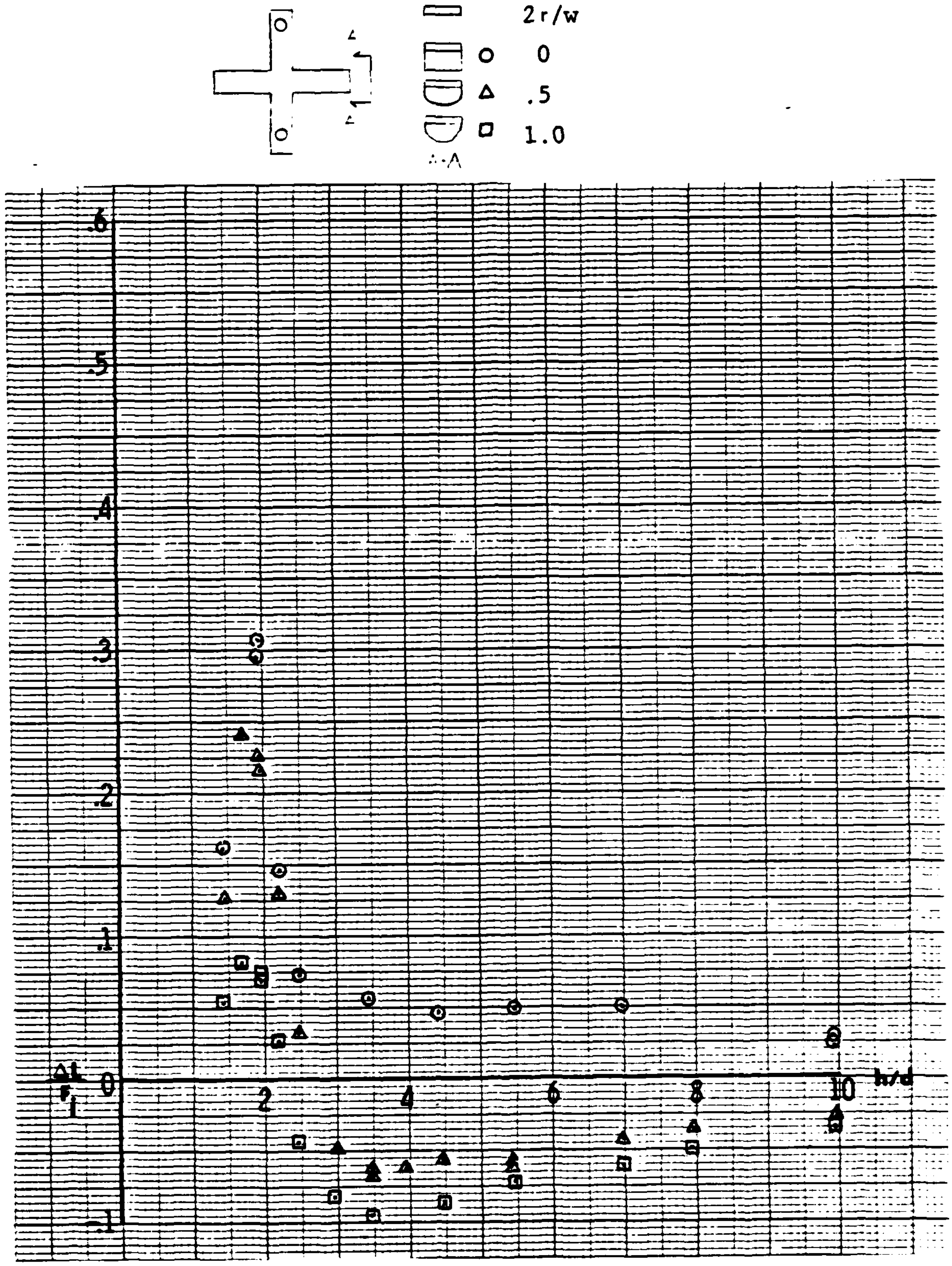

Figure A-1. Configuration 1

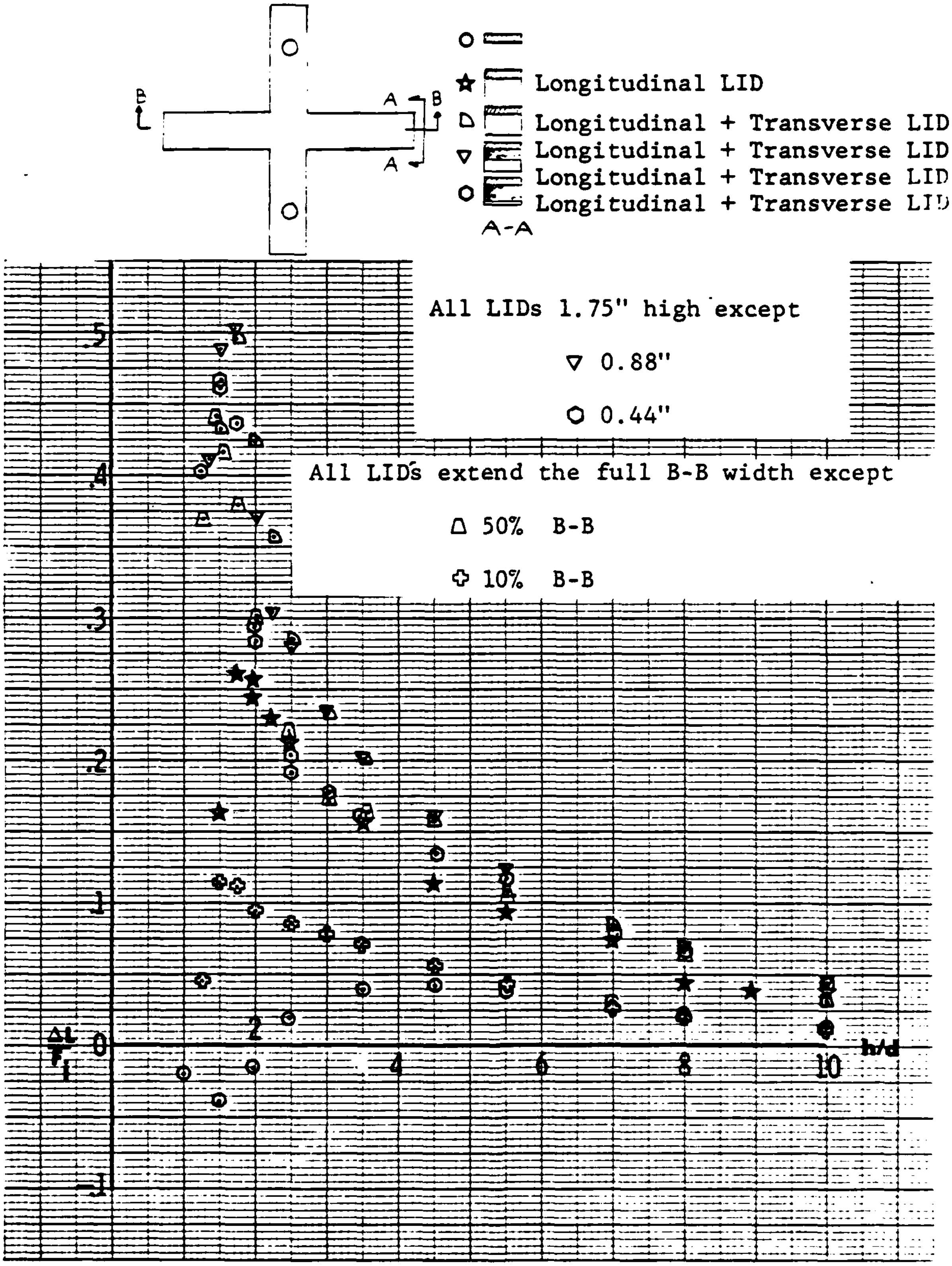

Figure A-2. Configuration 1

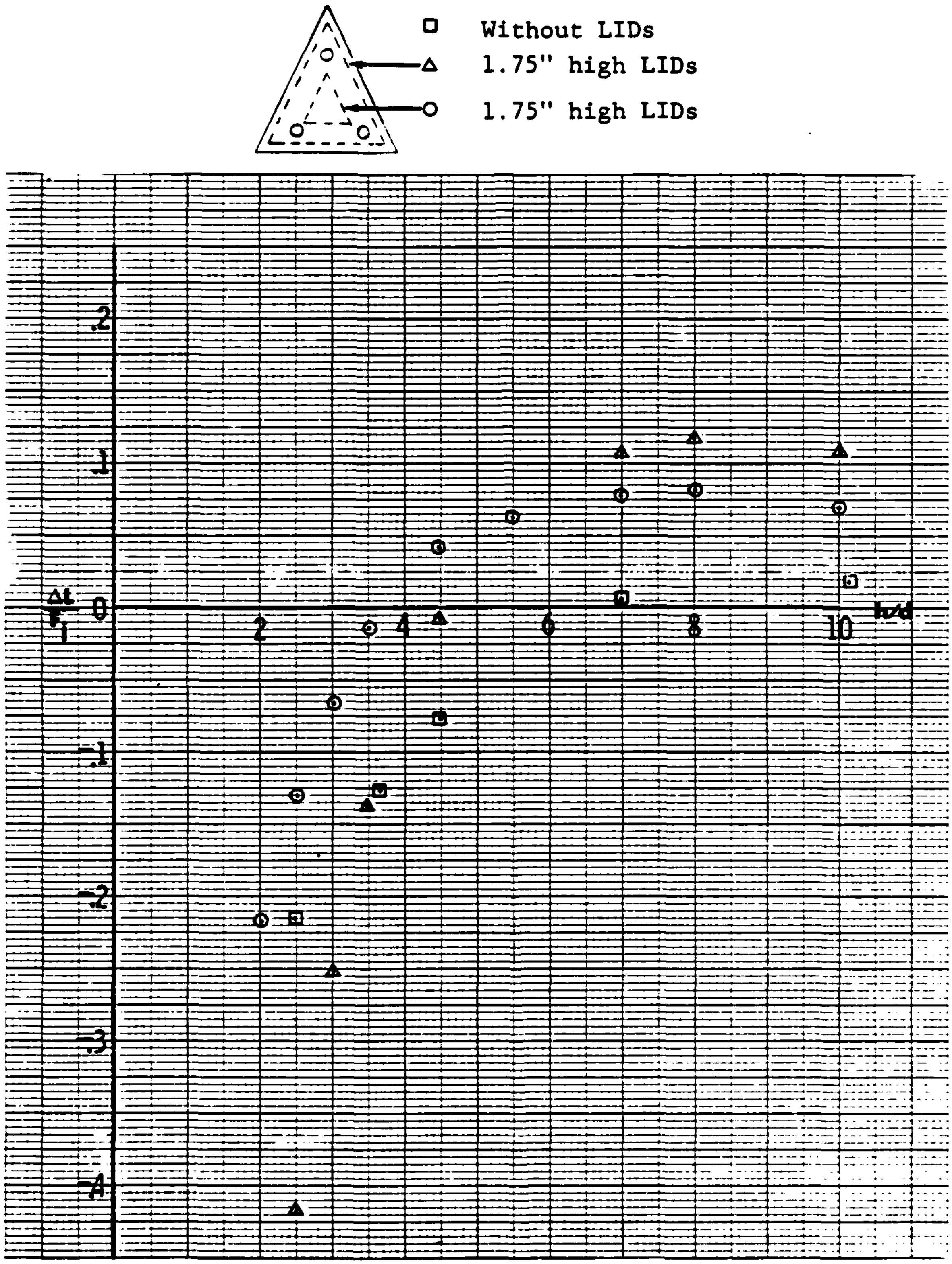

Figure A-3. Configuration 6

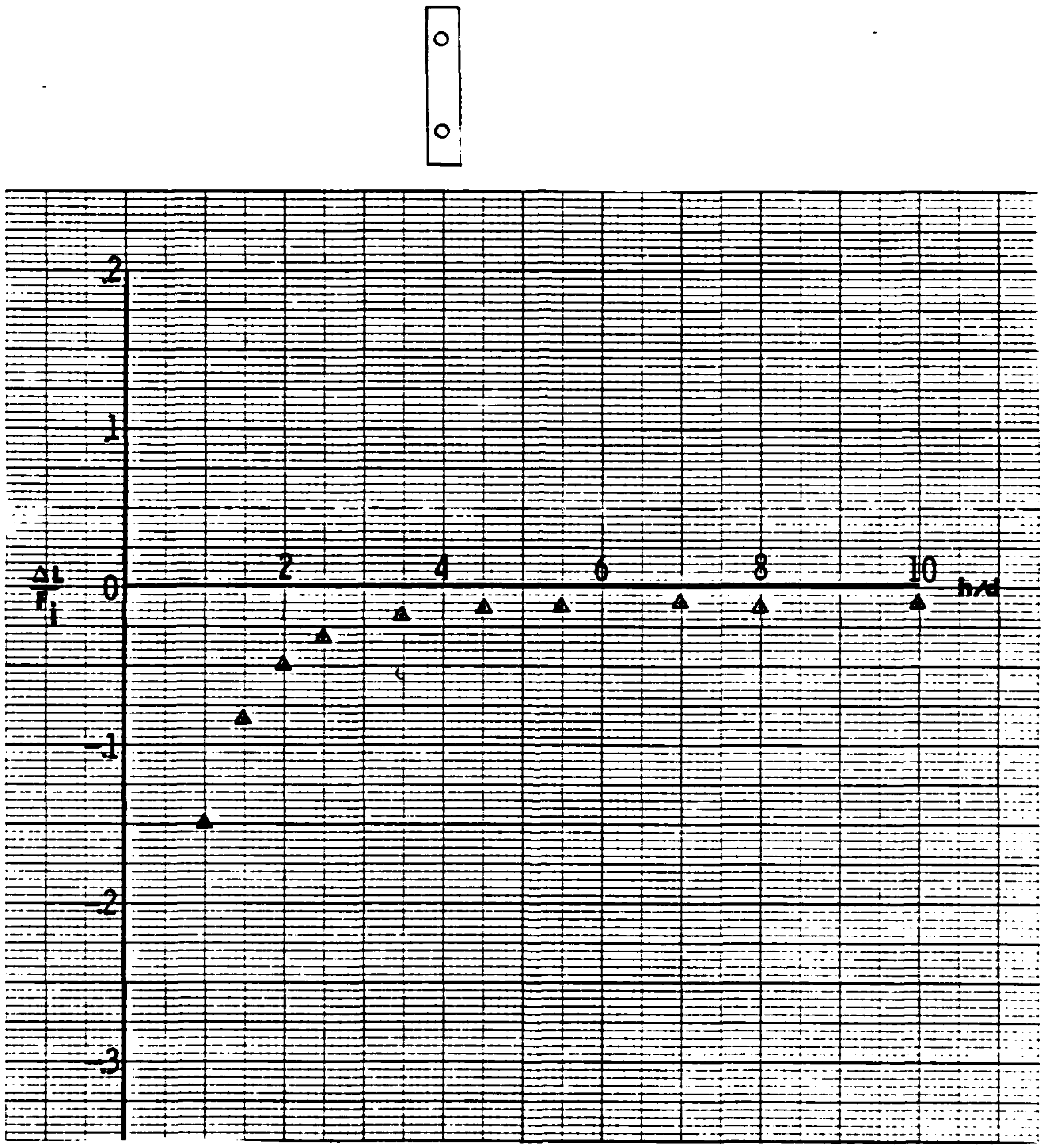

Figure A-4. Configuration 10

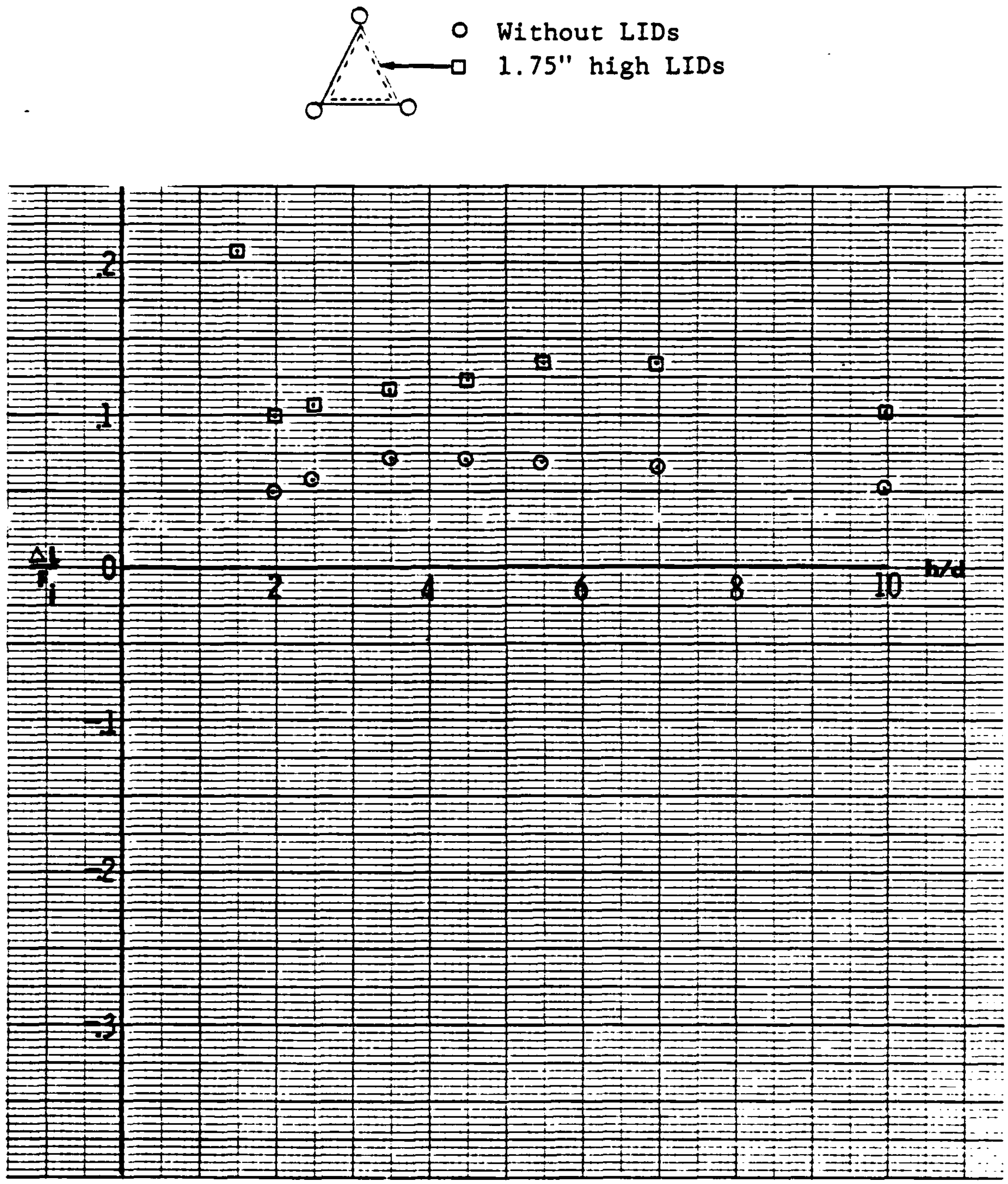

Figure A-5. Configuration 12

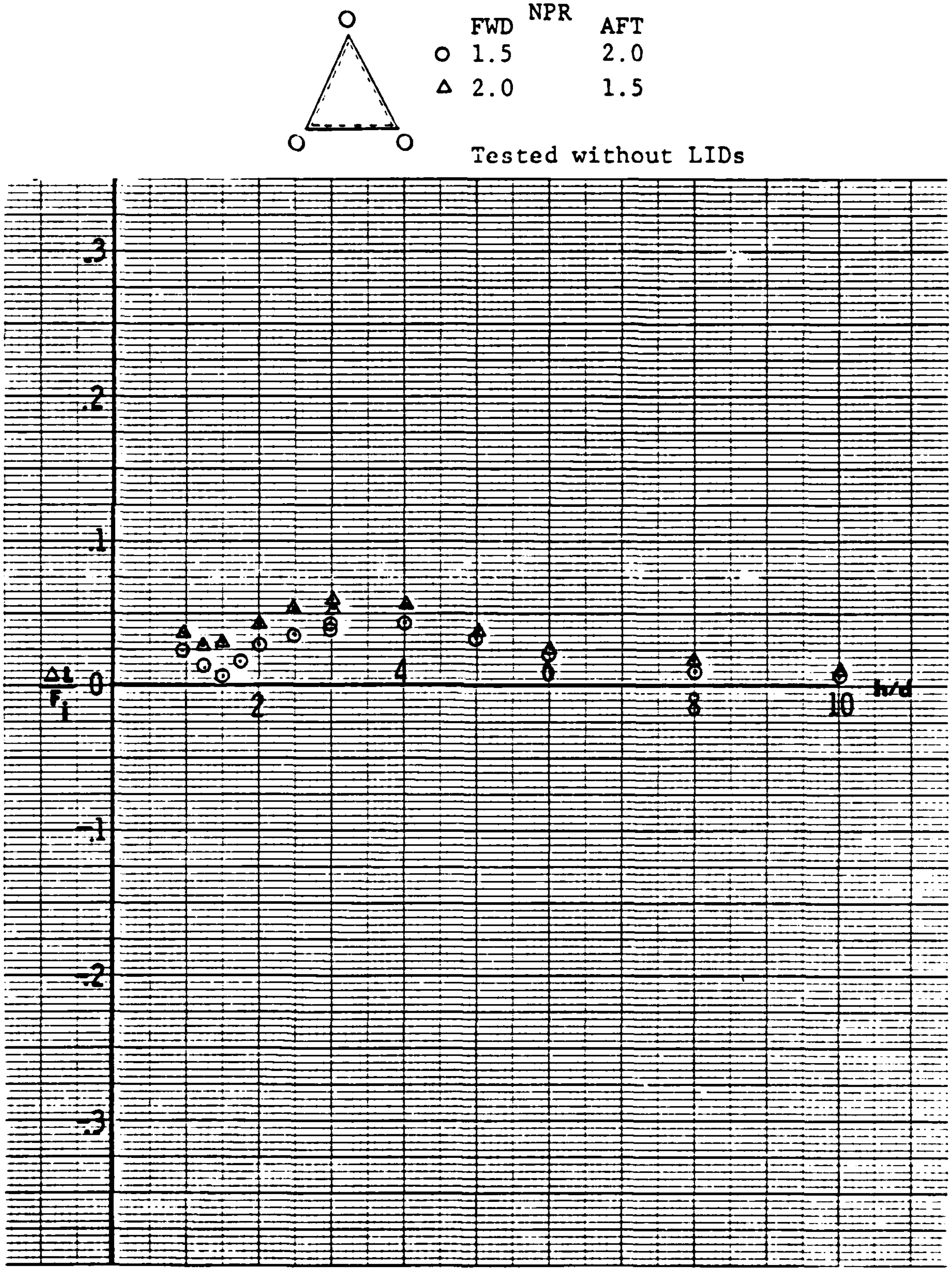

Figure A-6. Configuration 12

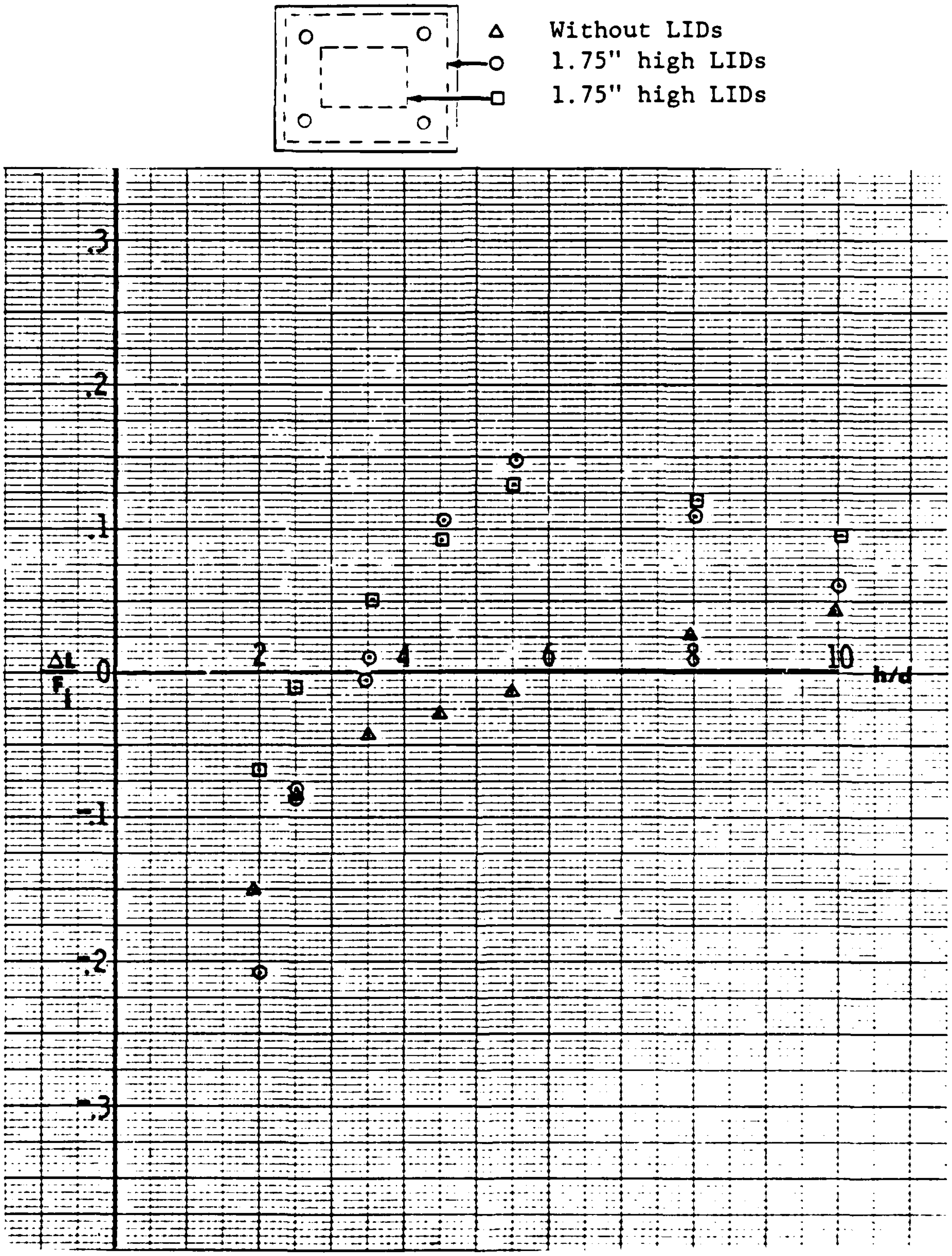

Figure A-7. Configuration 13

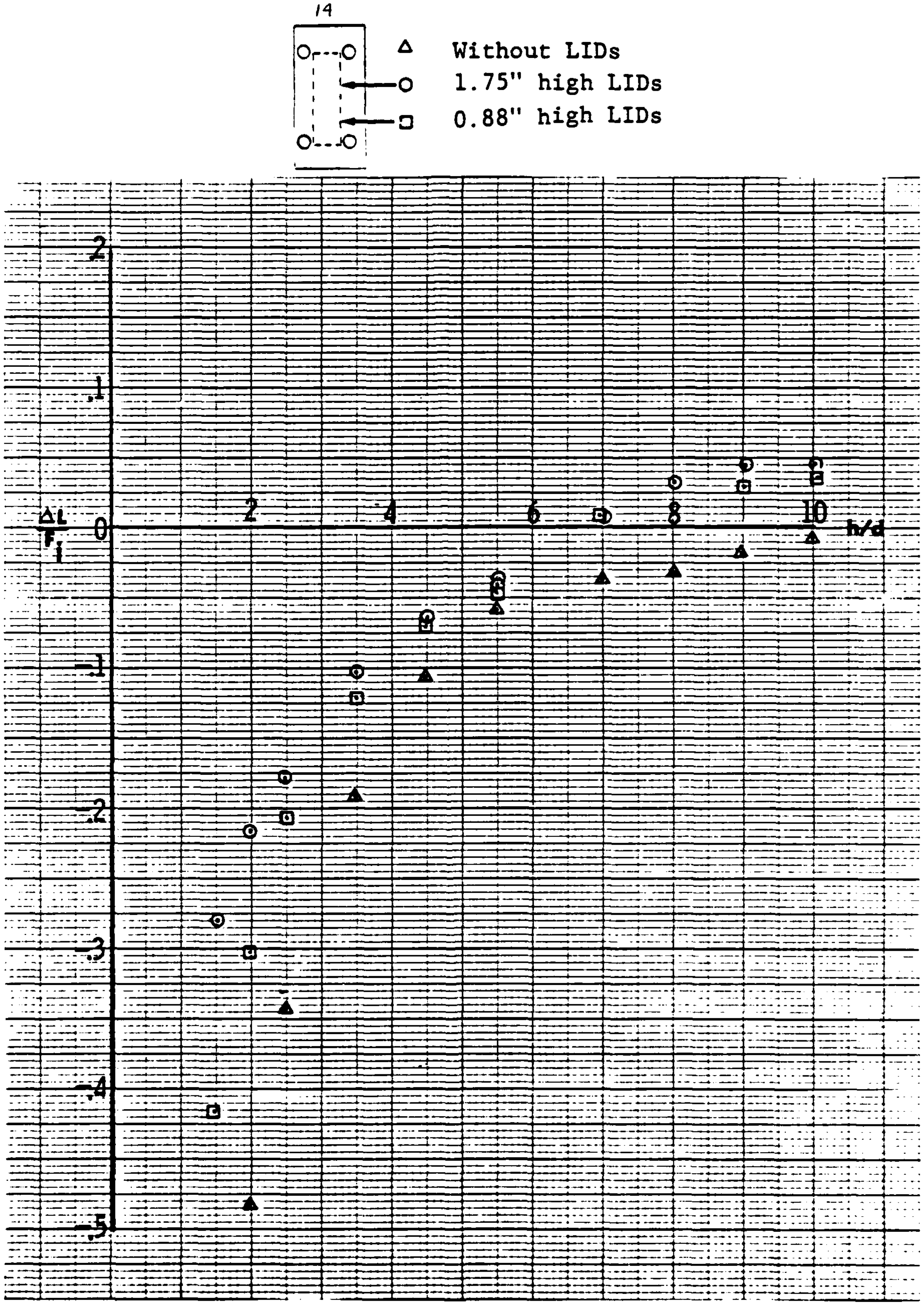

Figure A-8. Configuration 14

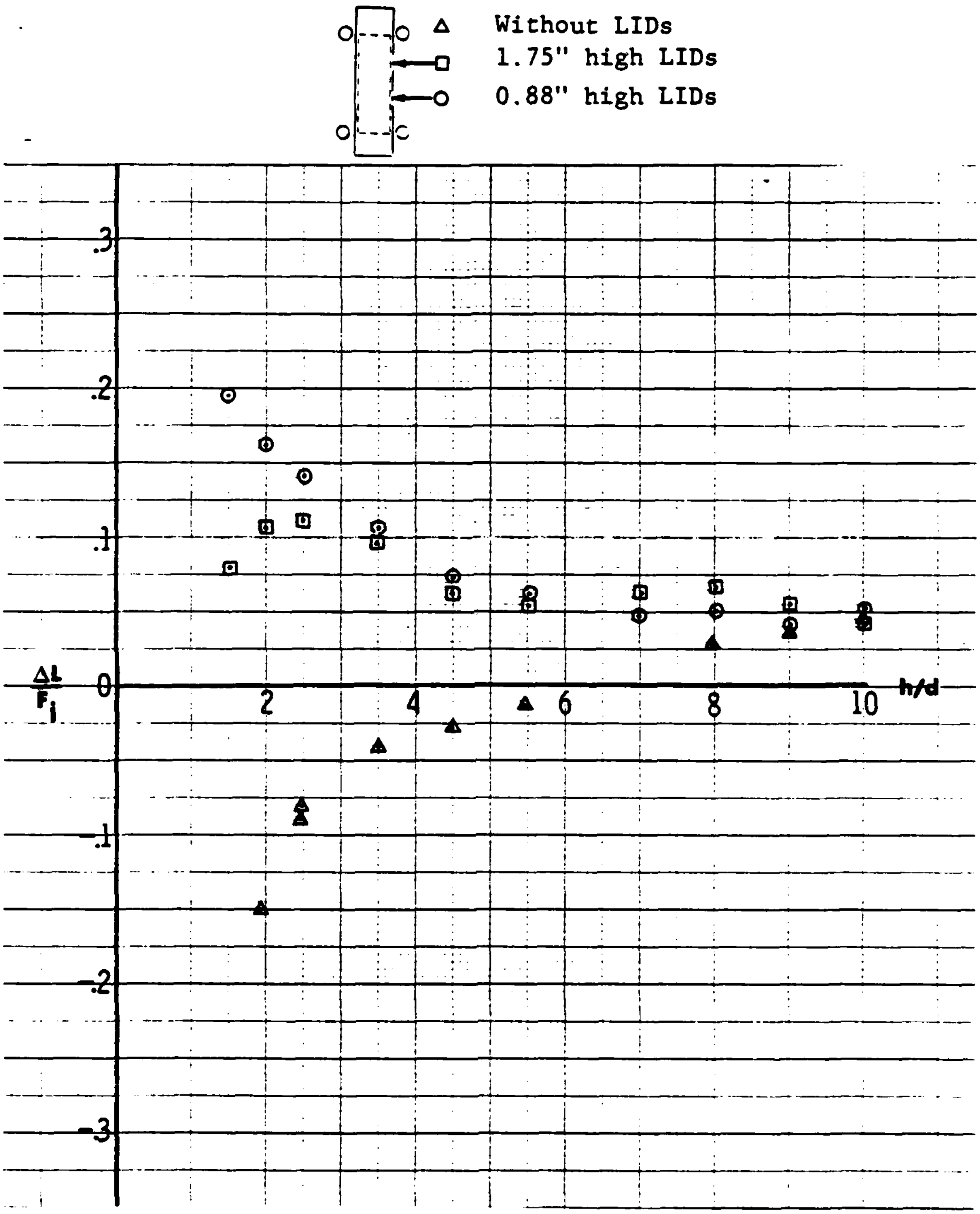

Figure A-9. Configuration 15

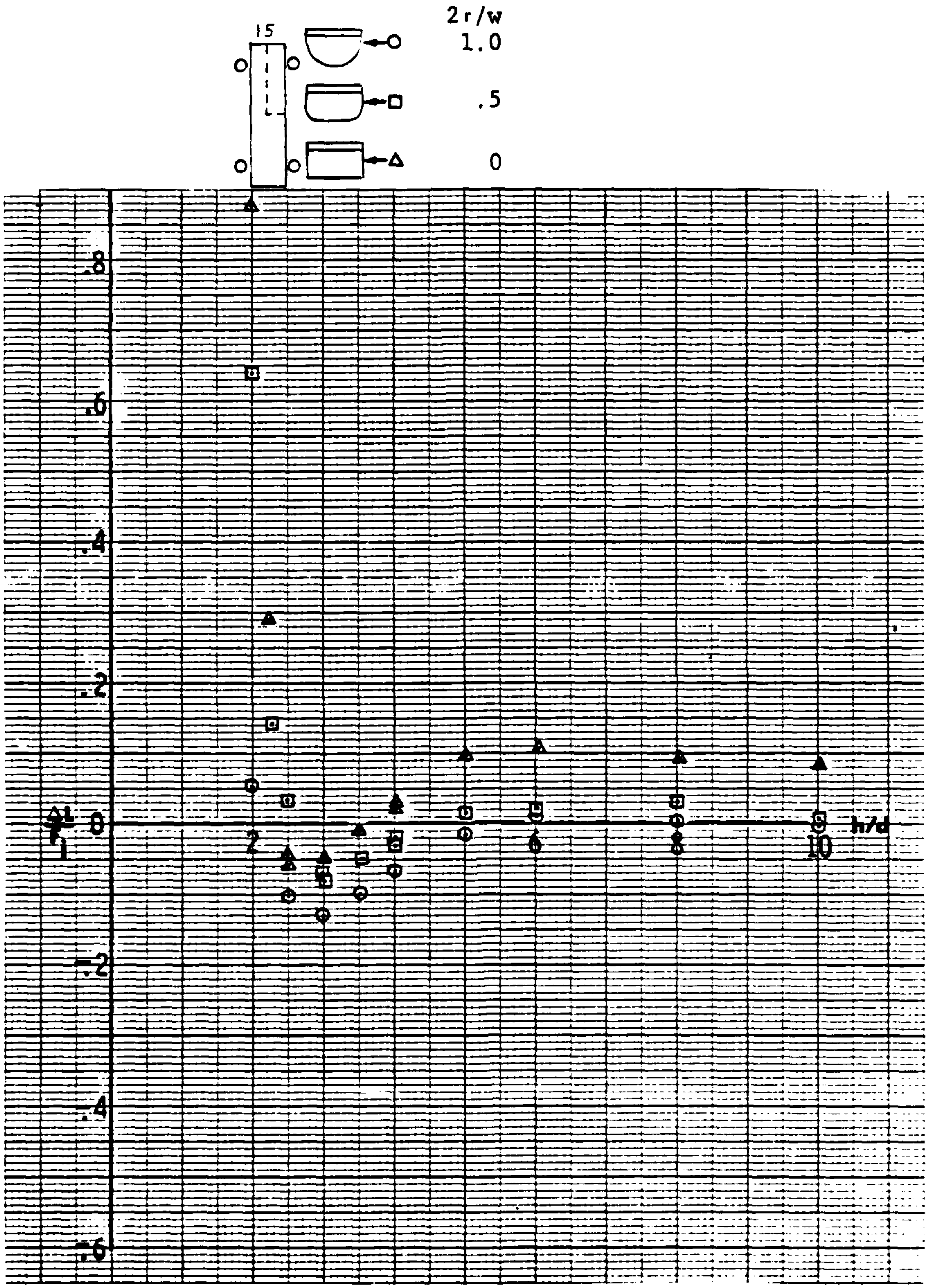

Figure A-10. Configuration 15

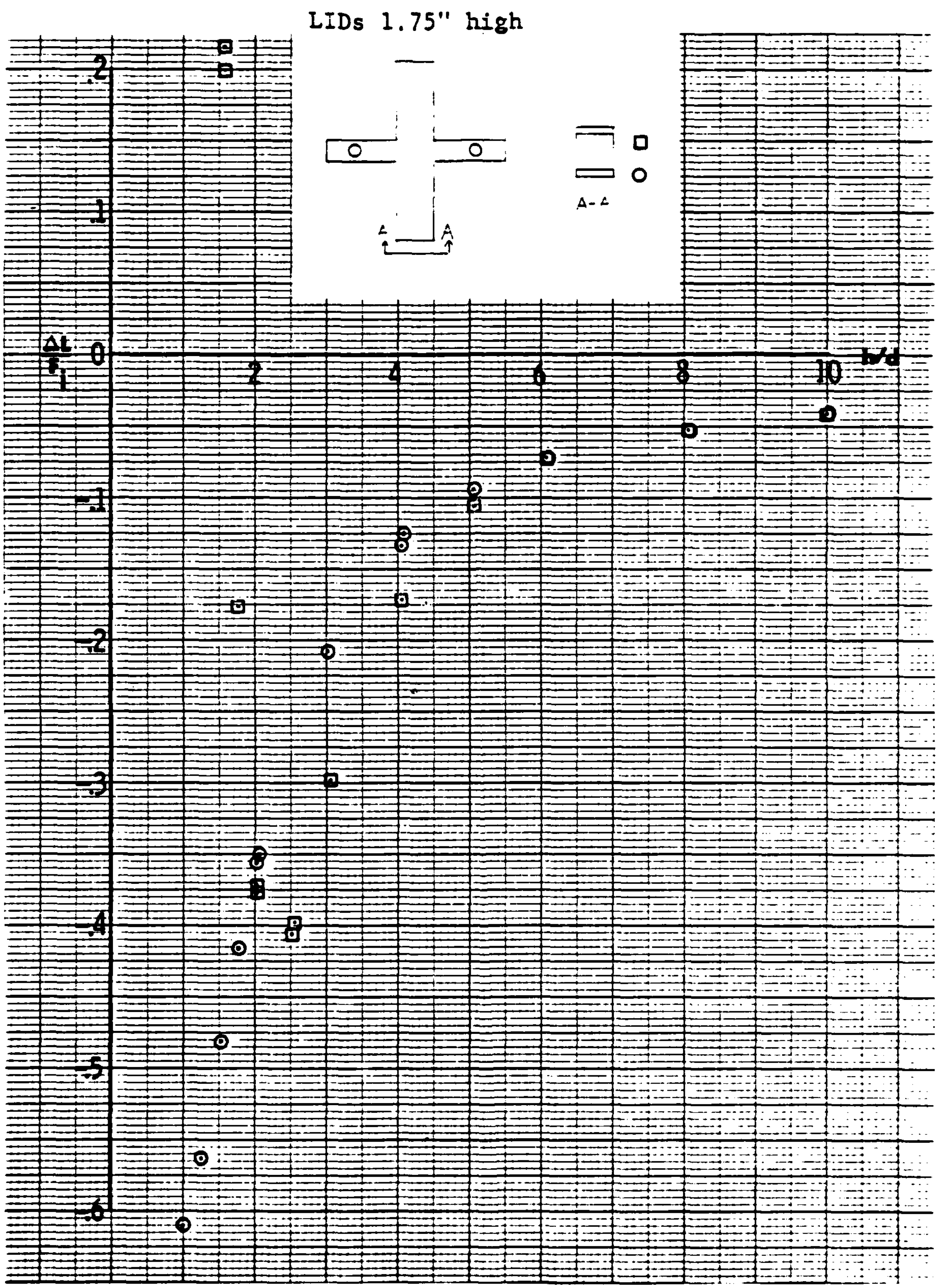

Figure A-11. Configuration 21
Single Jet Operation

LIDs 1.75" high

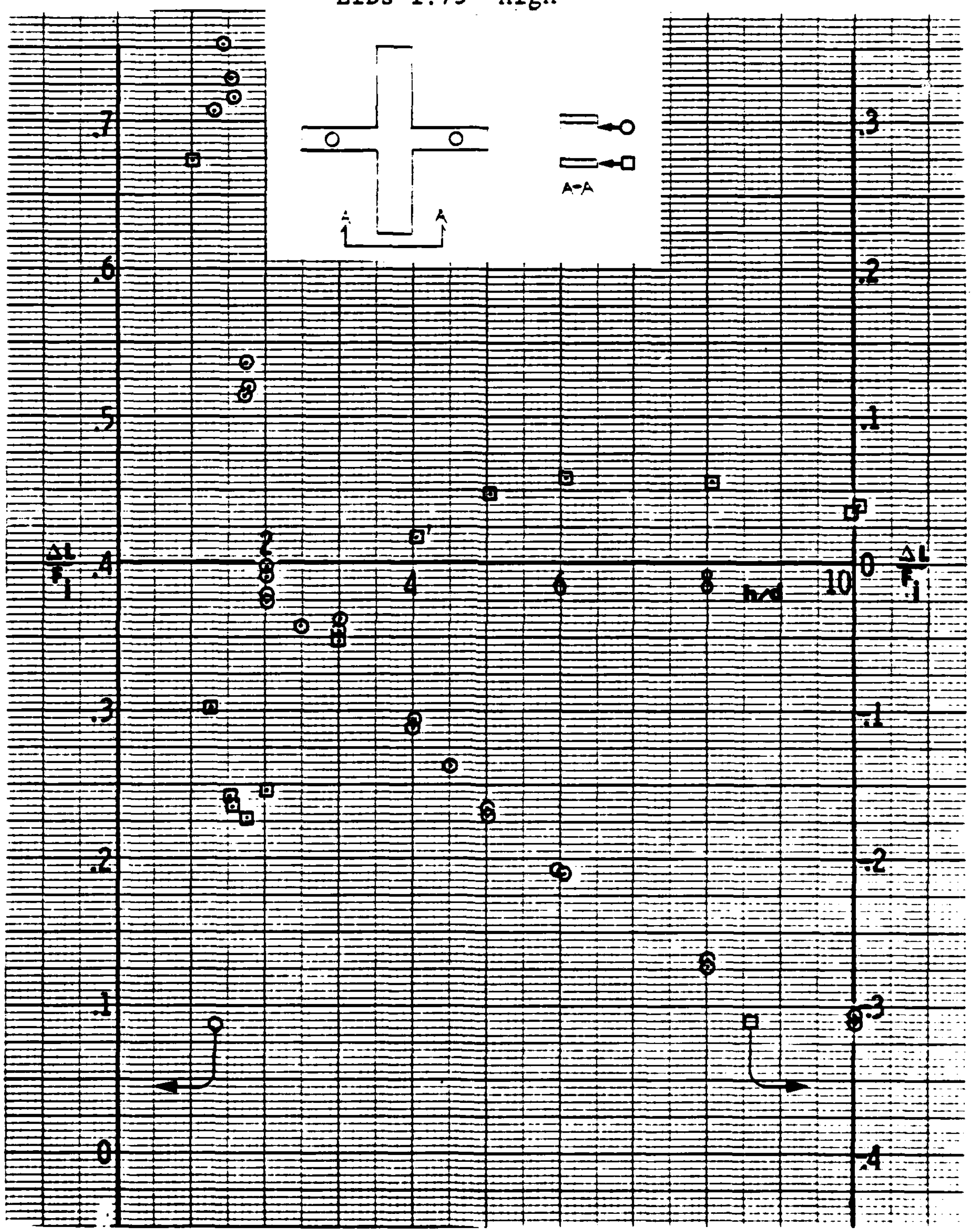

Figure A-12. Configuration 21

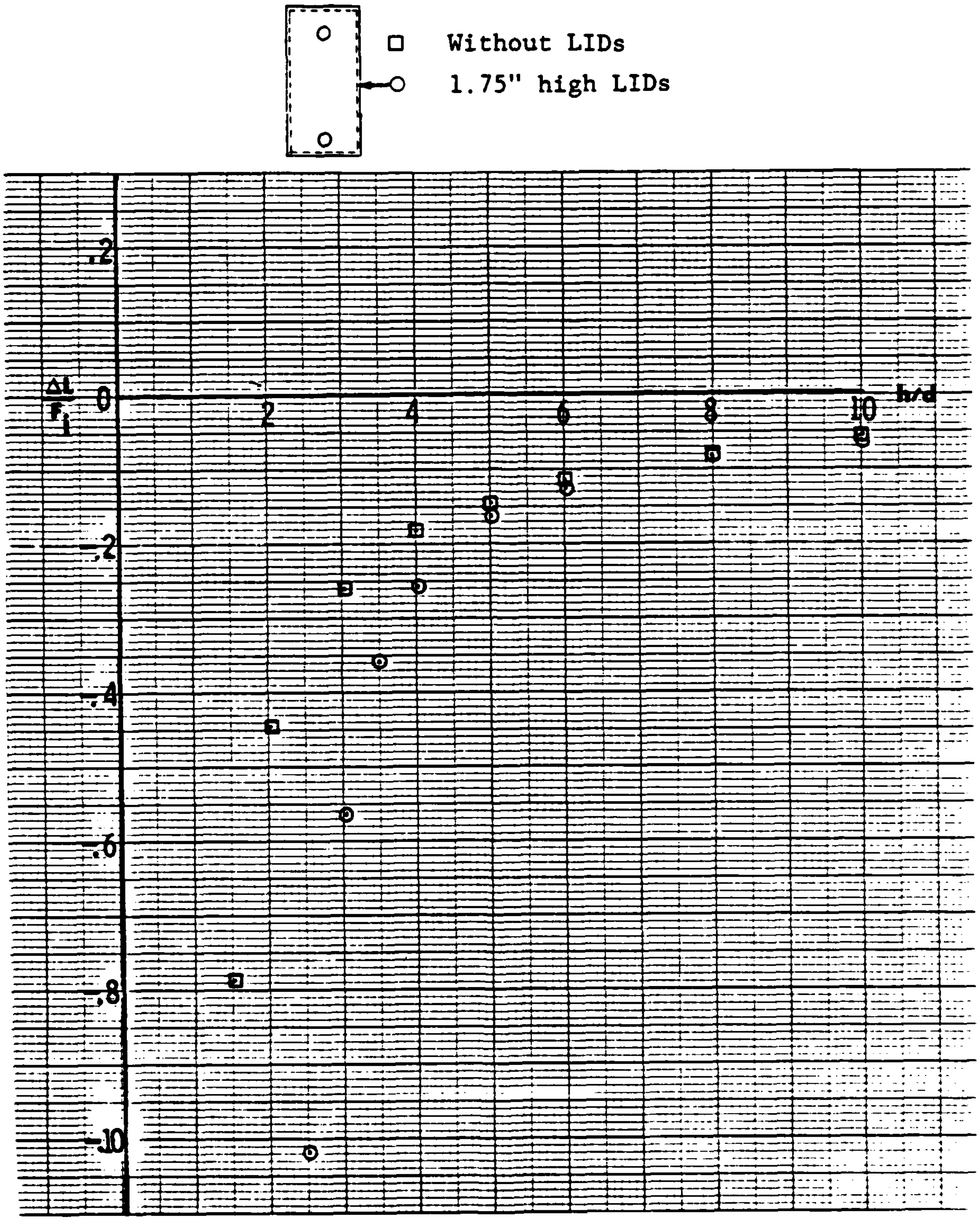

Figure A-13. Configuration 22

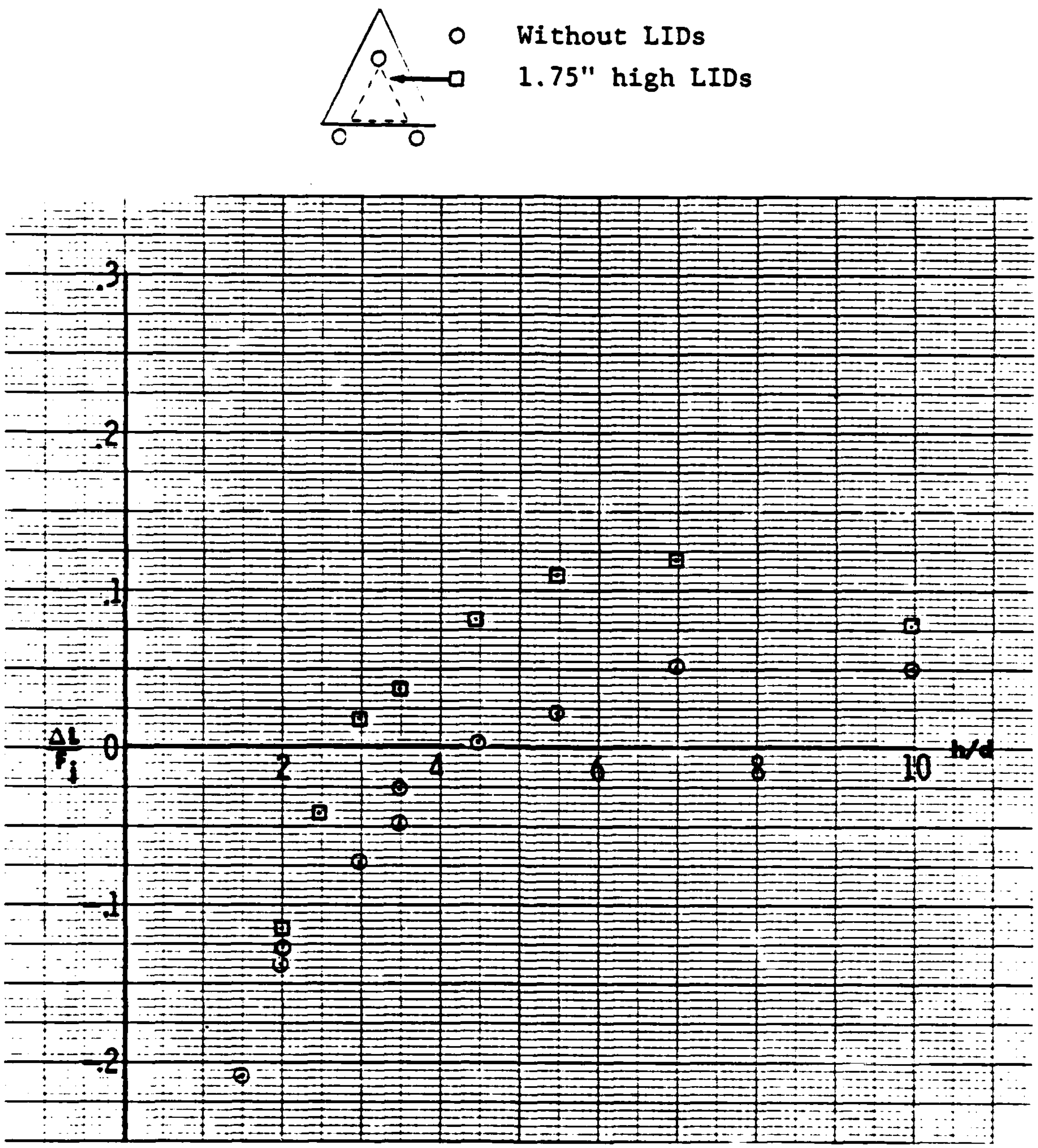

Figure A-14. Configuration 26

DISTRIBUTION LIST

Commander
Naval Weapons Center
China Lake, CA 93555

Commanding Officer
Naval Air Propulsion Center
Trenton, NJ 08628

Commander
Naval Air Test Center
Patuxent River, MD 20670

Commander
David Taylor Naval Ship Research
& Development Center
Bethesda, MD 20034

Chief
Office of Naval Research
800 N. Quincy Street
Arlington, VA 22217

Institute of Defense Analysis
400 Army Navy Drive
Arlington, VA 22202
Attn: J. Attinello

Director
National Aeronautics & Space
Administration
Ames Research Center
Moffett Field, CA 94035
Attn: D. Hickey

Director
National Aeronautics & Space
Administration
Flight Research Center
Edwards Air Force Base, CA 93523

National Aeronautics & Space
Administration
Langley Research Center
Hampton, VA 23365

Director
National Aeronautics & Space
Administration
Lewis Research Center
21000 Brooke Park Road
Cleveland, OH 44135

Director
Air Force Flight Dynamics Laboratory
(ASD/ENFDH)
Wright-Patterson Air Force Base
Dayton, OH 45433

Commander
Air Force Aeronautical Systems
Division
Wright-Patterson Air Force Base
Dayton, OH 45433

Superintendent
Naval Postgraduate School
Monterey, CA 93940

Commanding Officer
Army Aviation Systems Test Activity
Edwards Air Force Base, CA 93523

Commanding General
Army Aviation Ssytems Command
St. Louis, MO 63102

Commander
Naval Air Systems Command (AIR-954)
Department of the Navy
Washington, DC 20361
7 copies: (2) for retention
(2) for AIR-320D
(1) for AIR-5301
(1) for PMA-257
(1) for AIR-03PA)

DISTRIBUTION LIST (CONTINUED)

General Dynamics
Convair Division
P.O. Box 80986
San Diego, CA 92138

McDonnell-Douglas Corporation
P.O. Box 516
St. Louis, MD 63166

Lockheed-California Company
P.O. Box 551
Burbank, CA 91503

The Boeing Company
Seattle, WA 98101

LTV Aerospace Corporation
Dallas, TX 75221

Rockwell International
Columbus, OH 43216

General Dynamics
P.O. Box 748
FortWorth, TX 76101

Commander
Air Force Flight Test Center
Edwards Air Force Base, CA 93523

Administrator
Defense Documentation Center for
Scientific & Technical Information
(DDC)
Building #5, Cameron Station
Alexandria, VA 22314
(12 copies)

Office of Naval Research
800 N. Quincy Street
Arlington, VA 22214
Attn: Dr. R. Whitehead

Commander
Naval Air Development Center
Warminster, PA 18974
13 Copies: (3) for Code 813
(10) for Code 6053
Attn: C. Henderson

McDonnell-Douglas Corporation
3855 Lakewood Boulevard
Long Beach, CA 90808

Pratt & Whitney Aircraft Division
Division of United Aircraft
Corporation
East Hartford, CT 06108

Northrop Corporation
Hawthorne, CA 90250

Lockheed-Georgia Company
Marietta, GA 30061

Grumman Aerospace Corporation
Bethpage, Long Island, NY 11714

Rockwell International
Los Angeles, CA 90053

Fairchild-Republic Corporation
Farmingdale, Long Island, NY 11735

Royal Aeronautical Establishment
Bedford, England
Attn: A. Woodfield

Hughes Aircraft Company
Culver City, CA 90230

DISTRIBUTION LIST (CONTINUED)

A. L. Byrnes
Lockheed-California Company
Burbank, CA 91520

W. G. Hill, Jr.
Research Department, A-08-35
Grumman Aerospace Corporation
Bethpage, NY 11714

R. J. Kita
Grumman Aerospace Corporation
Bethpage, NY 11714

D. Koenig
Mail Stop 247-1
NASA Ames Research Center
Moffett Field, CA 94035

D. R. Kotansky
Section Chief, Aerodynamics
McDonnel Douglas Corporation
McDonnell Aircraft Company
P.O. Box 516
St. Louis, MO 63166

P. T. Wooler
Aerosciences Research
Department 3811, Zone 82
Northrop Corporation, Aircraft Group
3901 W. Broadway
Hawthorne, CA 90250

R. R. Jeffries
AFWAL/FIMM
Wright Patterson AFB, Ohio 45433

E. D. Spong
Branch Chief, Propulsion
Dept. 343, Bldg. 32/2
McDonnell Aircraft Company
P.O. Box 516
St. Louis, MO 63166

J. W. Paulson, Jr.
Mail Stop 286
NASA Langley Research Center
Hampton, VA 23665

S. Perkins
Nielsen Engineering & Research Inc.
510 Clyde Avenue
Mountain View, CA 94043

R. Perkins
Deputy Chief V/STOL Project Office
Naval Air Systems Command
Washington, DC 20361

M. F. Platzer
Code 67Pl
Department of Aeronautics
Naval Postgraduate School
Monterey, CA 93940

D. B. Schoelerman
Vought Corporation
P.O. Box 5907
Dallas, TX 75222

C. J. Martin
David W. Taylor Naval Ship Research and Development Center
Bethesda, MD 20014